When water becomes an unexpected efficient solvent for polar s-block organometallic compounds : H-bond networks and mechanism

Samuel Danladi Mador

THÈSE

Pour obtenir le grade de

DOCTEUR DE L'UNIVERSITÉ GRENOBLE ALPES

École doctorale : CSV- Chimie et Sciences du Vivant
Spécialité : Chimie Physique Moléculaire et Structurale
Unité de recherche : Département de Chimie Moléculaire

Quand l'eau devient un solvant efficace et inattendu pour les composés organométalliques polaires du bloc s : réseaux de liaisons H et mécanisme

When water becomes an unexpected efficient solvent for polar s-block organometallic compounds: H-bond networks and mechanism

Présentée par :

Samuel Danladi MADOR

Direction de thèse :

Anne MILET — Directrice de thèse
PROFESSEURE DES UNIVERSITES, Université Grenoble Alpes

Rapporteurs :

Carine MICHEL
CHARGE DE RECHERCHE HDR, ENS Lyon
Hélène GERARD
PROFESSEUR DES UNIVERSITES, Sorbonne Université

Thèse soutenue publiquement le **27 janvier 2023**, devant le jury composé de :

Anne MILET PROFESSEUR DES UNIVERSITES, Université Grenoble Alpes	Directrice de thèse
Carine MICHEL CHARGE DE RECHERCHE HDR, ENS Lyon	Rapporteure
Hélène GERARD PROFESSEUR DES UNIVERSITES, Sorbonne Université	Rapporteure
Guy ROYAL PROFESSEUR DES UNIVERSITES, Université Grenoble Alpes	Président
Hassan OULYADI PROFESSEUR DES UNIVERSITES, Université de Rouen Normandie	Examinateur

Acknowledgement

My sincere gratitude to the jury members Dr. Carine Michel, Pr. Hélène Gerard, Pr. Guy Royal and Pr. Hassan Oulyadi for accepting and making out time to evaluate my thesis. I am honoured to have your presence as the jury and I hope to sustain your interest in the work even more so during the defence.

I am profoundly grateful to my thesis supervisor Pr. Anne Milet for the support and encouragement. The conducive working environment and the kindness you showed during the course of the thesis is remarkable and greatly encouraging. I appreciate the guidance and the time you have given to see to the success of this work and also for your advice and patience during the period of this work. Indeed, it was a nice working with you and I have learnt a lot from you. Thank you.

I also want to express my gratitude to the members of my Comité de Suivi Individuel (CSI), Dr. Pascale Maldivi and Dr. Frederic Minassian for the time you gave to be part of the committee and for the encouraging and helpful discussions and advices. My sincere gratitude to Dr. Florian Berthiol for accepting to be my tutor in the CSI committee. You have always given me a listening ear and have always been ready to render assistance and guidance even pertaining administrative procedures. Thank for the warm atmosphere you create in the lab.

For every successful completion of a work lies a number of people that play one role or the other. I first want to express my indebted gratitude to Dr. Pierre Girard the Research Engineer and cluster manager of the SITh team of DCM laboratory, for the kind technical support and advice, always making out time and always being ready to assist whenever approached. I sincerely thank all the members of the SITh team researchers; Pr. Mark Earl Casida, Dr. Hélène Jamet, Dr. David Gatineau, Dr. Yves Gimbert and Dr. Baptiste Leforestier and also colleagues and friends; Océane Mangel and Subash Arjunan, for the wonderful working environment and group meetings and discussions over the years. I am grateful to the secretaries of the DCM laboratory and ED-CSV for their assistance.

I am thankful to the TETFund, Nigeria for the scholarship funds awarded for this thesis and to the University of Jos, Nigeria.

My deep thanks to my family for the support and encouragement during this period of study. I could always rely on you for your tireless love and support. I am also very grateful to my friends in the lab, in Grenoble and other places and also to the family of St. Marc Anglican Church, Grenoble who have made living here wonderful and bearable especially during the lockdown. God bless.

Table of Contents

Table of Figures

Table of Tables

Atom Caption

Hydrogen

Lithium

Carbon

Nitrogen

Oxygen

Sulphur

Magnesium

Chlorine

Bromine

Abstract

Organometallic compounds of polar *s*-block metals especially organolithium and Grignard reagent have found vast applications in organic transformations. Due to the polarity of their C—Metal bonds, a significant thing to note in their use is their extreme sensitivity to moisture and therefore, their manipulation must be in anhydrous solvents under controlled conditions. Yet, recently, interesting and surprising use of these class of compounds in organic transformations under uncontrolled environment (under air and at room temperature) and in the presence of water were reported with improved performance and yield in most cases. This thesis sort to understand the mechanism of this reaction and the role of water, with emphasis on the synthesis of 2,2-disubstituted tetrahydrofuran by reaction of 4-chloro-1-phenyl butan-1-one (γ-chloroketone) with methyllithium "on water" by DFT and the biased QM/MM dynamics such as metadynamics method. We first, studied the different aggregation states and nature of solvation of the MeLi in ethereal solvents (diethyl ether and THF). The prominent states were found to be the dimer and tetramer with the tetramer being the most stable state. The solvent coordination number observed with THF is higher than the corresponding diethyl ether solvation. This is chiefly due to the steric repulsion pose by the alkyl chains of the diethyl ether. A similar trend was observed for the clusters with docked ketone (acetone, γ-chloroketone) on the lithium of the methyllithium (MeLi—Ketone clusters). Study of intermolecular interaction energy between solvents or ketones and MeLi clusters by symmetry-adapted perturbation theory (SAPT) showed the direct interaction energy is dominated by electrostatic interaction with contributions from induction and dispersion interactions.

Reaction mechanism of addition of MeLi aggregates to the ketones were studied in the conventional (diethyl ether and THF) and unconventional media ("on water"). The solvents were found to have significant effect on the reactions. For the reaction on water, a hydrogen bonding network formed by water and the partly hydrolysed ketone-cluster system postulate an insight to this reaction without complete consumption of the organometallic reagent by the water.

We also studied the organometallic nucleophilic addition of sulfinyl ketimines and found the difference in stability and quick addition relative to isomerism of the diastereomers and the effect of steric to be the reasoning behind the high selectivity of the 1,2-addition obtained for the reaction.

INTRODUCTION

The chemistry of compounds containing direct bonding interaction between carbon and metal have been in existence for more than two centuries. This group of compounds are referred to as 'organometallic' compounds, a term coined by Edward Frankland in 1849. The metal may be a main-group metal of the *s* and *p* blocks of the periodic table or transition metal of the *d* and *f* blocks.

Historically, in 1760, in a Paris military pharmacy, Cadet made the first organometallic compound, cacodyl oxide, $[CH_3)_2As]_2O$ which was later isolated and characterized by Bunsen, as a component of the inflammable malodorous mixture termed 'Cadet's fuming arsenical liquid' made from heating arsenic trioxide with potassium acetate (eq. I).[1,2]

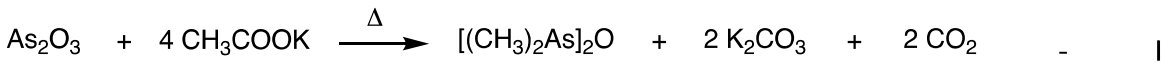

$$As_2O_3 + 4\,CH_3COOK \xrightarrow{\Delta} [(CH_3)_2As]_2O + 2\,K_2CO_3 + 2\,CO_2 \quad \text{- I}$$

After more than half a century of Cadet's discovery, William Christopher Zeise synthesised the first transition metal organometallic compound known as the Zeise's salt, $K[PtCl_3(C_2H_4)].H_2O$ presented in a paper in 1830, by dissolving platinic chloride in alcohol, evaporating the alcohol and reacting the residue with potassium chloride to obtain the yellow crystal salt.[3,4] With growing interest in alkyl radicals inspired by the isolation of the relatively stable cacodyl by Bunsen, Edward Frankland attempting to isolate ethyl radical by reacting ethyl iodide with zinc metal, prepared diethylzinc instead (eq. II).[5]

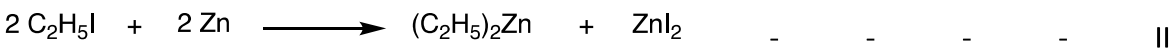

$$2\,C_2H_5I + 2\,Zn \longrightarrow (C_2H_5)_2Zn + ZnI_2 \quad \text{- - - - II}$$

Onward from Frankland's discovery in 1849, the chemistry of organometallic gain wide spread especially as reagents in synthesis and many new organometallic compounds were discovered. To mention a few are: organosilanes by Friedel and Crafts; the synthesis of the first metal-carbonyl complex, $[Pt(CO)Cl_2]_2$ by Schützenberger in 1868; the first binary metal carbonyl, $Ni(CO)_4$ by Ludwig in 1890; and in 1900 came the discovery of one of the most versatile class of organometallic compound, the Grignard reagents by Victor Grignard who shared a noble price in 1912 for its development. Preceded by the findings of Barbier (who was Grignard's supervisor) of the replacement of zinc by magnesium in Saytzeff reaction, Grignard sorted to isolate organo compounds of magnesium by treatment of magnesium with akylhalide in absolute ether at room temperature, before subsequent reaction with reactive compounds, notably carbonyl compound, in a next step. He followed this path to prepare alcohol as shown in scheme I.[6]

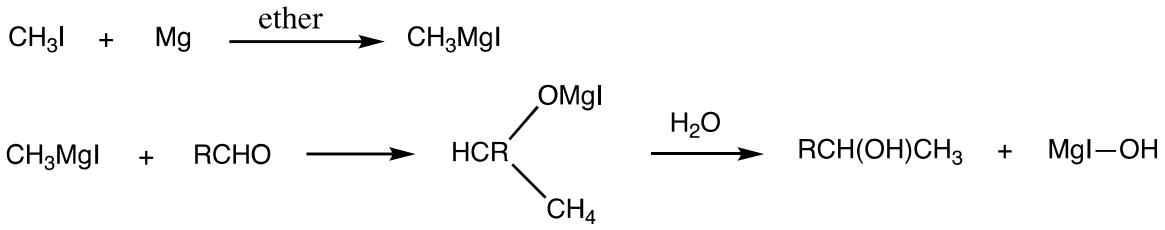

Scheme I: Grignard reaction for the preparation of alcohol

In 1917, organometallic alkali compounds, organolithiums were first prepared by Schlenk, which came to be another widely used organometallic reagents in organic synthesis. He reported the synthesis of the organolithium compounds, MeLi, EtLi, n-propylLi and PhLi illustrated in scheme II. [7,8]

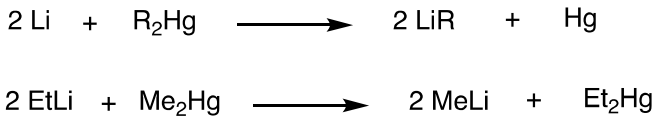

scheme II: Schlenk's preparation of organolithium

Other discoveries in the field of organometallic chemistry and by no means exhaustive, are:[9–11] the first use of organometallic compound, in homogeneous catalysis in hydroformylation (the oxo process) by Otto Roelen; Pauson's and Miller's groups independently discovered ferrocene, $(C_5H_5)_2Fe$, **I** in 1951 and its sandwich structure was proposed by Wilkinson, Fischer and Woodward; Ziegler and Natta used mixed metal catalysts, transition-metal halide/AlR_3 in developing olefin ploymerisation at low pressure, earning them a noble prize in 1963; the first metal carbene, **II** and metal carbyne, **III** complexes by Fischer in 1964 and 1973 respectively; the use of palladium catalyst in coupling of aryl boronic acids (Suzuki coupling) by Suzuki and Miyaura in 1979; and more recently, the first Zn(I) organometallic compound, $Zn_2(Cp^*)_2$, **IV** by Carmona in 2004.

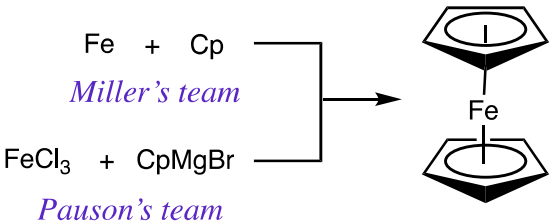

I

scheme III: Synthesis of ferrocene by Miller's and Pauson's group

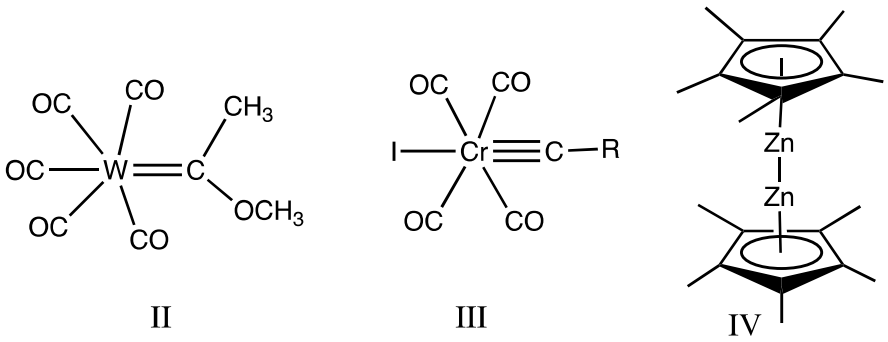

II III IV

Fig I: structures of some early discovered organometallic compounds

Organometallic compounds, (OMCs) have continued to gain wide acceptance and applications. They find utility as reagents in synthesis where they act as sources of carbanions. Due to the metals being more electropositive than carbon, polarisation of the carbon-metal bond results, making it possible for electrophilic attack on the carbon and also the use of the organometallic compounds as nucleophiles. Organometallic compounds have also found applications as additives in modifying properties of compounds especially in the 20th century and early 21st century. Examples of this are: the use of tetraethyllead and methyl cyclopentadienyl manganese tricarbonyl (MMT) as antiknocking agents before their ban in most countries; the use of ferrocene as soot suppressant in combustion systems which unfortunately can form conductive coating of iron oxide on the sparkplug surfaces resulting in their failure in vehicles. Another well-known application of OMCs is in homogeneous catalysis. This application is prominent with OMCs of the transition metals with few from the main-group compounds. Many books have been written about organometallic catalysis in synthesis and industrial production. Here, to mention a few examples are: the use of Wilkinson's catalyst, $(Ph_3P)_3RhCl$, Schrock-Osborn catalyst, $[Rh(COD)(PPh_3)_2]^+PF_6^-$, Crabtree's catalyst, $[Ir(COD)(PCy_3)(Py)]^+PF_6^-$ and Marks' catalyst, $(Cp^*_2LuH)_2$ in hydrogenation of alkenes and alkynes; use of palladium organometallic catalyst in C—C and C-N cross coupling; employing cobalt carbonyl, cobalt catalyst, $Co_2(CO)_8$ or rhodium-phosphine complex, $HRh(CO)(PPh_3)_3$ to catalyse hydroformylation; $Ni(CO)_4$ in reaction of unsaturated organic compounds with CO and an active compound such as H_2O, ROH or RNH_2 to give carboxylic acid derivative; alkene metathesis with Grubbs' or Schrock's catalyst which are derived from transition-metal halides and carbanion donors; formation of urethanes from isocyanates and alcohols using trialkyltin-alkoxide such as $(Bu_3Sn)_2O$; esterification of terephthalic acid with ethylene glycol to produce polyester utilising dialkyltin oxide, R_2SnO as catalyst.

Here, the focus of this thesis is on the polar *s*-block OMCs in particular organolithium and organomagnesium (Grignard reagents) compounds. The ease of synthesis and commercial availability of these compounds give them their broad usage as reagents in organic transformation. A notable application of these compounds is in the synthesis of alcohol by their addition to carbonyl compounds (scheme IVa). In this sense, organolithiums in general form addition product while their counterpart Grignard reagents especially with sterically hindered carbonyl compound mostly lean more towards reduction product. An example is the reactions of diisopropyl ketone with isopropyl magnesium bromide and with isopropyl lithium (scheme IVb). [12]

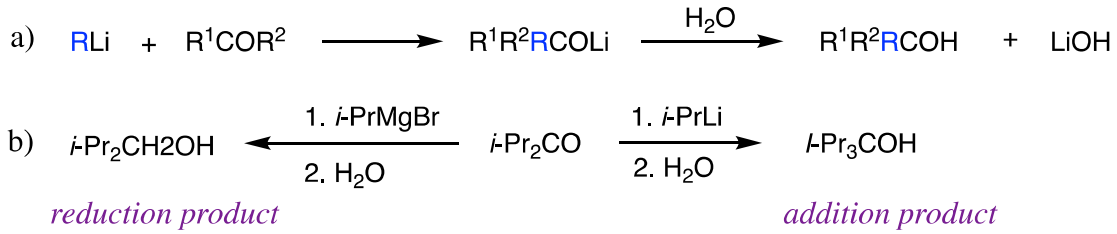

scheme IV: a) synthesis of alcohol by addition of organolithium to carbonyl compound
b) reduction and addition product for Grignard and organolithium reaction

Another addition reaction of organolithium reagents is conjugate addition to double bonds such as alkenes, α,β-unsaturated esters and α,β-unsaturated imines which may generate stereogenic centers in which case organic chemists always sort to develop asymmetric conjugate addition which may be by using external chiral ligand or by use of chiral auxiliary.

Like organolithiums, Grignard reagents also react with alkenes although often times metal catalyst are employed. Coupling reactions of Grignard reagents with organic halides are also common in literature. Many interesting reactions of Grignard reagents with carbonyl and C=N compounds yielding good stereoselective product continue to gain popularity among synthetic chemists. A good review of these reactions have been put together by Bartolo and co-workers.[13] However, the challenge lies in the difficult to explain their stereoselectivity by simple models like the Felkin-Anh or chelation-control model.

A significant and almost the first thing to note about the use of these OMCs of *s*-block elements in organic transformation is their extreme sensitivity to moisture due to their highly polarized metal-carbon bonds. Their manipulations must therefore be in anhydrous solvents and under controlled atmosphere, and so it is preposterous to think of adding water as a ligand or solvent. Yet, recently, an interesting development in the chemistry of this class of *s*-block polar organometallic-compounds, is their application in organic transformations under uncontrolled

environment (under air and at room temperature) and in unconventional solvents as water and deep eutectic solvents (DES). In most cases, improved performance and yield results. A good number of such unconventional reactions have been performed by Capriati and collaborative workers including Hevia and Garcia-Àlvarez. Notable works involving this unconventional reactions have been nicely highlighted in reviews by Capriati and collaborative workers. [14–16] This development instigates many questions such as how these reagents survive hydrolysis and the role of the unconventional solvents in the reactions which prompted our interest, driving us into this project.

Therefore, the main aim of the project revolves around understanding the aggregation state and nature of solvation of this polar organometallic compounds in ethereal solvents and deciphering the mechanism of their nucleophilic addition reaction in conventional ethereal solvents and in unconventional reaction media (reaction in the presence of water under atmospheric conditions) with emphasis on the role of the solvents and importance of hydrogen bonding. In addition, we studied the mechanism and stereoselectivity of nucleophilic addition to sulfinyl ketimines. These studies were conducted by theoretical methods using state of the art molecular modelling techniques such as the density functional theory (DFT) computation, molecular dynamics with metadynamics enhanced sampling technique, symmetry-adapted perturbation theory (SAPT) and the ab initio coupled-cluster method, details of which will be discussed in the next chapter.

The particular reaction under consideration is the reported work by Capriati and co-wokers where they synthesised 2,2-disubstituted tetrahydrofuran, **VII** by reaction of 4-chloro-1-phenyl butan-1-one, **V** (also referred to as 4-chlorobutyrophenone or simply γ-chloroketone) with methyl lithium or methyl magnesium chloride “on water” under air and at room temperature (scheme V).[17] The product, **VII** was formed via cyclization of an intermediate chlorohydrin **VI**. A 3 to 6 equivalent of 3.0 M MeMgCl in THF or 1.6M MeLi in diethyl ether (Et_2O) was spread over a suspension of 0.5mmol of **V** in 1mL water. A yield of 72 to 80 and 75 to 82% of product was gotten at 3 to 6 equivalents of MeMgCl and MeLi, respectively, after 10mins. Compared with the conventional tetrahydrofuran (THF) solvent under controlled atmosphere, only 3% yield was reported after 10mins. Also, in the reaction in the conventional THF solvent, by changing to room temperature from -40°C, a reduction in yield from 60 to 10% at 3 equivalent of MeMgCl and from 70 to 30% at 3 equivalent of MeLi were observed. A good yield of up to 75% at 3 equivalent and up to 85% at 6 equivalent were recorded for other organometallic reagents and γ-chloroketones with bulkier organic substrates

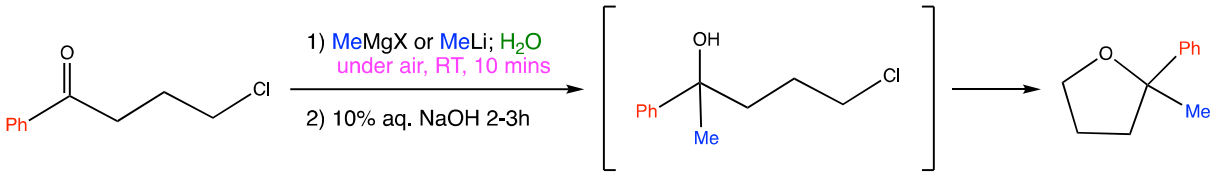

V VI VII

scheme V: unconventional synthesis of 2,2-disubstituted tetrahydrofuran

The thesis is thus, divided into four parts. The first part comprises of the study of the nature of aggregation and solvation of MeLi in Et_2O and THF solvents. It is important to understand how the structures of this compound are affected by solvation. This understanding of the likely predominant and more stable aggregation state will help in elucidating the mechanism and the most likely aggregation form our alkyl lithium takes in the reaction.

The second part is dedicated to the study of the mechanism of 1,2-addition of the polar *s*-block organometallic compounds to sulfinyl ketimines. The insight is given to the stereoselectivity of these reactions despite the existence of the sulfinyl ketimines as mixtures of *E* and *Z* isomers in equilibrium which can undergo interconversion and cannot be separated. The third part comprises of the study of the mechanism of the reaction of γ-chloroketones with methyl lithium (scheme IV) in conventional conditions and solvents, Et_2O and THF. In the last part is the study of the addition of the methyl lithium to the γ-chloroketone in unconventional media, the "on water" reaction.

CHAPTER ONE

1 Computational Methods

Molecular modelling entails simplified approximation of theories into more general forms for practical utility which may or may not involve incorporation of experimentally derived quantities. Beyond the theoretical approximations, the computational chemist also uses a chemical model which is a simplified system designed to best represent the chemical system to be studied. Therefore, a computational chemist is one who models chemical system of interest and uses or develop computational tools to study the system and find solution to practical chemical problems. It is worthy of note that computational chemistry and molecular modelling are terms that are often used interchangeably.

There is always a question of "what is the accepted limit of simplicity of a theory or to what extend can approximations (model and/or theory) be made that will still capture close enough representation or result of the practical chemical system?" Also, another important question is, "is it practical, do we have the resources or the luxury of time to solve problems with a chosen level of approximation?"

In this chapter attention is brought to the different computational methods employed in this work. A general introduction to the theories behind the methods are given, followed by the level of the theory specifically employed in solving each particular task for our systems. Herein, the theories and methods involved are density functional theory, coupled cluster theory, molecular dynamics, metadynamics and symmetry-adapted perturbation theory. Before diving into these aforementioned theories and computational details, the concepts of molecular mechanics and quantum mechanics would be first discussed.

1.1 Molecular Mechanics

Molecular mechanics (MM) involves the treatment of the chemical systems following the classical laws of physics. The molecules are simplified as a collection of balls or spheres and springs to model the atoms and bonds, respectively. This theory was designed for studying nonreactive and non-excited state systems. It is basically for the study of properties that do not depend on electronic distribution of the atoms. MM is most significantly used for the study of systems with large number of atoms.

In MM also referred to as force field method, simple models of nuclear interaction within a molecular system are used. The interactions are either bonding or non-bonding interactions. The energy of the system is associated with these interactions and any distortion on the components associated with these interactions causes a change in energy. The component or terms that describe the bonding interaction are: bond length, bond angle, torsional angle and out-of-plane bending term (such as improper torsion); while the non-bonding interaction is described by the electrostatic interaction and the van der Waals interaction. These are the major components which are contained in all force fields. Most force fields contain an additional term known as the cross term which takes into account coupling between the fundamental terms mentioned above. A force field is therefore an equation that gives the approximate potential energy of a molecular system (eq. 1.1).

$$U_{r^N} = U_{str} + U_{bend} + U_{rot} + U_{vdw} + U_{elst} + U_{cross} \quad 1.1$$

where U_{str}, U_{bend} and U_{rot} are energy functions due to bond stretching, angle bending and torsional angle rotation. U_{vdw} is the energy due non-bonded van der Waals interaction, U_{elst} is the energy due to electrostatic non-bonded interaction and U_{cross} is the cross term covering coupling between the first three terms.

Different force fields may differ by having different additional components to the aforementioned. Force fields also differ in the way they are parameterized. That is, the representation of structural units (referred to as atom type) which are similar in different molecules. The different atom types are generated with respect to the neighbour atom or atoms. Parametrization is an important aspect of force field development and determines the suitability and of a force field to a particular system.

1.1.1 Force Field Potential Energy Functions

For the bond stretching from the natural bond length, r_{eq} to a length r, different functional forms are used to describe the energy term, U_{str}. This include the simple harmonic potential from the second order of a Tylor expansion around the natural bond length for bonds between atom say, A and B, r_{AB} given by:

$$U_{str}(r_{AB}) = U(r_{eq}) + \frac{dU}{dr}(r - r_{eq}) + \frac{1}{2!}\frac{d^2U}{dr^2}(r - r_{eq})^2 + \cdots \quad 1.2$$

The first term is set to zero and the second term is zero by virtue of the expansion being around the natural bond, r_{eq}. Truncating after the third term gives eq. 1.3 known as the Hooke's law.

$$U_{str}(r_{AB}) = \frac{1}{2!}k(r - r_{eq})^2 \quad 1.3$$

where k is the force constant for the bond.

Higher order potentials such as the quartic approximation (forth order term) may also be used to describe the bond stretching energy term. Another function to calculate the energy due to bond stretching is the Morse potential[18] given by eq. 1.4

$$U_{str,morse}(r_{AB}) = D_e[1 - e^{-\alpha(r-r_{eq})}]^2 \quad 1.4$$

where D_e is the depth of the potential energy minimum or dissociation energy and α is a fitting constant related to the force constant, k by: $\alpha = \sqrt{k/2D_e}$

The Morse potential and the quartic approximation reproduces well the bond-stretching potential energy curve over a wide range of distances. The Morse potential up to 0.8Å and the quartic up to 0.3Å from an electronic structure calculation for a CH_4 molecule.[19] However, there are some difficulties with the application of the Morse potential. For instance, the restoring force is quite small making distorted structures slow to converge. Fortunately, for majority of systems, their important degrees of freedom are close to their equilibrium values which is within 10 kcal mol^{-1} situated at close to the bottom of the energy curve for interatomic separation. At this region, the quartic approximation almost perfectly matches the Morse potential and even the simple harmonic potential performs well and so the harmonic potential can be used to describe the bond stretching energy term.

Similarly, the bond angle bending energy term defined by an angle say ABC can be described by the harmonic potential given by eq. 1.5. where θ_{eq} is the natural bond angle.

$$U_{bend}(\theta_{ABC}) = \frac{1}{2}k(\theta - \theta_{eq})^2 \quad 1.5$$

The energy term associated with rotation about a bond C—D from a four atoms sequence say ABCD, is derived from a Fourier series to capture periodicity as the torsional angle, ω between bonds AB and CD is periodic. The general equation for the rotational energy term is given by eq. 1.6.

$$U_{rot}(\omega_{ABCD}) = \sum_{\{n\}ABCD} \frac{1}{2}V_n[1 + \cos(n\omega - \gamma)] \quad 1.6$$

where V_n is the barrier height of the rotation, γ is the phase factor which determines where the dihedral angle passes through its minimum value and n is the term that describe the periodicity. For instance, n=1,2 and 3 describe rotation that is periodic at 360, 180 and 120°, respectively. The factor of one is added to shift the zero point of the rotation potential.

In general, the first three terms of the Fourier series are sufficient for reproducing the energy profile of the rotation for all organic molecules which essentially have a maximum valence of four and showing at most three minima (with exceptions) on the rotational energy profile. Most force fields use terms up to n=3.

The van der Waals interaction term shows a non-polar non-bonded attractive or repulsive interaction. The force associated with this interaction is known as the 'dispersion', 'London' or 'van der Waals' force. At infinite distance between two atoms, the interaction between them is zero. As the distance between the atoms shortens, an attractive force is felt between the electron clouds from induced dipole-dipole interaction due to electron correlation that causes charge polarization of an atom by its neighbour atom. The attractive force varies as the inverse sixth power of the distance between the atoms. The potential energy continues to decrease towards the negative until its minimum at a distance equivalent to the sum of the radii of the atoms. The interaction becomes repulsive and the energy rises to positive at distance lower than the sum of the radii of the atoms. The repulsive energy rises to zero on shortening the atomic distance faster than in moving the atoms to infinite distance. Therefore, the repulsive term is expected to be steeper than the attractive term. A function that captures this is the Lennard-Jones potential[20] given by eq. 1.7.

$$U_{vdw,LJ} = 4\varepsilon_{ij}\left[\left(\frac{\sigma_{ij}}{r_{ij}}\right)^{12} - \left(\frac{\sigma_{ij}}{r_{ij}}\right)^{6}\right] \qquad 1.7$$

where σ_{ij} is the interatomic separation at which the attractive and repulsive forces are equal, that is, $U = 0$, ε_{ij} is the Lennard-Jones well-depth and r_{ij} is the interatomic distance calculated from the Cartesian coordinates (eq. 1.8).

$$r_{ij} = \sqrt{\left(x_i - x_j\right)^2 + \left(y_i - y_j\right)^2 + \left(z_i - z_j\right)^2} \qquad 1.8$$

The other non-bonded energy term of the force field is a polar interaction which is due to internal redistribution of electrons in a molecular system resulting in positive and negative parts of the molecule. The approach is to assign each atom a partial charge. The charge can be permanent for atom types in all systems or can vary depending on the electronegativities of the atoms to which it is connected. The interaction energy between this point charges is defined by the Coulomb potential, eq. 1.9. In some force fields, the bond dipole moment is used instead of the atomic charges and other force fields include polarization, both of which will not be discussed here.

$$U_{elst} = \frac{q_i q_j}{\varepsilon_0 r_{ij}} \qquad 1.9$$

where q_i and q_j are the partial charges and r_{ij} is the distance of separation of atoms i and j. ε_0 is the dielectric constant.

The last term of eq. 1.1 captures the coupling between the bonding interactions (that is, the bond length, bond angle and torsional angle). Cross terms are important in obtaining better structural properties especially vibrational frequencies. Most cross terms are functions of two coordinates with rare instances involving three coordinates. In general, only few cross terms are necessary in reproducing good structural properties. The components in cross terms are usually obtained as products of the first-order Taylor expansion of the individual coordinate terms. For example, eq. 1.10 for stretch-rotation coupling for systems with eclipsing conformation that causes some strain.

$$U_{str-rot}(r_{BC}, \omega_{ABCD}) = \frac{1}{2} k_{BC,ABCD}(r - r_{eq})[1 + \cos(n\omega + \gamma)] \qquad 1.10$$

where $k_{BC,ABCD}$ is the stretch-rotation constant and all other terms are as defined above.

In summary, force fields have the general form (not strictly same) with the fundamental terms shown in eq. 1.11 with additional terms such as the cross term, depending on the force field.

$$U_{r^N} = \sum_{bonds} \frac{1}{2} k(r - r_{eq})^2 + \sum_{angles} \frac{1}{2} k(\theta - \theta_{eq})^2 + \sum_{torsions} \frac{1}{2} V_n[1 + \cos(n\omega - \gamma)] + \sum_{i=1}^{N} \sum_{j=i+1}^{N} 4\varepsilon_{ij} \left[\left(\frac{\sigma_{ij}}{r_{ij}} \right)^{12} - \left(\frac{\sigma_{ij}}{r_{ij}} \right)^{6} \right] + \sum_{i=1}^{N} \sum_{j=i+1}^{N} \frac{q_i q_j}{\varepsilon_0 r_{ij}} + U_{cross} \qquad 1.11$$

1.2 Quantum Mechanics

In chemistry, the study of the properties of a system that depend upon the electronic distribution of molecules (such as reactivity and spectroscopic properties) is an important field and requires the use of quantum mechanics (QM).

Early works leading to the development of this theory includes the idea of quantization of energy by Max Planck and the wave-like properties of matter by de Broglie in addition to the particle-like properties. A key postulate in QM is that an operator, the Hamiltonian (H), acting upon a wave function, Ψ returns the observable property, energy (E), of the system (eq. 1.12). This is the Schrödinger equation.

$$H\Psi = E\Psi \qquad 1.12$$

The Hamiltonian is given by eq. 1.13 running over electrons i and j, and over nuclei k and l. The typical contributions that account for the Hamiltonian are: the kinetic energies of the

electrons and nuclei (first and second terms of eq. 1.13), the attraction of electrons to nuclei (third term), and the inter-electronic and inter-nuclear repulsions (fourth and fifth terms, respectively).

$$H = -\sum_i \frac{\hbar^2}{2m_e}\nabla_i^2 - \sum_i \frac{\hbar^2}{2m_k}\nabla_k^2 - \sum_i \sum_k \frac{e^2 Z_k}{r_{ik}} + \sum_{i<j} \frac{e^2}{r_{ij}} + \sum_{k<l} \frac{e^2 Z_k Z_l}{r_{kl}} \qquad 1.13$$

where $\hbar = \left(\frac{h}{2\pi}\right)$ and h is the Planck's constant. m_e and m_k are the mass of electron and nucleus, respectively, Z is the atomic number, e is the electronic charge, r_{ab} is the distance between particles a and b and ∇^2 is the Laplacian operator for the Cartesian coordinates x, y and z.

In principle, the expression of the wave function for many-particle molecular system is extremely complex due to the correlation motion of the particles, therefore the exact solution to the Schrödinger equation is not trivial. For simplicity, the Born-Oppenheimer approximation is applied. The Born-Oppenheimer approximation is based on the knowledge that the mass of the nucleus is much higher than the electron and so moves much more slowly relative to the motion of the electrons. Therefore, the motion of the electrons and motion of nuclei are decoupled and thus, the electronic energies are computed for fixed nuclear positions. With this, the kinetic energy term of the nuclear in eq. 1.13 is cancelled out and the repulsive nuclear-nuclear term is taken as a constant for a given geometry. The wave function is invariant for a given set of fixed nuclear coordinate in the Hamiltonian and so in practice, the Schrödinger equation is solved without including the fifth term to obtain the eigenvalue before adding the nuclear-nuclear repulsion term to obtain the so-called "electronic energy". The potential energy surface is thus defined by the BO approximation-calculated-energy over all possible nuclear coordinate. But despite this approximation, the electronic correlation from many-electron system still poses a difficult challenge.

In constructing a guess wave function, ϕ a linear combination of exact hydrogenic functions term "basis set" is used to represent the wave function (eq. 1.14)

$$\phi = \sum_{i=1}^{N} a_i \varphi_i \qquad 1.14$$

where φ_i is a set of N functions referred to as the basis set and a_i is its associated coefficient. The lower and lower the calculated energy, the closer and closer the guess wave function is to the true ground-state wave function. Therefore, by varying the coefficient for a chosen basis set we can minimize the energy for all possible linear combinations of the basis. This is regarded as the variational principle. From calculus, for the energy to be at its minimum, its derivation with respect to all a_i must be zero.

Some attempts have been made to find an approximated method to treat the many-electron system. In the Hartree approach for instance, the Hamiltonian operator is separable and its many-electron wave function can be constructed as the products of one-electron wave function referred to as 'Hartree-product', $\Psi_{HP} = \psi_1\psi_2 \ldots \psi_N$ and the Schrödinger equation takes the form:

$$H\Psi_{HP} = \left(\sum_{i=1}^{N} \varepsilon_i\right)\Psi_{HP} \qquad 1.15$$

The separable Hamiltonian operator, $H = \sum_{i=1}^{N} h_i$ (where N is the total number of electron) and the one-electron Hamiltonian, h_i is:

$$h_i = -\frac{1}{2}\nabla_i^2 - \sum_{k=1}^{M}\frac{Z_k}{r_{ik}} + \sum_{j\neq i}\int\frac{\rho_j}{r_{ij}}dr \qquad 1.16$$

where M is the total number of nuclei, ρ_j is the probability density of electron j given by $\rho_j = |\psi_j|^2$. The third term of the equation is the interaction potential of j with all other electrons occupying the same orbital. The essence of the calculation is to determine ψ but this undetermined function is included in the Hamiltonian. To get by this challenge, Hartree proposed a 'self-consistent field', SCF method where in a first step, guess wave functions for all the occupied atomic orbitals are used to determine the one-electron Hamiltonian operators. Solution of each differential one-electron Schrödinger equation provides a new presumably more accurate set of wave functions which is used to form a new one-electron Hamiltonians to determine each necessary probability density. The process is repeated until the difference between a newly determined set of wave functions and the immediately preceding set falls below some set threshold and at this point the final set of wave functions is referred to as converged SCF orbitals.

A notable conclusion of the Hartree product is that the probability of finding an electron at a particular place is independent of the probability of finding another electron at that point. It assumes that specific electrons are assigned to specific orbitals. This does not satisfy the antisymmetry principle which requires that the electrons are indistinguishable and that exchange of electrons is independent of electron labels. In 1929, Slater harnesses the use of determinant in constructing wave functions for a polyelectronic system that satisfy the antisymmetric principle. The Slater determinantal wave function, Ψ_{SD} is given by:

$$\Psi_{SD} = \frac{1}{\sqrt{N!}} \begin{vmatrix} \chi 1(1) & \chi 1(1) & \cdots & \chi N(1) \\ \chi 1(2) & \chi 2(2) & \cdots & \chi N(2) \\ \vdots & \vdots & & \vdots \\ \chi 1(N) & \chi 2(N) & \cdots & \chi N(N) \end{vmatrix} \quad 1.17$$

where N is the total number of electrons; χ is the spin orbital which is the product of a spatial orbital function and an electron spin function and $\chi x(x)$ indicate a function that depends on the space and spin coordinates of the labelled electron $'x'$. The factor $1/\sqrt{N!}$ ensures normalization of the equation. In exchanging any two rows, that is for a process that corresponds to exchanging two electrons, the sign of the determinant is changed and therefore directly lead to the antisymmetry property. This agrees with a feature of relativistic quantum field theory that electron wave functions must change sign whenever the coordinates of two electrons are interchanged. A multiple of any column can be added to another column and the value of the determinant remains unchanged. This indicate that, the spin orbitals are not unique. If two rows are identical, corresponding to two electrons assigned the same spin, then the determinant vanishes. This account for the Pauli's principle which states that no two electrons can have the same set of quantum numbers. The spatial orbital can only have two electrons of opposite spins. An extension of the Hartree SCF procedure to represent wave functions as single Slater determinant was proposed by Fock. The molecular orbitals are individually determined as eigenfunctions of a set of one-electron operators and the interaction of each electron with the static field of all other electrons includes exchange effects on the Coulomb repulsion. The Hartree-Fock (HF) theory also follows a SCF process where an initial guess of the density matrix is made. The challenge of choice of basis set and the attempt to improve the accuracy of the HF method led to introduction of parameterization on one hand and the inclusion of electron correlation without approximation on the other hand.

1.3 Coupled-Cluster Theory

The coupled-cluster, (CC) theory is one of the method developed in an attempt to account well the electron correlation as an improvement from the HF method. The HF method can be thought of as ignoring the correlation motion of other electrons or intrinsically being a single-determinant process. That is, only the first term is taking into account in eq. 1.18 which is the construction of wave function as a linear combination of multiple determinants.

$$\Psi = c_0\Psi_{HF} + c_1\Psi_2 + c_2\Psi_2 + \cdots \quad 1.18$$

In CC, the exact wave function (full configuration interaction wave function) is defined as:

$$\Psi_{CC} = e^{T}\Psi_{HF} \qquad 1.19$$

T is the cluster operator given by $T = T_1 + T_2 + T_3 + \cdots + T_n$

where n is the number of electrons and all possible excitations i, have determinants generated from the operators T_i. For instance, for a double excitation, $T = T_2$, Taylor expansion of the exponential function in eq. 1.19 yields:

$$\Psi_{CCD} = \left(1 + T_2 + \frac{T_2^2}{2!} + \frac{T_2^3}{3!} + \cdots\right)\Psi_{HF} \qquad 1.20$$

Each T_2 generates double excitation, so the square of T_2 gives quadruple excitation and the cube gives hextuple. Therefore, using the exponential of T ensures size consistency. Generally, including single excitation in addition to the double increase accuracy with a practical cost. But inclusion of a connected triple excitation is very expensive with a scaling of N^6 order and so unpractical. Hence, approximated iterative or non-iterative triples corrections are more practical rather than the full triples inclusion. The most commonly used non-iterative method that estimate the effect of the connected triple excitation via perturbation theory, is the CCSD(T) method,[21] which also include a correction term from both singles and doubles. The triples correction in the (T) approach is slightly overestimated by an equal amount to the ignored quadruples and so kind of balances the estimation. Despite the high performance of this bench mark method, it is limited to chemical systems with not more than about 1000 basis. Here, we use the domain based local pair-natural orbital coupled-cluster theory with single-, double- and perturbative triple excitations, DLPNO-CCSD(T)[22–25] method by Neese *et al* which expand the implementation of this method to medium-sized chemical systems. Its approximation is based on locality of the dynamic electron correlation. It combines the concept of pair natural orbitals with local correlation treatment. The pair natural orbital is said to constitute a set of correlating orbitals that is as local or non-local as the actual bonding of electron pair.

1.4 Density Functional Theory

One of the widely used and successful approach to solving the Schrödinger equation is the density functional theory, DFT. The theory considers the density of electrons, $\rho(r)$ at a particular coordinate in space in which integration over all space give the total number of electrons, N. (eq. 2.21). The density is said to contain information that is physically observable

from the full wave function solution to the Schrödinger equation and the density in terms of individual electron wave function, ψ_i is given by eq. 1.22.

$$N = \int \rho(r)dr \qquad 1.21$$

$$\rho(r) = 2\sum_i \psi_i^*(r)\psi_i(r) \qquad 1.22$$

where ψ_i^* is a complex conjugate and the 2 indicates the 2 spins of electrons.

DFT is rooted based on two fundamental theorems set by Hohenberg and Kohn in 1964[26] and also on some set of equations by Kohn and Sham[27] the following year. The Hohenberg-Kohn first theorem is that the ground-state energy from the Schödinger's equation is a unique functional of the electron density. By finding a functional of electron density having just three spatial variables, the Schrödinger equation can be solved. But what is this functional? The property of the functional is given in the second theorem which state that "the electron density that minimizes the energy of the overall functional is the true electron density corresponding to the full solution of the Schrödinger equation"[26,27]. The energy functional in terms of single-electron wave functions, ψ_i is given by:

$$E[\{\psi_i\}] = \frac{h^2}{m}\sum_i \int \psi_i^* \nabla^2 \psi_i dr + \sum_k \int \frac{Z_k}{|r - r_k|}\rho(r)dr + \frac{e^2}{2}\iint \frac{\rho(r_1)\rho(r_2)}{|r_1 - r_2|}dr_1 dr_2 + E_{ion} + E_{XC}[\{\psi_i\}] \qquad 1.23$$

The terms on the rhs respectively refer to: the electron kinetic energies, the Coulomb interactions between electrons and nuclei, the Coulomb interaction between electron pairs, the Coulomb interaction between nuclei pairs, and the exchange-correlation functional that include all quantum mechanical effects not included in the other terms. Kohn and Sham showed that finding the right electron density can be done in a way that involves solving a set equations, of the form eq. 1.22, in which each equation only involves a single electron.

$$\left[-\frac{h^2}{2m}\nabla_i^2 - \sum_k \frac{Z_k}{|r-r_k|} + e^2 \int \frac{\rho(r')}{|r-r'|}dr' + V_{XC}(r)\right]\psi_i(r) = \varepsilon_i \psi_i(r) \qquad 1.24$$

where the second term on the lhs is the potential that defines the interaction between electrons and nuclei as in eq. 1.21. Next, is the Hartree potential describing the Coulomb repulsion between the considered electron and the total electron density. $V_{XC}(r)$ is the functional derivative of the exchange-correlation energy given by: $V_{XC}(r) = \frac{\delta E_{XC}(r)}{\delta \rho(r)}$. It defines exchange and correlation contributions to the single-electron equations.

The Kohn-Sham set of equations is solved in an iterative way where first an initial trial electron density is defined and using this trial density, the equations are solved to find the single-particle wave function, $\psi_i(r)$. The electron density is then calculated from $\psi_i(r)$ and compared with the initial electron density. If the two densities are similar meeting some set threshold, it is taken as the ground-state electron density and used to calculate the total energy. Otherwise, the trial density is updated and the cycle repeated.

The question of the true form of the exchange-functional that is the exact or accurate representation of nature remains valid till date. Some good approaches have been made over the years. One approach is based on approximation of constant electron density at all points in space, the "uniform electron gas approximation". The exchange-correlation potential at each point in space is set to be the known exchange-correlation potential from this so called uniform electron gas at the electron density observed at that point. This makes use of local density to define approximate exchange correlation functional and is termed local density approximation (LDA). Another approach is the use of information from the local electron density and the local gradient in the electron density thereby including information on the spatial variation in electron density. This class of functional is referred to as the generalized gradient approximation (GGA). A notable example is the Becke gradient-corrected exchange-energy functional which is often used in combination with the Lee-Yang-Parr correlation-energy functional, together referred to as the BLYP[28,29] functional. More classes of functional that include more physical information were developed such as the hyper-GGA or hybrid-GGA which uses mixture of the exact or Hartree-Fock exchange and GGA exchange functional. In this class is the famous B3LYP.[11,30,31] Other functionals include: the meta-GGA that uses the Laplacian of the density and/or the non-interacting positive kinetic energy density; the hybrid-meta-GGA that combines exact exchange with meta-GGA; the range-separated hybrid functional that introduces a long-range correction scheme with HF exchange energy for long-range electron-electron interaction and density functional approximation (DFA) exchange energy for the complementary short-range interaction; and in recent times, there is also the double-hybrid functional which depend on virtual orbitals. With all these functionals developed, the choice of the functional to use for a particular system of interest is an important one but by no means trivial.

Having introduce the basic theories for the methods employed in this thesis, the practical methods and computational setup details will be the focus of the following sections of this chapter.

1.5 Geometry Optimization and Energy Calculations

The energy of a molecule is a function of it atomic coordinates. Where the first derivation of energy with respect to each degree of freedom (bond lengths, bond angles and dihedrals) is zero corresponds to a stationary point on the potential energy surface (PES). These stationary points can correspond to reactant, product, intermediate or transition state of a reaction system. Optimization entails finding either of these points. In minimization, the minimum with the lowest energy referred to the global minimum on the PES is preferably desired but its location is not trivial and in most cases the interesting structure may not be that from the global minimum. Therefore, in minimization, the local minimum is often sorted. On the path between two minima is a saddle point which is a minimum in all direction except in the path of the reaction. The geometry associated with the saddle point is the transition structure with respect to that path. To categorize the stationary point as minima or saddle point a second derivative of the potential energy is taken with respect to the degrees of freedom. For a minimum, the second derivatives are all positive while for the saddle point the second derivatives are positive except in the direction along the reaction coordinate where it is a negative (that is, $\frac{\partial E}{\partial x_i} = 0; \frac{\partial^2 E}{\partial x_i^2} > 0;$ for all geometric parameters x, except along the reaction coordinate where $\frac{\partial^2 E}{\partial x_i^2} < 0$). It is therefore important to calculate the eigenvalues of the Hessian matrix. An 'n' negative eigenvalues termed imaginary frequencies corresponds to an n^{th}-order saddle point.

Vibrational frequencies are calculated from the eigenvalues to identify the optimized structures as reactant, product, intermediate or transition structure. The transition structure must have a single imaginary frequency (first-order saddle point) which is in the direction of the transformation, such as bond making, bond breaking, angle bending or dihedral rotation as the case may be. The reaction path connecting the reactant and product can be determined from intrinsic reaction coordinate (IRC) calculations which constitute moving along the steepest descent path from the transition structure to each minimum with infinitely small step.

The frequency calculation is also used to calculate the thermodynamic terms. The Gibbs free energy is defined by:

$$G = H - TS \qquad 1.25$$

where H, is the enthalpy and TS is the entropy contributions given by:

$$TS = T(S_{el} + S_{vib} + S_{rot} + S_{trans}) \qquad 1.26$$

S_{el}, S_{vib}, S_{rot}, and S_{trans} are electronic, vibrational, rotational and translational entropy, respectively, and T is the temperature. The enthalpy is given by:

$$H = U + k_B T \quad (1.27)$$

where k_B is the Boltzmann's constant and U is the internal energy at T defined by:

$$U = E_{el} + E_{ZPE} + E_{vib} + E_{rot} + E_{trans} \quad (1.28)$$

where E_{el} is the total energy from the electronic structure calculation. In reality, molecules are never actually stationary with zero kinetic energy. They vibrate continuously and possess zero-temperature vibrational energy referred to as zero-point energy, E_{ZPE} (Fig. 1.1). E_{vib} is the finite temperature correction to the zero-point energy due to population of excited vibrational states, E_{rot} is the energy due to thermal rotation and E_{trans} is the translational thermal energy. The harmonic oscillator equation and the rigid rotor approximations are used for the description of the vibrational and rotational energy terms, respectively.

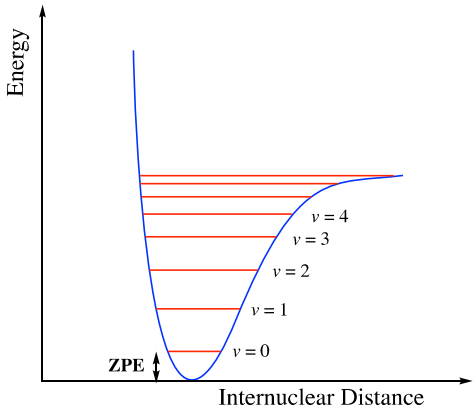

Fig. 1.1: vibrational energy levels a molecule can occupy and zero-point energy level

1.5.1 $(MeLi)_n$ Aggregates and Ketone—$(MeLi)_n$ Systems

The optimization of the systems of methyllithium aggregates and the systems of the aggregates coordinated to ketone were performed at the DFT level using the combined Becke exchange and Lee-Yang-Parr functional, BLYP with the Karlsruhe def2-TZVPP basis.[32,33] The Grimme's dispersion correction with Becke-Johnson damping, D3BJ[34,35] was added to account for dispersion effects. Solvent effect was added via implicit solvation with solvation model based on quantum mechanical charge density of the molecular system interacting with a continuum definition of the solvent, referred to as the SMD model.[36] The thermodynamic properties were calculated at 298.15 K and 1 atm. The energies were also calculated by single-point calculation of the optimized geometries at the *ab initio* domain based local pair natural orbital coupled-cluster method, DLPNO-CCSD(T) with the extended basis def2-TZVPP and implicit solvation with the SMD model for comparison and validation of the chosen functional and basis. To calculate the Gibbs free energy, the zero-point energy correction, thermal corrections, enthalpy

correction and entropy terms from the preceded optimization and frequency calculations at BLYP/def2-TZVPP were added to the single point calculation. The calculations were performed with the ORCA 5.0.2[37–39] software package.

1.5.2 Molecular Systems of Sulfinyl ketimines Bonded to Organometallic Compounds

In the study of the nucleophilic 1,2-addition of organometallic compounds to sulfinyl ketimines which will be reported in chapter three, the geometry optimizations were performed by DFT using the hybrid functional B3LYP with the def2-SVP basis [32,33] and the dispersion effects were accounted for by the D3BJ dispersion correction. In selecting this level of theory, the electronic energy barriers for the nucleophilic organometallic addition to a sulfinyl ketimine, $\mathbf{5a}_{E(S)}$ (refer to chapter 3 for the labelling) was calculated at the benchmark DLPNO-CCSD(T) level with def2-TZVP and compared with the DFT calculation at B3LYP-D3BJ with def2-SVP and 6-31+G(d,p) basis.[40] A close agreement between the coupled-cluster calculation and the DFT calculation with def2-SVP basis was observed with energy difference of 1.87 kcal.mol^{-1} (Table 1.1). This pushed for the choice of the B3LYP/def2-SVP with D3BJ correction as a good compromise between accuracy and cost. Analytical frequencies were calculated and the thermodynamic properties calculated from contribution resulting from translational, electronic, rotational and vibrational modes at 298.15 K and 1 atm. Implicit solvation was done via single-point correction on the optimized geometries by conductor-like polarizable continuum model (CPCM)[41] method with an expanded def2-TZVP basis. In the CPCM model, the molecule in placed in a cavity of approximate size of the molecule and the solvent reaction field is described the polarizable charges on the cavity surface which were in turn determined by the molecule. The calculations were done with the ORCA 4.2.1[20,21] and Gaussian16[42] programs.

Table 1.1: Comparison of levels of theory calculations

Level/Functional	Basis	Energy Barrier, ΔE* (kcal/mol)	Energy Difference (kcal/mol)
DLPNO-CCSD(T)	Def2-TZVP	18.96	0.00
B3LYP	6-31+G(d,p)	21.82	+2.87
B3LYP	Def2-SVP	17.07	-1.87

1.6 Molecular Dynamics

Molecular dynamic, MD involves the evolution of the molecular system as a function of time. The trajectory of the system is generated by solving the classical Newton's laws of motion. With a set of initial position and momenta and forces acting on each particle at any instance thereby deriving the acceleration, a true phase-space trajectory is obtained. From the initial position at time $t = 0$, the potential energy is calculated from eq. 1.11 (the force field equation). The potential energy, $\vec{\nabla}U_r$ is related to the force by:

$$\vec{F} = -\vec{\nabla}U_r \qquad 1.29$$

The resultant force $\vec{F}_i = \sum_{i \neq i} F_{j \to i}$ on each atom is calculated. From Newton's law of motion and knowing force is the derivative of the potential energy at position, r, eq. 2.28 is obtained.

$$-\frac{dU_r}{dr} = m\frac{d^2r}{dt^2} \qquad 1.30$$

By numerical integration of the equation, a new velocity and position at new time $t + \delta t$ is obtained and with the new position, a new energy and force is calculated. The cycle is repeated to get the ensemble of all the atoms with time. There are many algorithms for integrating the equations of motion such as the Verlet algorithm, Beeman's algorithm and leap-frog algorithm, to mention a few. Note that the time step choosing, δt must be sufficiently small to allow for proper integration of the equation.

In this thesis, use if made of the hybrid *ab initio* quantum mechanics/molecular mechanics method, QM/MM[43,44] for the dynamics simulation. In this method, a small part of the system, usually the reactive part or part of interest is calculated at the QM level and the larger part, usually the solvent is treated at the less expensive classical level. Two schemes are known for calculating the total energy of the system: the subtractive and the additive scheme. Here, the additive scheme is used, given by:

$$E_{QM/MM} = E_{MM} + E_{QM} + E_{QM-MM} \qquad 1.31$$

where E_{MM} and E_{QM} are the energies of the MM and QM subsystems calculated at the classical and quantum level, respectively, and E_{QM-MM} is the energy term for the interaction between the two subsystems, details of which will not be discussed here.

1.6.1 Molecular Dynamics Set-up

The MD simulation was done for the systems of methyl lithium clusters and the system of the clusters coordinated to ketone. The cluster or cluster coordinated to ketone and in some

instances with few water or hydroxyl molecules (in the "on water" case) is treated at the QM level while the solvent molecules are treated at the MM level. The MM charges were generated by restrained electrostatic potential, RESP[45] method and the parameterization was defined by the AMBER GAFF force field.[46] The molecular systems with the solvent molecules are loaded into a box with periodic boundary conditions applied. The system was first minimized in a total of 10,000 steps with constraint of the QM molecules/atoms with a global force constant of 100 $kcalmol^{-1}Å^{-2}$ to prevents the molecules from moving away from the center of the solvent. A time step of 0.5 fs was used. The nonbonding interactions were calculated with the smooth particle mesh Ewald[47,48] method with a cutoff of 10Å. After the minimization, the system was heated to reach an equilibrium temperature of 300 K over 10ps using a Langevin thermostat[49] and a collision frequency of $5ps^{-1}$ in the NVT ensemble. Next, the equilibration of the system was done in the NPT ensemble to ensure attainment of the correct density. Like the minimization, a constraint of 70 and 50 $kcalmol^{-1}Å^{-2}$ global force constant was applied to the assigned QM molecules. Average densities of 0.716±0.001 and 0.881±0.001g/cm^3 at 300 K for the systems in diethyl ether and THF systems, respectively were obtained. These were in close agreement with experimental densities of 0.715 at 293.15 K[50] and 0.882 g/cm^3 at 298.15 K[51] for diethyl ether and THF, respectively. The minimization, heating and equilibration were carried out with the AMBER 18 software program.[46]

After equilibration by the force field method, the systems were allowed to equilibrate for 3000 steps in the NVT ensemble by the QM/MM method before the production run at the NVT ensemble. The QM part were calculated at the DFT level with BLYP functional and DZVP-MOLOPT[52] basis and dispersion correction were added by the D3 Grimme[53] approximation. Integration of the core electrons were done using the Goedecker-Teter-Hutter, GTH[54–56] type pseudopotential. An auxiliary plane-wave cutoff of 400Ry and density cutoff of 10^{-10} was set. Temperature of the system was maintained around 300K by the canonical sampling/velocity rescaling, CSVR thermostat[57]. The time step for the simulations was set at 0.5fs. All QM/MM molecular dynamics simulations were performed with the CP2K 6.1 software.[58]

1.7 Metadynamics

Exploration of rare event such as protein folding, conformational changes in solvents, and chemical reactions entails crossing large energy barriers on the free energy surface which is unattainable in practical time by the ordinary molecular dynamics simulation. One of the methods used to enhance the exploration of the free energy surface is the metadynamics[59–61]

enhance sampling method. Metadynamics involves addition of history-dependent bias potential constructed as a sum of Gaussian functions in the region of some selected slow degrees of freedom (termed collective variables, CVs) which constitute major molecular changes. The Gaussian potential is added every τ_G defined MD steps. The metadynamics potential acting on the molecular system at time t is given by:

$$V_G(S(x),t) = w\sum exp\left(-\frac{\left(S(x)-s(t')\right)^2}{2\delta s^2}\right) \quad 1.32$$

where $t' = \tau_G, 2\tau_G \cdots and\ t' < t$; w is the Gaussian height; δs is the Gaussian width;

$S(x)$ and $s(t')$ are the values of the CV at t and t'

The time dependent potential defined by the sum of Gaussians deposited over time provides an unbiased estimate of the free energy, F in the explored region (eq. 2.31)

$$\lim_{t\to\infty} V_G(S(x),t) = -F \quad 1.33$$

It is often a challenge to know when to terminate a metadynamics run. Continuing a run may lead to the irreversible access of irrelevant configuration. The free energy does not converge but fluctuates around the correct value with an error proportional to the square root of the rate of deposition of the bias potential. To address this challenge, the well-tempered[62] metadynamics is used. In this improved method, the Gaussian heights are rescaled at each step and the bias is thus, given by:

$$V_{WT}(S(x),t) = \omega e^{-[V(s,t)/\Delta T]}\tau_G\sum exp\left(-\frac{\left(S(x)-s(t')\right)^2}{2\delta s^2}\right) \quad 1.34$$

where ω is the initial bias deposition rate, τ_G is the interval at which the Gaussians are deposited and ΔT is the temperature. However, this bias does not fully compensate for the free energy. The free energy surface is determined by:

$$F(s,t) = -\frac{T+\Delta T}{\Delta T}V(s,t) \quad 1.35$$

For $\Delta T = 0$, the bias is 0 and as $\Delta T \longrightarrow \infty$, the deposition rate is constant and the standard metadynamics is followed. Therefore, by tuning the bias factor ΔT, the barrier crossing can be facilitated and more regions in the space of the CVs can be sampled.

The choice of the CVs is very crucial to the performance and accuracy of metadynamics. In this thesis, two CVs are chosen for each study. For the study of dissociation of MeLi tetramers to dimers in solvents (Chapter 2), the distance between centers of mass (Fig 1.2a) and the coordination number of the Li ions to the solvent molecules were chosen as the CV1 and CV2, respectively. In the study of the nucleophilic addition of methyl lithium to ketones (chapters 4

and 5), the bond distance between the methyl carbon of MeLi and carbonyl carbon of the ketone was chosen as CV1 for the reactions involving the dimers while for the tetramers, the coordination number of the carbonyl carbon with the carbons of the methyl lithium groups was taken as CV1. The CV2 for both dimer and tetramer systems was chosen as the bond angle between the carbonyl carbon, carbonyl oxygen and Li ion on which the ketone in bonded (Fig 1.2b and 1.2c).

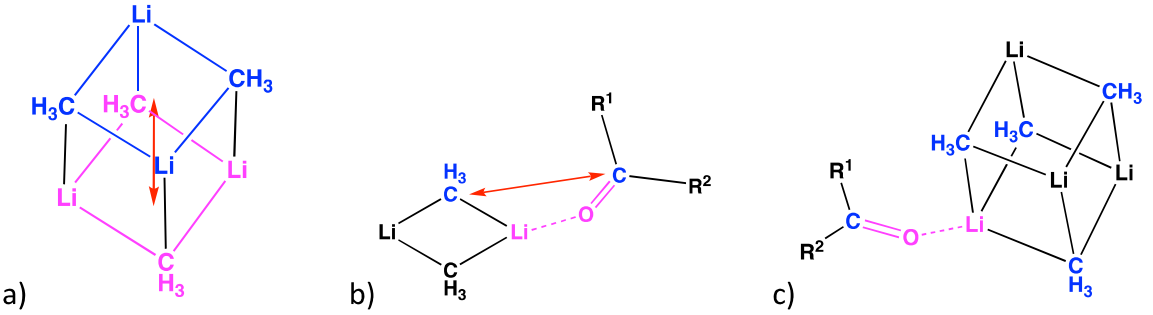

Fig. 1.2: Structures showing CVs for the metadynamics simulations a) the CV1 is the distance between center of mass of atoms in blue and atoms in pink; CV2 is the CN of Li ions with solvent molecules b) CV1 is the C—C bond distance (blue) and CV2 is the C—O—Li bond angle (pink) c) CV1 is the CN of carbonyl carbon with the methyl groups (blue) and CV2 is the C—O—Li bond angle (pink).

The coordination number, CN is defined as:

$$CN_{ij} = \sum_{i,j} \frac{1 - (r_{ij}/r_0)^p}{1 - (r_{ij}/r_0)^q} \qquad 1.36$$

where r_{ij} is the distance between the two sets of atoms and r_0 is the reference distance; p and q are constants, used for tuning the smoothness of the function.

The parameters set for the well-tempered metadynamics: $w, \delta s, \tau_G$ *and* biasfactor are given in Table 1.2. The temperature, T is set at 300 K for all systems. The values of p, q *and* r_0 for the MeLi tetramer dissociation calculations are 4, 8 and 2.2 Å, respectively, while for the tetramers of the nucleophilic addition reaction studies are 3, 6 and 2.1 Å, respectively. The metadynamics parameters were set with the open-source community-developed PLUMED 2.7.0 plugin[63–65] to the CP2K 6.1 software package.

Table 1.2: well-tempered metadynamics parameters set-up

System	w	δs		τ_G	Biasfactor
	(kcal/mol)	CV1	CV2		
$(MeLi)_4$ in ETH	0.5	0.70 Å	0.15	50	30
$(MeLi)_4$ in THF	0.5	0.70 Å	0.15	50	30
$(MeLi)_2$—Acetone in ETH	0.5	0.55 Å	18.1°	20	45
$(MeLi)_2$—Acetone in THF	0.5	0.70 Å	18.5°	20	60
$(MeLi)_4$—Acetone in ETH	0.6	0.08	19.0°	20	80
$(MeLi)_4$—Acetone in THF	0.6	0.08	18.8°	20	95
$(MeLi)_2$—Chloroketone in ETH	0.5	0.44Å	19.0°	20	90
$MeLi)_2$—Chloroketone in THF	0.5	0.38Å	19.5°	20	85
$MeLi)_4$—Chloroketone in ETH	0.6	0.09	19.0°	20	75
$MeLi)_4$—Chloroketone in THF	0.6	0.09	20.0°	20	100

1.8 Intermolecular Interaction by Symmetry-Adapted Perturbation Theory

The symmetry-adapted perturbation theory (SAPT) method is a method to compute directly molecular interaction energy. It combines perturbation expansion with imposition of permutational symmetry of the wave function. In this method, the basis set superposition error, BSSE is eliminated. [66] The fundamental interactions (electrostatic, induction, dispersion and exchange) are described in this method. The sum of contributions to the interaction energy is given by eq. 2.37. [67]

$$E_{int}^{SAPT2} = E_{elst}^{(10)} + E_{exch}^{(10)} + E_{ind,resp}^{(20)} + E_{disp}^{(20)} + E_{exch-ind,resp}^{(20)} + E_{exch-disp}^{(20)} + \delta_{HF}^{(2)} + E_{elst,resp}^{(12)} + E_{exch}^{(11)} + E_{exch}^{(12)} + E_{ind}^{(22)} + E_{exch-ind}^{(22)} \quad 1.37$$

Where the first number in the parenthesis indicate the perturbation order in computing the difference between the full dimer Hamiltonian and the sum of two monomer Hamiltonian while the second number is the perturbation order for the fluctuation potential accounting for electron correlation on monomers. $E_{elst}^{(10)}$ and $E_{elst,resp}^{(12)}$ are electrostatic energy contributions; $E_{exch}^{(10)}$,

$E_{exch}^{(11)}$ and $E_{exch}^{(12)}$ are exchange energy contributions; $E_{ind,resp}^{(20)}$ and $E_{ind}^{(22)}$ are the induction energy contributions; $E_{disp}^{(20)}$ is the dispersion energy; $\delta_{HF}^{(2)}$ is the Hartree-Fock interaction energy; $E_{exch-ind,resp}^{(20)}$ and $E_{exch-ind}^{(22)}$ are additional exchange repulsions due to coupling of electron exchange and induction interaction and $E_{exch-disp}^{(22)}$ is repulsion due to coupling of electron exchange with dispersion interaction. The term *resp* included in the subscript denotes that orbital relaxation effect is included. Detailed description of SAPT(2) and the terms can be found in Ref. 66 and 67. Here, we calculate the interaction energies by SAPT2[67] with basis aug-cc-pvdz[68] using Psi4[69] software package.

CHAPTER TWO

2 Methyllithium Aggregates and Solvation

The chemistry of organolithium, discovered in the late forties and developed in the following decades, now occupies a prominent place in the synthetic chemist's toolbox[70] and are probably the most widely used building blocks. However, this area of organometallic chemistry remains a non-trivial field since, beyond the factors usually influencing any chemical reaction, organolithium compounds, have a fascinating ability to make multiple non-covalent interactions in solution that allow them to self-assemble and/or to adopt preferential conformations with the reactive organic partners. The versatile and interesting applications of this organometallic compounds of alkyllithium in organic transformation drew interest and the need for the study of their structure and especially in solvents so as to be able to study the mechanism of reactions involving this class of widely used reagent and as well help in planning synthetic strategies. In most cases, when writing the mechanisms involved or when mentioning the compound, organolithium reagents are usually pictured schematically as mononuclear species (i.e. a single Li^+ cation and a single "R" group: methyllithium is "MeLi" for example), but the structure of these compounds is expected to involve aggregates and is complex and flexible. It has been established over the years from literature that this alkyllithium reagents are capable of existing in different aggregation states. Many researchers have worked in the determination of their structures in different solvent through different means. Theodore L. Brown for instance, in over five decades past put together in a review some determined structures of organolithium compounds as of that time. The structures included dimeric, tetrameric and hexameric species of organolithium compounds.[71] Günther and co-workers use two-dimensional NMR spectroscopy to determine the structures of organolithium in THF solvent. They used a combination of ^{1}H-, ^{13}C-, ^{6}Li-, and ^{7}Li-NMR to confirm the dimeric, tetrameric and hexameric aggregates of alkyllithium.[72] Through the use of ^{1}H-, ^{13}C-, and ^{7}Li-NMR also, Baker *et al* were able to determine the structure of methyllithium (MeLi) in tetrahydrofuran, diethyl ether and trimethylamine solutions. From the results of the ^{13}C—^{7}Li spin-spin coupling, they were able infer that the tetramer is the preferred structure of the MeLi in these solvents. They reported that each lithium is bound to interact with three adjacent methyl groups due to the sufficiently slow inter- and intra-aggregate (fluxional) exchange in the MeLi

solution. The resulting structure is a tetrahedron formed by the four lithium atoms and the methyl groups are positioned over each facial plane of the tetrahedron. Single-crystal X-ray structure of [$(MeLi)_4$.4THF] by Ogle and co-workers revealed similar geometry.[73] Baker and co-workers also reported in the study that the Li—C carbon bond in the aggregate is predominantly covalent and the carbon is sp3 hybridized.[74] In like vein of the observation of slow exchange that was reported by Baker *et al,* Thomas and co-workers also reported slow fluxional exchange of *tert*-butyllithium (*t*-BuLi) tetramer in cyclopentane from J-coupling values from ^{13}C and ^{6}Li NMR studies.[75]

Numerous theoretical studies have also been devoted to the study of organolithium compounds. From the 80s, the pioneering work of Schleyer[76] has studied, in particular, the different conformers of MeLi dimers, trimers and tetramers at the HF and MP2 level, then in the 90s and beginning of the 2000, DFT calculations were also performed.[77] For the MeLi clusters, the hexamer (D_{3d}) and octamer structures were found to be more stable than the tetrahedral tetramer (T_d). These static calculations do not include explicitly the solvent. Dynamics studies of MeLi have been performed by Gérard *et al* but still without explicit solvent.[78]

No doubt the nature of aggregation of alkyllithium depend on the solvent they are in and on the size of the alkyllithium. For instance, stable tetra-coordinated *t*-BuLi was found in equilibrium with the uncoordinated *t*-BuLi in diethyl ether from NMR study[79] while on the other hand X-ray of the crystal of MeLi crystalized from a cumene/THF solution revealed a tetrameric structure with one-tenth being a mixed crystal of [$Me_3Li_4Cl(THF)_4$].[73] In general, ethereal solvents such as diethyl ether and THF are considered to be good coordinating solvent to lithium. In a bid to study the behaviour of alkyllithium in solution, Pratt, Truhlar and Cramer with their co-workers have by DFT calculation using explicit solvent molecules bonded to the alkyllithium in combination with continuum solvent model (implicit-explicit model) studied the monomeric, dimeric and tetrameric methyllithium, ethyllithium, *s*-butyllithium and *t*-butyllithium in THF. The monomers could accommodate three THF while the dimers could have either one or two THF solvent molecules coordinated to each lithium. In the tetramers, the lithium atoms were each mono-solvated. However, stable tetramers were only optimized for methyllithium and ethyllithium. Steric effect of the alkyl groups pose a major effect on the solvation state of the alkyllithiums.[80]

Here in this chapter, we would like to get a picture on the different MeLi aggregation. Indeed, it is important to understand their complexity. First, we will study them in interaction with the first shell of solvent. Like for most of this work, we will compare the two solvents diethyl ether and THF. Using DFT calculations, we will characterize the geometrical parameters of the

aggregates and study the energy difference between the different clusters. As the number of solvent molecules around the aggregates change, it is important to get a thermodynamic model taking into account this feature. We will also study the ketone—MeLi interaction. The ketone we consider here is the 4-chloro-butyrophenone (for which we will mostly refer to simply as γ-chloroketone). The cost of the dissociation of the tetramer into dimers will be studied as well. A mixed implicit-explicit solvation model and an explicit solvation by QM/MM molecular dynamics will be applied in these calculations. Knowledge from this study will be used for the further study of the reaction mechanism of the nucleophilic addition of MeLi on ketone in conventional and unconventional solvent in chapter four.

2.1 Geometrical Parameters of the MeLi Aggregates

In 2013, a review by Hans Reich on the role of organolithium aggregates in organic transformation mechanisms involving organolithium put together the various characterized structural forms of organolithium in solid state and solution. The alkyl—lithium unit often pair to cancel out the dipoles or by stacking, the ring structures cancel out the dimer quadrupoles. [81] Here, we optimized different aggregate forms of methyllithium following the common established structures reported in the literature (Fig 2.1). The aggregates range from dimers to hexamer which have either ring, ladder or polyhedral structures and are named accordingly. The ring structures are found for the dimers, trimers and tetramers, that is, for n=2,3,4 in $(MeLi)_n$. The ladder structures exist also for n=2,3 and 4 while the polyhedral structures are only found in the tetramer and hexamer structures (n=4,6). Other forms of aggregates are those in which the MeLi pair disjoin to give an opened structure. This is notable in the dimer, trimer ladder and tetramer ladder aggregates. In the polyhedral tetramer, the four lithium atoms form a tetrahedral geometry with a T_d symmetry. The four methyl groups each bond to the triangular faces of the tetrahedron with the carbon atom positioned at the centre of the face. This is consistent with X-ray crystal structure observed.[73] The hexamer aggregate structure is a hexamer prism with the lithium ions forming a slightly distorted octahedral structure with a D_{3d} symmetry. As with the tetrahedral structure, the methyl groups in the octahedral hexamer are centred at the triangular faces except at the two distorted faces where there are no methyl groups coordinated.

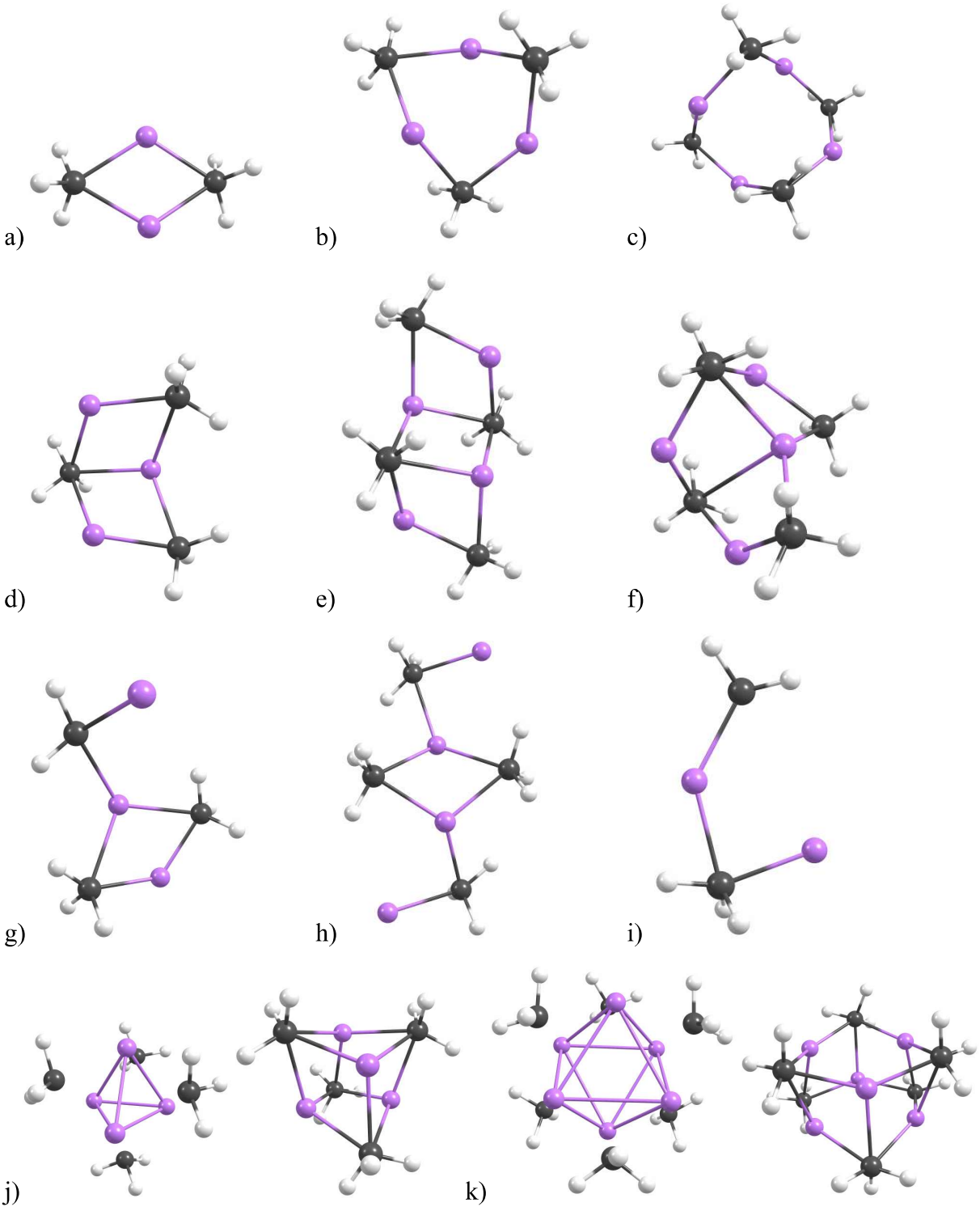

Fig. 2.1: Different optimized geometries of the studied MeLi aggregates (*a—b: ring structures; d—f: ladder structures; g—i: opened structures; j & k: polyhedral structures*)

Solvation of the lithium ions is geared towards attainment of the common coordination number of four on the lithium or in some cases three especially in the solvation with diethyl ether due to the steric repulsion pose by its chain-like structure compared to the ring structured THF. In

the dimer solvated with diethyl ether for instance, the dimer with four solvent molecules is less stable, with a +12.7 kcal mol^{-1} free energy difference than the corresponding dimer with two solvent molecules (from a DFT calculation at BLYP/def2-TZVPP).

In the ring structures, the Li^+ ions are mono-solvated with diethyl ether while solvation with up to two THF molecules is attainable on the other hand. In the ladder structures, the inner Li^+ ions of the ladder are mono-solvated to reach tetra-coordination in both diethyl ether and THF, while the Li^+ ions at the ends of the ladder are mono-solvated in diethyl ether and di-solvated with THF due to the effect of steric repulsion. The open-ladder structures are similarly solvated except on the dangling Li^+ ion, where it is di-solvated or tri-solvated with diethyl ether and always tri-solvated with THF. The inner Li^+ ion in the angled-ladder is not solvated haven already attained tetra-coordination. The outer Li^+ ions of the angled-ladder structures are mono-solvated with diethyl ether and di-solvated with THF. In the polyhedral structures, the Li^+ ions are each mono-solvated in both diethyl ether and THF solvents. The aggregates are categorized based on the nature of solvent coordination as either symmetric, having the solvated lithium atoms equally solvated (ring dimer, ring trimer, ring tetramer, angled-ladder tetramer, tetrahedral tetramer and octahedral hexamer), or termed as asymmetric, with the solvated lithium atoms having unequal solvent coordination (opened dimer, opened-ladder trimer and opened-ladder tetramer; Fig 2.2). The ladder trimer and ladder tetramer are symmetrically solvated with diethyl ether but asymmetrically solvated with THF.

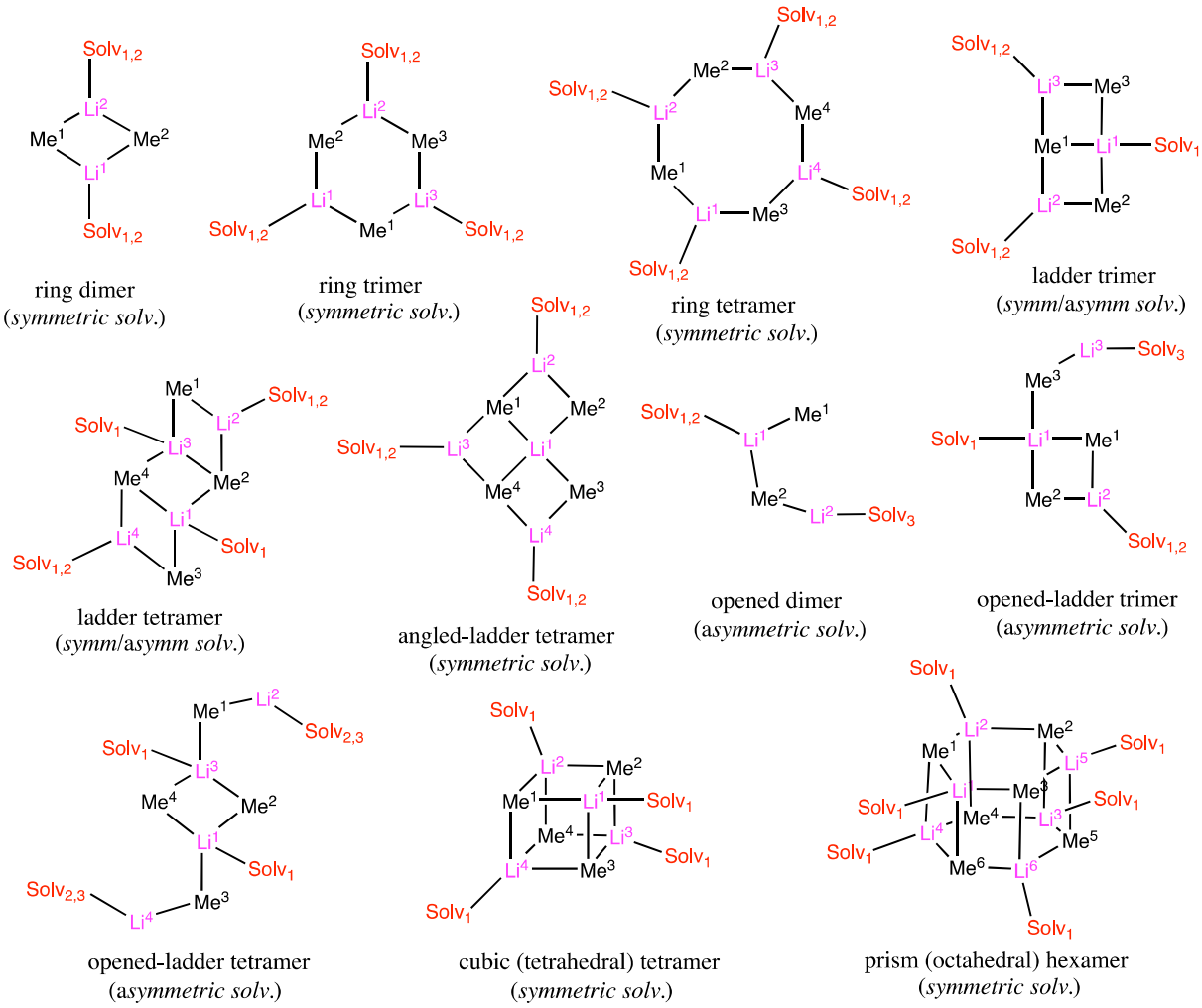

Fig. 2.2: MeLi aggregates with their nature of solvation (*the subscript in Solv indicate the number of solvent molecules; the higher number in a two-digits subscript is associated to THF solvation; the aggregates are termed either as symmetrically solvated or as asymmetrically solvated*)

The geometric parameters, Li—Li and C—C nearest neighbour distances, defining the structures of the MeLi clusters were measured and compared between the different solvents coordination. These parameters differ for same geometries depending on the coordinated solvent. For instance, the Li—Li and C—C distance in the dimer are 2.26 and 3.63 Å, respectively in Et_2O and 2.31 and 3.73 Å in THF. The more the number of coordinated solvent, the longer the Li—Li and C—C distances. The widening of these distances may be attributed to the crowdedness associated with higher solvent coordination. The average Li—C bond distances of the dimer bonded to Et_2O is 2.15 ± 0.01 Å while in THF it has a value of 2.20 ± 0.01 Å. This trend of increased Li—Li and C—C distances with increased number of coordinated solvent is more or less consistent in the MeLi aggregates (Table 2.1; higher values with THF solvated aggregates) especially among the clusters with symmetric solvation (ring

dimer, ring trimer, ring tetramer and angled-ladder tetramer). The inconsistent longer C—C value in Et_2O solvated angled-ladder tetramer (Table 2.1, row 11) comes from the effect of steric repulsion posed by the THF solvents on the outer Li^+ ions (Li^2, Li^3 and Li^4 Fig 2.2). The crowdedness from the solvent causes a distortion from the regular angled-ladder-tetramer structure depicted in Fig 2.2. The repulsion from the THF solvents pushes the methyl groups away elongating the Li—C distance and bringing the methyl groups a bit closer than in the Et_2O solvated cluster. The effect of steric from the coordinating THF solvents on the structure can be seen from the higher Li—Li distance (+0.58 Å in comparison to the Et_2O solvated cluster).

In the clusters asymmetrically coordinated to solvents (opened dimer, opened-ladder trimer and opened-ladder tetramer; Fig 2.2), the relation between the geometric parameters and the solvation is also seen. In the ladder trimer, a longer Li—Li and C—C distances in the Et_2O solvated structure (Table 2.1 rows 19-22) in comparison to its THF solvated counterpart, though having higher number of coordinated solvent, was observed. This is quite unusual as one would expect the higher solvent coordination with the THF would distort the ladder structure to a greater extent than the Et_2O would. Here, one may only suggest that the attainment of the preferred coordination number of four on the lithium atoms in the THF coordinated structure may play some role but this is not very clear.

In the opened-ladder trimer, ladder tetramer and opened-ladder tetramer, the Li^1—Li^3 distance in the Et_2O solvated structures is longer than in the THF solvated structures (Table 2.1 rows 24, 27 and 33). This is from the steric repulsion posed by the coordinated Et_2O solvents on the inner Li^+ ions (Li^1 and Li^3, Fig 2.2) which is otherwise less with the THF solvents. In these ladder and opened-ladder structures where the lithium ions are not uniformly solvated, elongation of the Li—C bonds in THF solvated complexes where there are higher number of coordinated solvents relative to the Li—C bonds in Et_2O solvated complexes, is observed at the Li^+ ions. For example, in open-ladder trimer, the Li^2—C^1 and Li^2—C^2 bond distances (Fig 2.2) both have values of 2.11 Å in Et_2O while in THF on the other hand they have values of 2.19 Å. Similarly, the Li—C bonds in ladder trimer, ladder tetramer and angled-ladder tetramer have average values of 2.16 ± 0.06, 2.14 ± 0.02 and 2.13 ± 0.02 Å, respectively in Et_2O compared to average values of 2.19 ± 0.05, 2.19 ± 0.02 and 2.27 ± 0.10 Å, respectively, in the THF coordinated aggregates.

Table 2.1: Measured geometric parameters of the MeLi aggregates in Å

System	Bond	Ether		THF	
		Mean dist.	Std. deviation	Mean dist.	Std. deviation
Symmetric solvation					
Dimer	Li—Li	2.26	—	2.31	—
	C—C	3.63	—	3.73	—
Ring trimer	Li—Li	2.63	0.0871	2.73	0.0876
	C—C	3.86	0.1132	3.97	0.0739
Ring tetramer	Li—Li	2.74	0.1821	3.02	0.1157
	C—C	3.83	0.2488	4.09	0.0574
Angled-lad. tetramer	Li—Li	2.50	0.1423	3.08	0.8666
	C—C	3.80	0.1389	3.68	0.0567
tetrahedral tetramer	Li—Li	2.51	0.0309	2.47	0.0108
	C—C	3.61	0.0411	3.64	0.0250
Octahedral hexamer	Li—Li	2.55	0.1150	2.41	0.0241
	C—C	3.52	0.0128	3.74	0.0503
Asymmetric solvation					
Open dimer	Li—Li	2.96	—	2.97	—
	C—C	4.03	—	4.18	—
Ladder trimer	Li^1—Li^2	2.65	—	2.42	—
	Li^1—Li^3	2.56	—	2.43	—
	C^1—C^2	3.94	—	3.77	—
	C^1—C^3	3.93	—	3.67	—
Opened-lad. trimer	Li^1—Li^2	2.35	—	2.41	—
	Li^1—Li^3	3.39	—	3.01	—
	C^1—C^2	3.67	—	3.74	—
	C^1—C^3	4.04	—	4.11	—
Ladder tetramer	Li^1—Li^3	2.68	—	2.49	—
	Li^1—Li^4	2.39	—	2.40	—
	Li^2—Li^3	2.39	—	2.45	—
	C^1—C^2	3.62	—	3.72	—
	C^2—C^4	3.68	—	3.75	—
	C^3—C^4	3.62	—	3.68	—
Opened-lad. tetramer	Li^1—Li^3	2.59	—	2.46	—
	Li^1—Li^4	2.53	—	2.96	—
	Li^2—Li^3	2.46	—	3.00	—
	C^1—C^2	3.74	—	4.09	—
	C^2—C^4	3.70	—	3.69	—
	C^3—C^4	3.68	—	4.09	—

In the polyhedral aggregates with symmetric solvation in both Et_2O and THF, the Li—Li distances are shorter in THF than in Et_2O, while conversely, the C—C distances are shorter in Et_2O than in THF (Table 2.1, rows 7 to 10). A closer look at the Li—C bond distances in tetrahedral tetramer showed an average value of 2.24 ± 0.01 Å in Et_2O and 2.24 ± 0.02 Å in THF. No major difference in the bonds were observed except a slight uneven distribution of the Li—C bond distances was noted with the THF coordinated cubic tetramer as evident in its higher standard deviation (0.02 compared to 0.01).

2.2 Energies of the Methyllithium Aggregates

The standard electronic energy, E and the standard free energy, G of the optimized geometries of the aggregates were calculated. The equilibrium energy between the aggregates were calculated and the tetrahedral tetramer was found to be the most stable of the calculated aggregates. The relationship between the tetrahedral tetramer, noted to be the most stable cluster, with the other clusters is expressed as:

$$a[(\mathrm{MeLi})_4.4(\mathrm{solv}) + \mathrm{x(solv)}] \rightleftharpoons \mathrm{b}[(\mathrm{MeLi})_n\mathrm{y(solv)}] \quad (2.1)$$

where a, b, x and y are constants showing the number of moles of cluster or solvent and n = 1, 2, 3, 4 or 6 corresponding to the kind of aggregate.

The standard electronic energy difference, ΔE and the standard free energy difference, ΔG of the clusters with respect to the most stable tetrahedral tetramer structures are shown in Table 2.2. In the same vein, the electronic energies for the clusters were calculated by the coupled-cluster method, DLPNO-CCSD(T) with the def2-DZVPP basis. To calculated the free energy, G, the total corrections (enthalpy correction, entropy correction, total thermal correction and zero-point corrections) from the DFT calculation is added to the electronic energy from the coupled-cluster calculation (eq. 2.2) and the result given in Table 2.3.

$$G_{CCSD(T)} = E_{CCSD(T)} + Corr_{BLYP} \quad (2.2)$$

Since these energies were calculated in gas-phase at standard state corresponding to 1 atm, it is pertinent to convert to standard state for solution which we take as 1M. The solution standard state free energy is thus given by:

$$\Delta G^0_{sol} = \Delta G^0 + \Delta G^{0*} \quad (2.3)$$

where ΔG^0 is the free energy at 1 atm standard state and ΔG^{0*} is the standard state correction defined by:

$$\Delta G^{0*} = \Delta n R_1 T ln(R_2 T) \quad (2.4)$$

where $R_1 = 8.3144$ J K^{-1} mol^{-1}, $R_2 = 0.08206$ L atm K^{-1} mol^{-1}, T is the temperature (298.15 K) and Δn is the change in the number of moles (only the reactions where the number of moles change are affected). [80,82,83] Therefore, a correction of 1.89 kcal mol^{-1} is added to the calculated free energies and the resulting corrected solution standard state free energy is given in Table 2.4.

Again, since the solvents (diethyl ether or THF) are treated both as solvating species and as solvated species, an additional correction term is required on the second term in the square bracket on the LHS of eq. 2.1. The correction added is given by eq. 2.5 since we are adopting standard state of 1M for all species. [80,82,83]

$$\Delta G^{o*}_{solv} = -nRTln([solv]) \quad (2.5)$$

where n is the number of moles of solvent (that is, $a.x$ from eq. 2.1) and $[solv]$ is the molarity of the solvents calculated from their density at 298.15 K. Therefore, the correction added for diethyl ether and THF with calculated molarity of 9.52 and 12.33 M at 298K is $1.49n$ and $1.34n$ kcal mol^{-1}, respectively.

Table 2.2: Free energy differences of aggregates in kcal/mol calculated at BLYP/def2-TZVPP

Aggregate	Diethyl ether			THF		
	Solv	ΔE_{BLYP}	ΔG_{BLYP}	Solv	ΔE_{BLYP}	ΔG_{BLYP}
Monomer	3 ETH	14.40	70.27	3 THF	-5.67	49.54
Dimer	2 ETH	30.46	8.16	4 THF	-7.41	25.88
Ring trimer	3 ETH	15.17	8.31	6 THF	-10.53	35.96
Ring tetramer	4 ETH	13.73	11.40	8 THF	-6.98	42.51
Ladder trimer	3 ETH	13.75	6.97	5 THF	-7.25	18.72
Ladder tetramer	4 ETH	8.19	5.59	6 THF	-5.98	17.57
Angled-ladder tetramer	3 ETH	17.58	2.06	6 THF	6.79	30.99
Opened dimer	4 ETH	18.38	52.97	5 THF	-5.91	51.40
Opened-ladder trimer	5 ETH	13.87	41.15	6 THF	-9.96	33.01
Opened ladder tetramer	6 ETH	3.39	27.90	8 THF	-10.43	38.78
Tetrahedral tetramer	4 ETH	0.00	0.00	4 THF	0.00	0.00
Octahedral hexamer	6 ETH	4.37	9.58	6 THF	1.76	8.17

Table 2.3: Standard free energy differences in kcal/mol calculated at DLPNO-CCSD(T)

Aggregate	Diethyl ether		THF	
	Solv	$\Delta G_{CCSD(T)}$	Solv	$\Delta G_{CCSD(T)}$
Monomer	3 ETH	71.11	3 THF	48.21
Dimer	2 ETH	6.54	4 THF	25.03
Ring trimer	3 ETH	8.75	6 THF	35.21
Ring tetramer	4 ETH	12.01	8 THF	42.41
Ladder trimer	3 ETH	7.16	5 THF	19.39
Ladder tetramer	4 ETH	6.48	6 THF	19.13
Angled-ladder tetramer	3 ETH	2.38	6 THF	32.71
Opened dimer	4 ETH	54.87	5 THF	50.05
Opened-ladder trimer	5 ETH	41.90	6 THF	33.04
Opened ladder tetramer	6 ETH	28.75	8 THF	39.27
Tetrahedral tetramer	4 ETH	0.00	4 THF	0.00
Octahedral hexamer	6 ETH	10.72	6 THF	10.07

Table 2.4: Standard state corrected energy differences in kcal/mol

Aggregate	Diethyl ether			THF		
	Solv	ΔG^*_{BLYP}	$\Delta G^*_{CCSD(T)}$	Solv	ΔG^*_{BLYP}	$\Delta G^*_{CCSD(T)}$
Monomer	3 ETH	50.11	50.94	3 THF	28.19	26.84
Dimer	2 ETH	10.05	8.43	4 THF	14.26	13.40
Ring trimer	3 ETH	8.94	9.38	6 THF	23.08	22.32
Ring tetramer	4 ETH	11.40	12.01	8 THF	29.00	28.89
Ladder trimer	3 ETH	7.60	7.79	5 THF	10.33	11.00
Ladder tetramer	4 ETH	5.59	6.48	4 THF	10.81	12.37
Angled-ladder tetramer	3 ETH	5.29	5.61	6 THF	24.23	25.95
Opened dimer	4 ETH	41.94	43.84	4 THF	33.01	31.66
Opened-ladder trimer	5 ETH	33.17	33.92	6 THF	20.12	20.15
Opened ladder tetramer	6 ETH	21.44	22.29	8THF	25.26	25.75
Tetrahedral tetramer	4 ETH	0.00	0.00	4 THF	0.00	0.00
Octahedral hexamer	6 ETH	8.95	10.09	6 THF	7.54	9.44

It was seen from the results that the tetrahedral tetramer structure is the most stable geometry of the MeLi aggregates. The higher stability of the tetrahedral tetramer structures is consistent with experimental works reported where it is found to be the dominating structure and in some case the only isolated aggregate. [73,74] For instance, the tetrahedral structure of the MeLi did not disrupt even in the presence of a strong chelating agent, tetramethylethylenediamine, TMEDA (in 1:1 ratio of MeLi to TMEDA) in THF solution.[74] Work by Verstraete and co-workers drew similar conclusion where in general, the polyhedral structures were found to be more stable than their corresponding ring structures. They reported that the hexamer structure is the most stable. However, their calculations were done without the inclusion of coordinated solvent molecules. [77]

From Table 2.2, the effect of entropy contribution can be seen from the difference in the ΔE and the ΔG values. Taking for example the closed-dimer structure for which an equilibrium relationship with the more stable tetrahedral tetramer can be written as follows in diethyl ether (ETH) and tetrahydrofuran (THF) solvents:

$$[(\mathrm{MeLi})_4 4\mathrm{ETH}] \rightleftharpoons 2[(\mathrm{MeLi})_2 2\mathrm{ETH}] \qquad 2.6$$

$$[(\mathrm{MeLi})_4 4\mathrm{THF}] + 4\mathrm{THF} \rightleftharpoons 2[(\mathrm{MeLi})_2 4\mathrm{THF}] \qquad 2.7$$

Here, in ETH, the entropic contribution is favoured in the dimer direction where there are higher number of molecules on the RHS of eq. 2.6 than on the LHS, hence, a more disordered state on the dimer side compared to the tetramer. This higher entropic contribution favouring the dimer results in the drop of energy difference from ΔE of 30.46 kcal mol^{-1} to ΔG of 8.16 kcal mol^{-1} (Table 2.2 row 4 columns 3 and 4). On the other hand, in THF, the entropic contribution is higher on the tetramer side of the equilibrium (eq. 2.7) thereby moving the energy difference from ΔE of -7.41 kcal mol^{-1} to ΔG of 25.88 kcal mol^{-1} (Table 2.2 row 4 columns 6 and 7).

It is evident from the results in Table 2.3 that the DFT calculation at BLYP functional and def2-TZVPP basis with D3BJ dispersion correction agrees well with the coupled-cluster, DLPNO-CCSD(T) calculation as found in chapter one when optimizing the level of theory. The calculated energy values from the DFT calculation differ at the most by about 2 kcal mol^{-1} from the coupled-cluster calculated energies. The comparison can also be clearly seen in Table 2.4.

The introduction of standard state correction for solution and the correction from the treatment of the diethyl ether and THF as both solvating and solvated species indeed showed some effect in the calculated energy values (Table 2.4). Again, considering the dimer and tetramer equilibrium in the two solvents, ETH and THF (eq. 2.6 and 2.7), a significant change in the energy values can be seen. The effect of the corrections is more pronounced in the THF as both

the standard state correction for solution and the solvent-in-solvent correction are added. A decrease of about 12 kcal mol^{-1} in the ΔG value was observed (From 25.88 kcal mol^{-1}, Table 2.3 row 4 column 7, to 14.26 kcal mol^{-1}, Table 2.4 row 4 column 6). In ETH, on the other hand, there is no solvent-in-solvent correction as there are no explicit ETH molecules as reactant (from eq. 2.6) contrary to the THF solvated species. Therefore, only the standard state correction for solution is added and hence, the lower effect of correction observed (from 8.16 to 10.05 kcal mol^{-1}). It is worth noting that, the corrections are only added where there is a change in the number of moles between the forward and reverse side of the equilibrium equation (that is, when there is unequal number of moles of reactant and product). For instance, in the equilibrium of tetrahedral tetramer and ring tetramer in ETH where the number of coordinated solvent is equal and hence, equal number of moles in both structures, there is no visible added correction (Table 2.2 row 6 column 4 and Table 2.4 row 6 column 3). The correction cancel out (see eq. 2.4 and 2.5).

Looking at the dissociation of the stable tetrahedral tetramer into simpler aggregates, for example, the dissociation of the stable tetrahedral tetramer into ring trimer and monomer, the chemical equilibrium relationship between the tetrahedral tetramer and ring trimer can be written as:

$$[(MeLi)_4 4ETH] + 2ETH \rightleftharpoons [(MeLi)_3 3ETH] + [(MeLi)3ETH] \quad 2.8$$

$$[(MeLi)_4 4THF] + 5THF \rightleftharpoons [(MeLi)_3 6THF] + [(MeLi)3THF] \quad 2.9$$

The ΔG_{DFT} for the tetramer equilibrium with trimer and monomer in diethyl ether (eq. 2.8) was calculated to be 23.8 kcal mol^{-1}. A similar value of 24.3 kcal mol^{-1} was obtained by coupled-cluster calculation ($\Delta G_{CCSD(T)}$). In THF (eq. 2.9), the ΔG_{DFT} value is 39.4 kcal mol^{-1} and the ($\Delta G_{CCSD(T)}$ value is 38.5 kcal mol^{-1}. On addition of the standard state corrections for solution and solvent in solvent correction as discussed above, the calculated ΔG^*_{DFT} and $\Delta G^*_{CCSD(T)}$ values for the equilibrium in diethyl ether are 19.2 and 19.8 kcal mol^{-1}, respectively, while in THF, the ΔG^*_{DFT} and $\Delta G^*_{CCSD(T)}$ values are 24.4 and 23.5 kcal mol^{-1}, respectively.

Having found the tetrahedral tetramers and dimers to be more stable and the most commonly isolated aggregates, we henceforth, performed dynamic simulations on this aggregates in explicit solvent conditions. Furthermore, we included the presence of ketone bonded to the Li^+ of the clusters.

2.3 Explicit Solvation of $(MeLi)_n$ and $(MeLi)_n$—Ketone Clusters by Molecular Dynamics

Molecular dynamics simulation of the MeLi dimer and tetramer aggregates in explicit solvation showed the coordination of the solvent molecules on the Li^+ ions differ for the different solvents, diethyl ether and THF. The radial distribution function, g(r) of the dimer in the solvents showed two solvation spheres at about 2 and 4 Å (Fig 2.3). Integration of the g(r) yielded the number of coordinating solvent on the Li^+ ions in the solvation spheres. In diethyl ether, the first solvation sphere showed one coordinated solvent per Li^+ ion while in THF on the other hand, two solvents molecules are bonded per Li^+ ion. The second solvation sphere showed two solvents around the Li^+ ion in diethyl ether and four in THF.

For the tetramers, all Li^+ ions are at most singly coordinated to a solvent molecule in both diethyl ether and THF in the first solvation sphere. The second solvation sphere have three and four solvents around the Li^+ ion in diethyl ether and THF, respectively. Solvent exchange was noted in diethyl ether solvated tetramer on especially two Li^+ ions (Fig 2.4). No solvent exchange was recorded for the tetramer in THF.

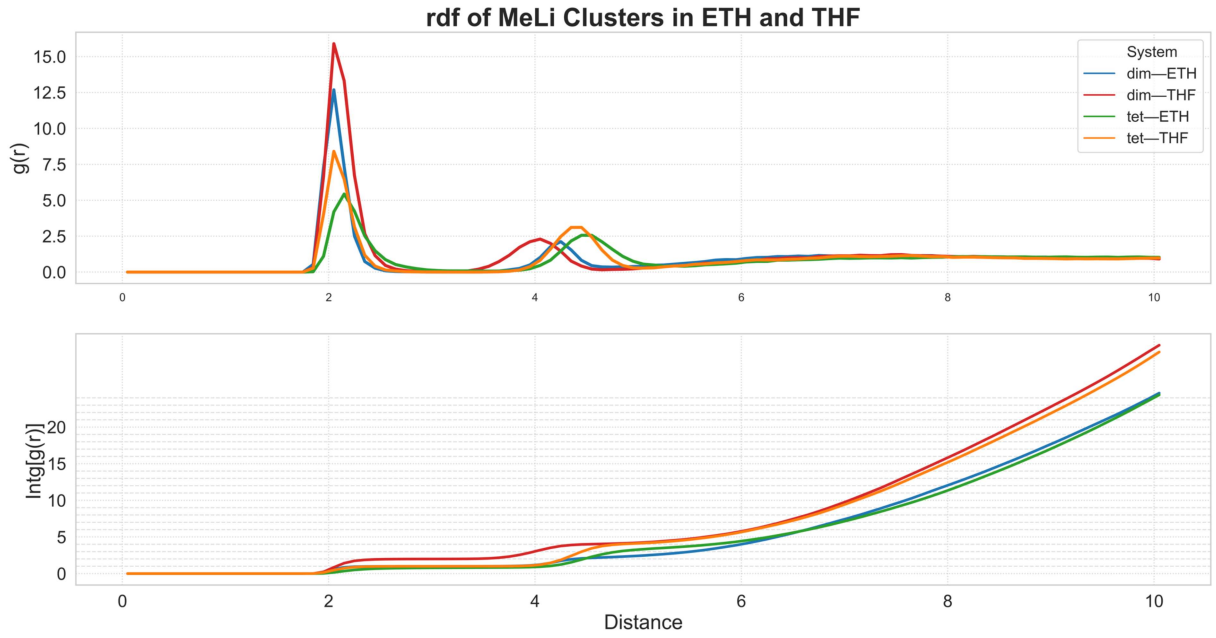

Fig. 2.3: radial distribution function, rdf of $(MeLi)_{2,4}$ solvation in ether and THF (top); integration of the rdf to give number of coordinated solvents (bottom)

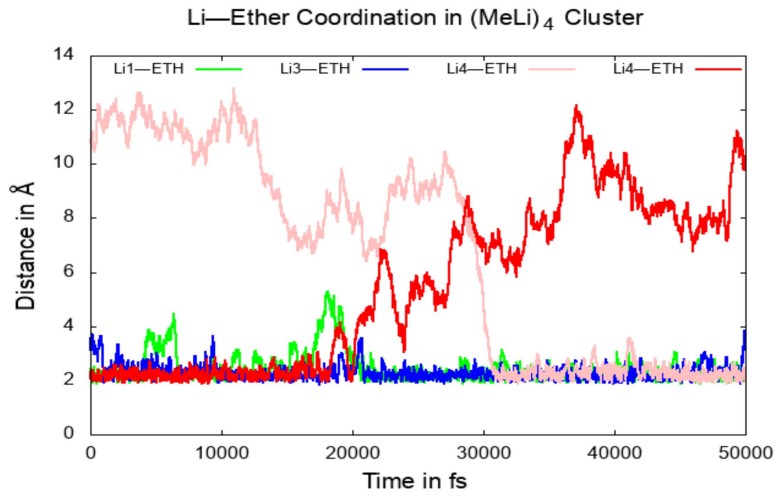

a)

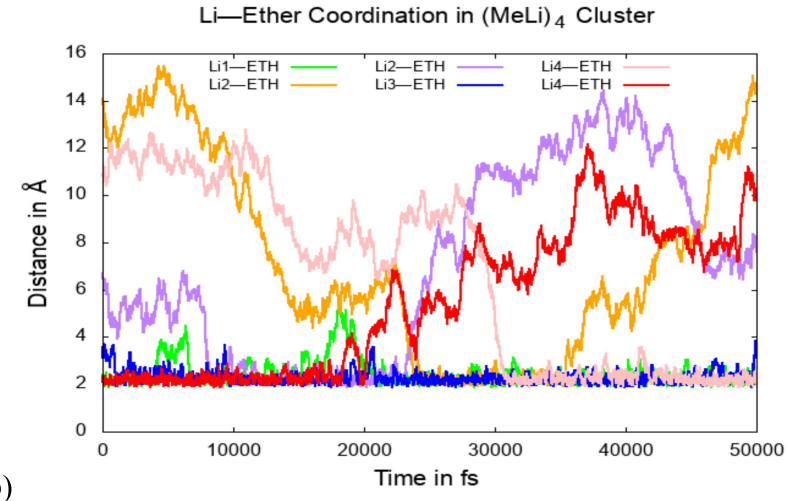

b)

Fig. 2.4: solvation in $(MeLi)_4$: a) showing solvent exchange on Li^4 in $(MeLi)_4$ and b) showing overall solvation with solvent exchange in $(MeLi)_4$

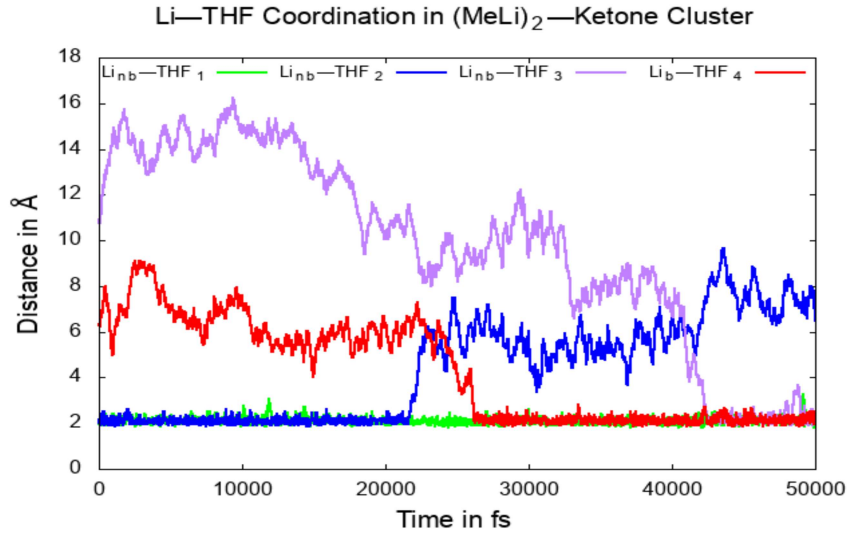

a)

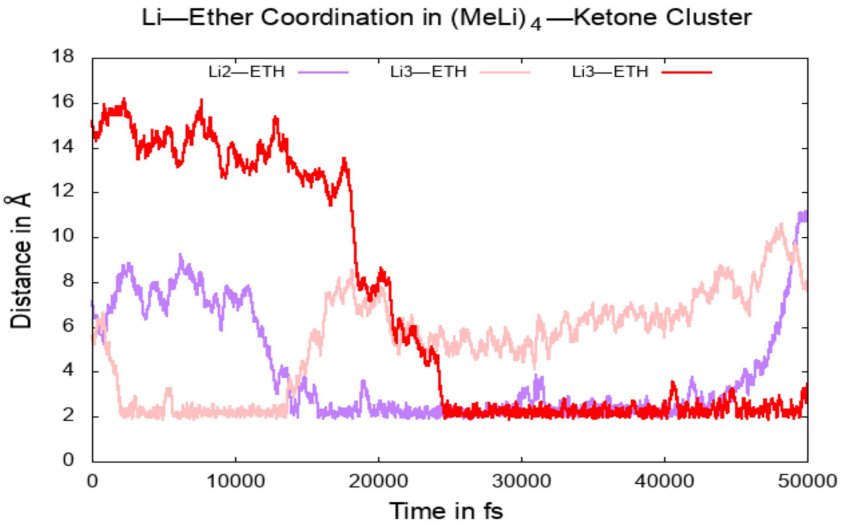

b)

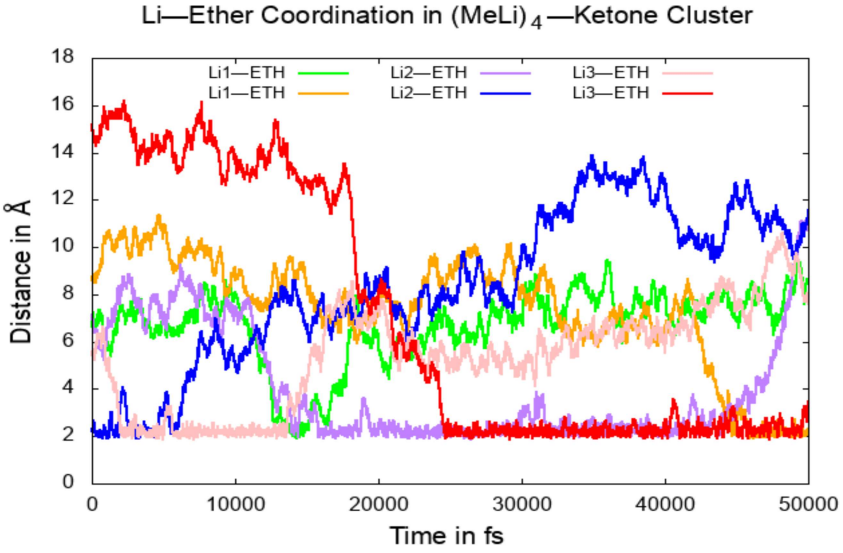

c)

Fig. 2.5: a) solvation in $(MeLi)_2$—ketone (b) graph emphasizing solvent exchange in $(MeLi)_4$—ketone solvation c) Overall solvation in $(MeLi)_4$—ketone

With the objective of studying the reactivity of the nucleophilic addition of MeLi on 4-chloro-1-phenylbutan-1-one (γ-chloroketone),[17] the explicit solvation of MeLi—ketone dimer and tetramer complexes were studied. For the system of $(MeLi)_2$—ketone cluster in diethyl ether, only the non-ketone-bonded lithium ion (Li^{nb}) is bonded to a solvent molecule. In THF on the other hand, the Li^{nb} is bonded to two solvent molecules. One of the solvent is lost after about 21 ps and at about the same moment, the ketone-bonded lithium ion (Li^{b}) becomes bonded to a solvent molecule (Fig 2.5a).

The solvation in $(MeLi)_4$—ketone is quite different. Only a maximum of two of the three Li^{nb} lithium ions were solvated at a time in diethyl ether. On most occasions, only one lithium ion is coordinated at a time (Fig 2.5b & c). Comparison of the Li^+ ion coordination number of

$(MeLi)_4$ and $(MeLi)_4$—ketone cluster is shown via a plot of the integral of radial distribution function (Fig 2.6). The limited diethyl ether coordination in $(MeLi)_4$—ketone is posed by the steric repulsion between the alkyl chain of the γ-chloroketone and the chain-like diethyl ether molecule. This is evident in the fact that the Li^+ ion in close proximity to the alkyl chain, **Li^1** in Fig 2.7b, was barely solvated. On the flip side, with THF, each Li^+ ion is solvated with a THF, and this without solvent exchange after 50ps dynamics run.

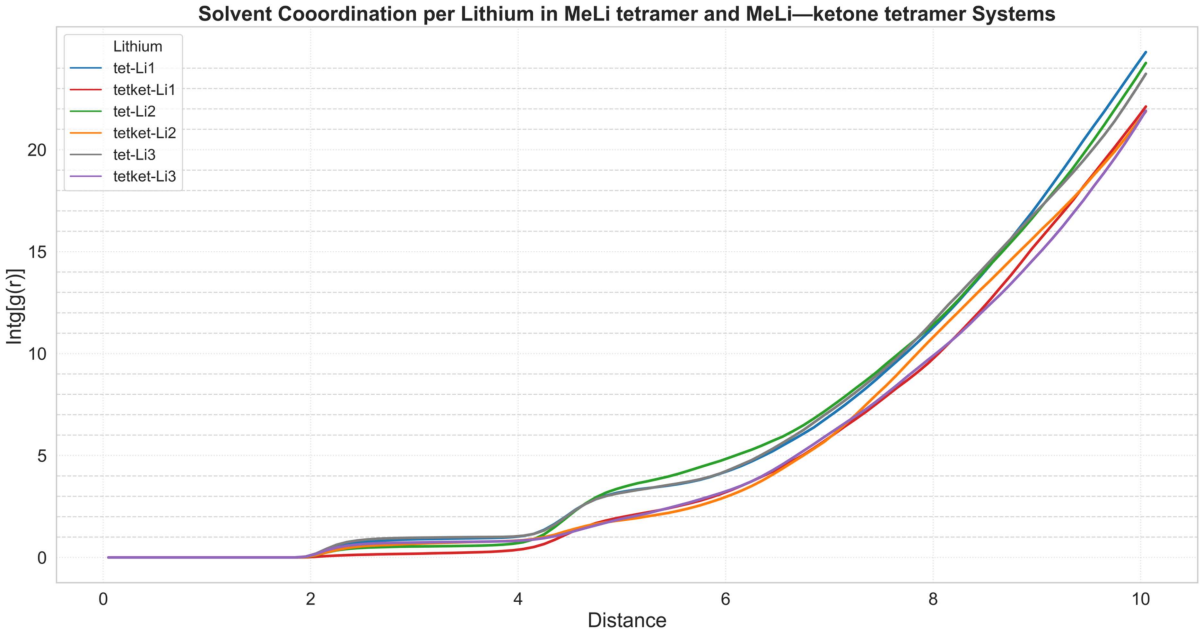

Fig. 2.6: integral of g(r) showing coordination number of solvent on Li+ in $(MeLi)_4$ and $(MeLi)_4$—ketone clusters (*where Li1, Li2 and Li3 are as shown in Fig. 2.7*)

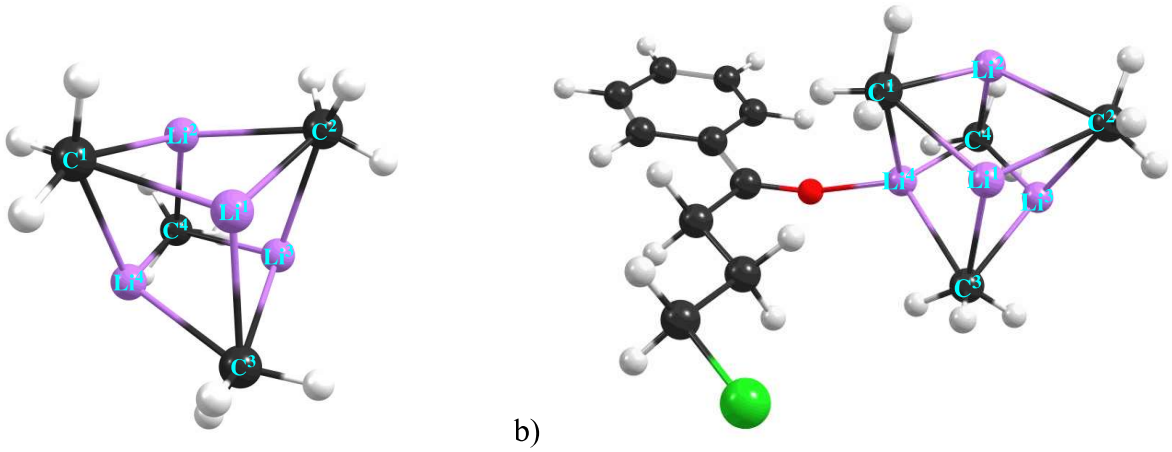

Fig. 2.7: $(MeLi)_4$ and $(MeLi)_4$—ketone clusters with the labels on the Li^+ ions and the methyl carbons

2.4 Structural Analysis of Aggregates in Solvents

The geometric parameters of the $(MeLi)_n$ and $(MeLi)_n$—ketone clusters were examined in explicit diethyl ether and THF solvents. The evolution of the Li—Li and C—C distances with time in the solvents were estimated. In the dimers, the Li—Li and C–C distances in THF are slightly stretched with mean values of +0.05 and +0.03 Å compared to those in diethyl ether for $(MeLi)_2$ and $(MeLi)_2$—ketone, respectively (Table 2.5). This stretched results from higher steric repulsion from the two bonded THFs as against one diethyl ether. This trend is not observed in $(MeLi)_4$ as the Li^+ are equally bonded to the solvents. These results are consistent with the DFT optimized geometries as earlier given. The geometry parameters from the molecular dynamics in comparison to the DFT optimized structures are given in Table 2.5. In $(MeLi)_4$—ketone, the Li—Li distances involving Li^1 (Fig 2.7) which is barely solvated due to the steric effect from the alkyl chain of the γ-chloroketone are shorter than their counterparts in THF (Table 2.5, column 3 rows 15-17). Larger standard deviations were observed for aggregates in which solvent exchange were noted, compared to their counterparts (Table 2.5, column 5 rows 5-6; column 4 rows 7-22) which is elaborate with aggregates in diethyl ether.

To check the effect of coordination of ketone on the clusters, a violin plot comparing the distribution of the Li—Li and C—C distances was made for $(MeLi)_4$ and $(MeLi)_4$—ketone clusters (Fig 8). No major disparity was observed between the two. The slight deviation comes from the distances involving Li^4 and Li^1 which are the lithium coordinated to the ketone and the lithium without coordinated solvent, respectively.

The ketone—lithium bond distances of $(MeLi)_n$—ketone aggregates in diethyl ether and THF were measured and the heat map plotted making comparison between the different solvation (Fig 2.9). The mean distance for the $(MeLi)_2$—ketone in diethyl ether and THF are 1.93 and 1.97Å with standard deviations of 0.10 and 0.12, respectively. The higher mean distance and standard deviation in THF which is the system with higher solvent coordination is a supportive indication of the effect of solvent in the cluster geometry. In $(MeLi)_4$—ketone a mean value of 1.97Å and standard deviation of 0.11 were recorded in both solvents. In general, the $(MeLi)_n$—ketone geometries are fairly stable in the solutions.

Table 2.5: Bond distances in $(MeLi)_4$ and $(MeLi)_4$—ketone clusters in Å

System	Bond	Ether		THF	
		Mean dist.	DFT opt. geometries	Mean dist.	DFT opt. geometries
$(MeLi)_2$	$Li^1—Li^2$	2.26 ± 0.0857	2.26	2.31 ± 0.0898	2.31
	$C^1—C^2$	3.65 ± 0.1016	3.63	3.71 ± 0.1040	3.73
$(MeLi)_2$—ketone	$Li^1—Li^2$	2.30 ± 0.0913	2.27	2.33 ± 0.0972	2.32
	$C^1—C^2$	3.66 ± 0.1044	3.67	3.69 ± 0.1088	3.70
$(MeLi)_4$	$Li^1—Li^2$	2.52 ± 0.1394	2.54	2.54 ± 0.1346	2.47
	$Li^1—Li^3$	2.57 ± 0.1385	2.53	2.54 ± 0.1359	2.48
	$Li^1—Li^4$	2.55 ± 0.1452	2.47	2.55 ± 0.1326	2.47
	$Li^2—Li^3$	2.54 ± 0.1389	2.48	2.55 ± 0.1374	2.50
	$Li^2—Li^4$	2.52 ± 0.1341	2.52	2.54 ± 0.1349	2.47
	$Li^3—Li^4$	2.56 ± 0.1399	2.54	2.53 ± 0.1343	2.47
	$C^1—C^2$	3.64 ± 0.1448	3.59	3.68 ± 0.1484	3.65
	$C^3—C^4$	3.68 ± 0.1583	3.59	3.67 ± 0.1448	3.65
$(MeLi)_4$—ketone	$Li^1—Li^2$	2.47 ± 0.1281	2.48	2.51 ± 0.1199	2.47
	$Li^1—Li^3$	2.48 ± 0.1324	2.35	2.53 ± 0.1185	2.49
	$Li^1—Li^4$	2.54 ± 0.1417	2.46	2.55 ± 0.1282	2.46
	$Li^2—Li^3$	2.54 ± 0.1419	2.49	2.51 ± 0.1249	2.47
	$Li^2—Li^4$	2.60 ± 0.1517	2.53	2.57 ± 0.1216	2.49
	$Li^3—Li^4$	2.58 ± 0.1475	2.46	2.56 ± 0.1287	2.46
	$C^1—C^2$	3.63 ± 0.1470	3.59	3.67 ± 0.1365	3.64
	$C^3—C^4$	3.70 ± 0.1514	3.55	3.70 ± 0.1473	3.66

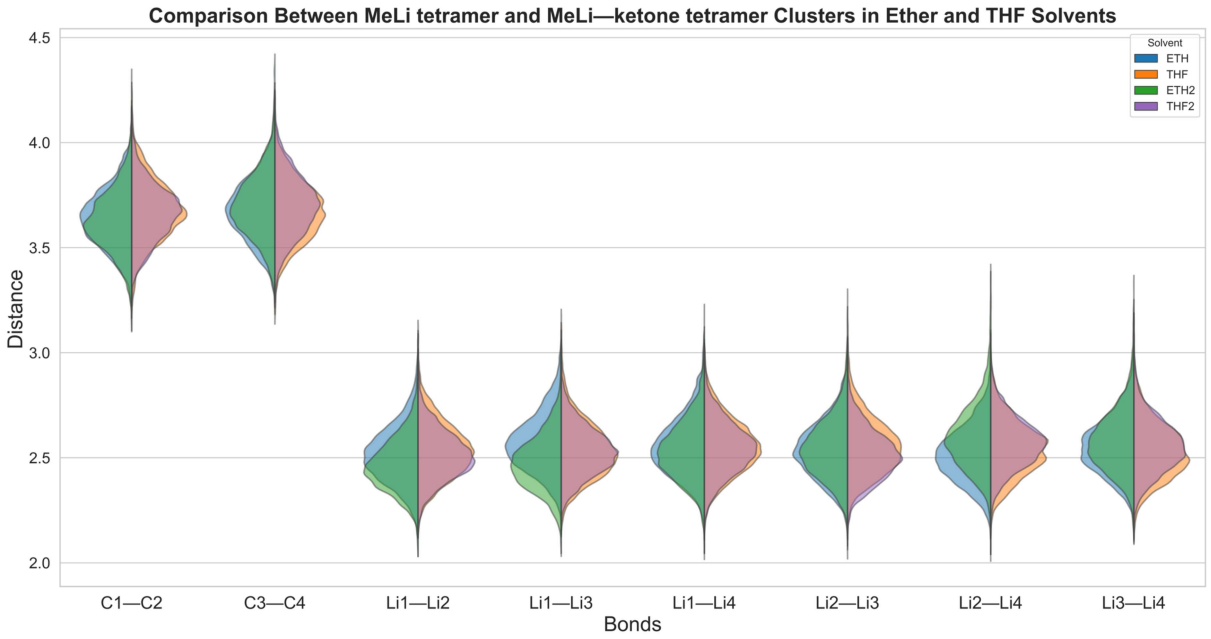

Fig. 2.8: violin plot for comparison of bond distances in clusters between $(MeLi)_4$ and $(MeLi)_4$—ketone clusters

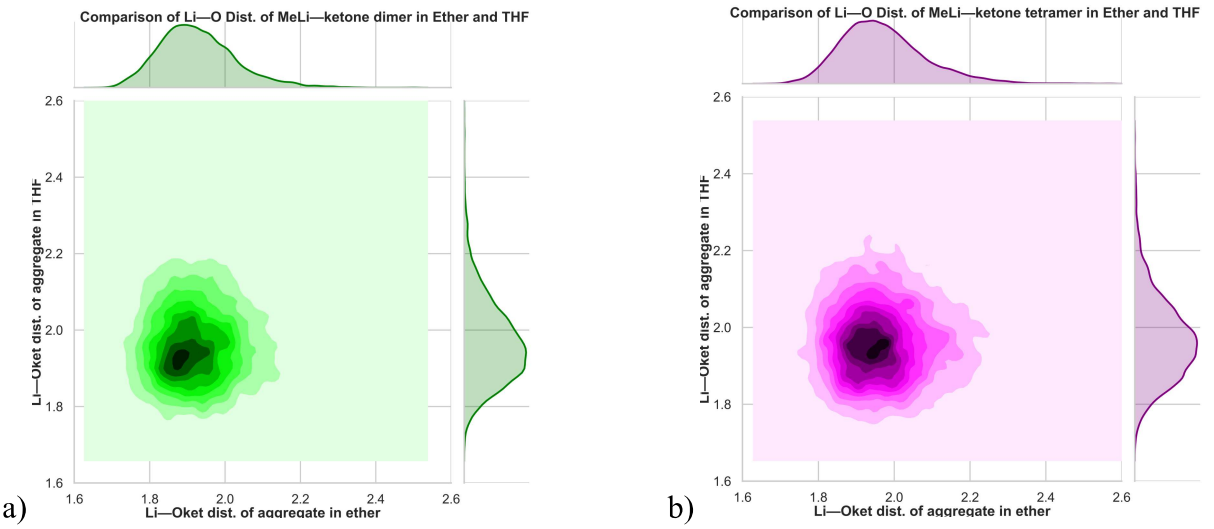

Fig. 2.9: ketone—Li distances heat map of clusters in ether and THF of a) dimers and b) tetramers

2.5 Interaction Energy

The intermolecular interaction energy of the solvent with the clusters ($[MeLi]_n$ and [ketone—$(MeLi)_n$]) and the interaction of the ketone with the clusters were calculated by symmetry-adapted perturbation theory, SAPT. The fundamental contributions: the electrostatic, exchange, induction and dispersion interactions are shown in Table 2.6. The induction column contains the sum of the induction interaction (attractive) as well as the exchange-induction contribution

and $\delta_{HF}^{(2)}$ (discussed in Chapter 1 section 1.8). Thus, these later contributions quench the induction interaction and in some case to a very large extent that the value on the induction column maybe positive (Table 2.6 column 4 row 15). In the dispersion column also exist an added exchange-dispersion repulsion contribution. But this is very minimal and thus the quenching very small. The bulk of the interaction comes from the attractive electrostatic interaction and the repulsive exchange interaction. The total energy of interaction of solvent with the rest of the aggregate varies significantly with the number of solvent molecules in the aggregate (Table 2.6, column 6) and to a lesser extent in the interaction of ketone with the aggregate. For example, $[(MeLi)_4.4THF]$ which has higher solvent coordination exhibited the lowest interaction energy (Table 2.6, row 2 columns 6). Nevertheless, the intermolecular interaction energies for this studied system are in the same range. In the ketone—$(MeLi)_n$ interaction, the interaction with the dimers is stronger than with the tetramers but globally, the interactions are in the same range.

Table 2.6: Intermolecular interaction energies of cluster—solvent and cluster—ketones in kcal/mol

$(MeLi)_n$—Solvent Interaction	**Elst.**	**Exch.**	**Ind.**	**Disp.**	**Total**
$[(MeLi)_2ETH]$—ETH	-21.89	15.30	-3.89	-5.10	-15.57
$[(MeLi)_23THF]$—THF	-19.77	17.27	-1.84	-8.09	-12.42
$[(MeLi)_43ETH]$—ETH	-22.21	20.87	-4.22	-10.51	-16.07
$[(MeLi)_43THF]$—THF	-23.37	17.68	-2.23	-7.83	-15.74
$[(MeLi)_n$—Ketone]—Solvent Interaction					
[Ketone—$(MeLi)_2$]—ETH	-20.27	13.00	-4.22	-4.67	-16.17
[Ketone—$(MeLi)_2$THF]—THF	-16.68	13.29	-5.35	-5.67	-14.42
[Ketone—$(MeLi)_4$]—ETH	-20.28	14.62	-3.47	-7.23	-16.35
[Ketone—$(MeLi)_4$2THF]—THF	-20.46	13.30	-1.59	-5.85	-14.60
$(MeLi)_n$—Ketone Interaction					
$[(MeLi)_2ETH]$—Ketone	-23.63	12.89	-1.67	-4.55	-16.96
$[(MeLi)_22THF]$—Ketone	-21.60	12.99	-2.60	-5.04	-16.24
$[(MeLi)_4ETH]$—Ketone	-19.24	11.87	-0.98	-6.30	-14.65
$[(MeLi)_43THF]$—Ketone	-18.20	11.22	0.07	-7.21	-14.12

2.6 Dissociation of Tetramer to Dimers

Next, the dissociation of $(MeLi)_4$ to $(MeLi)_2$ was investigated by the enhance molecular dynamics sampling method, metadynamics. We used two collective variables. First, the distance between the centre of mass of the upper dimer ring of the cube ($Li^1C^1Li^2C^2$ Fig 2.7) and the centre of mass of the lower dimer ring ($Li^3C^3Li^4C^4$ Fig 2.7) is set as a collective variable to represent the dissociation. A second collective variable set, is the coordination number of the lithium ions with the solvent molecules (Et_2O or THF). This second collective variable is there to induce the re-solvation of the dimers produced by the dissociation. The Gaussian potential during the metadynamics is added every 50 steps with height of 0.5 kcal mol^{-1} and the rescaling biasfactor of 30.

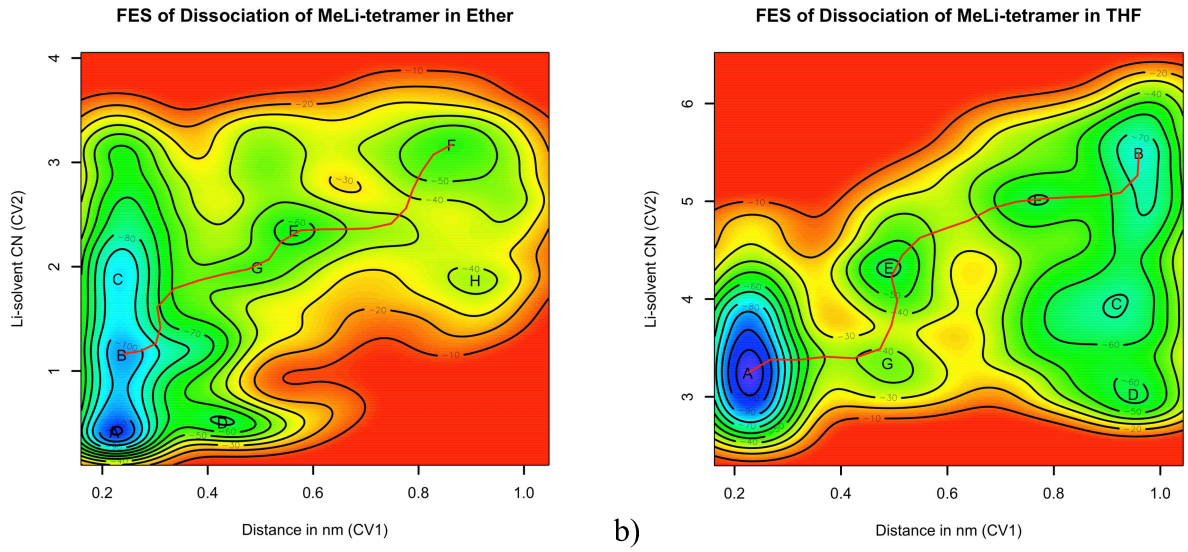

Fig. 2.10: FES of transformation of $(MeLi)_4$ to $(MeLi)_2$ in a) ether and b) THF

Transformation of tetramers to dimers is achieved by cluster splitting and solvent coordination. The tetramer splitting through the cleavage of the Li–C bond that stacks the dimer rings on one another is preceded by the Li^+ ions solvation. The path of this transformation is depicted in Fig 2.10. In diethyl ether solvent (Fig 10a), the path of the dissociation goes from the metastable state **B** where the tetramer is partially solvated (2 to 3 of the Li^+ ions solvated and solvent exchange occurring) to **F** where the two dimers are formed with each Li^+ coordinated to a solvent. It first with an estimated free energy barrier of 13kcal mol^{-1}, passes through an intermediate **E** where the tetramer is partially dissociated, which can be seen from the evolution of the collective variables. The Li—solvent coordination number goes from around 1.2 in **B** to 2.3 in **E**, preparing the expected solvation pattern of the dimers. This evolution was of course

done concurrently with the dissociation of the tetramer with the distance between the centre of mass of the two stacked dimer rings going from about 0.2 nm in **B** to about 0.6 nm in **E**. Next, it fully dissociated to the dimers in **F** at an estimated free energy barrier of 5 kcal/mol. The intermediate at **E** has +10 kcal mol^{-1} higher free energy than the initial tetrahedral tetramer structure at **B** (Fig 2.11). The dissociation of the tetramer **B** to dimers **F** in Et_2O can therefore be said to occur with an estimated free energy of activation of 13 $kcal.mol^{-1}$ taking into account the rate determining step as the transformation from the tetrahedral tetramer, **B** to the partially dissociated tetramer at **E**.

In THF, the transformation goes from a tetra-coordinated tetramer **A**, each Li^+ ion coordinated to a solvent, to tetra-coordinated dimers **B** with each Li^+ ion di-coordinated to the solvent molecules (Fig 10b). An intermediate **E** of partially dissociated tetramer structure was attained at a free energy barrier of 21 kcal mol^{-1}. At **E**, the tetramer is partially dissociated and there are incoming THF solvents for second solvent coordination on the Li^+ ions. The distance between the centre of mass (the first collective variable) evolve from about 0.2 nm in **A** to about 0.5 nm in **E**. Likewise, the coordination number (the second collective variable) increased from about 3.4 in **A** to about 4.4 in **E**. With a free energy barrier of 7 kcal mol^{-1} the intermediate **E** becomes fully dissociated in the dimers at **B**. The partially dissociated intermediate at **E** has a higher free energy of +13 kcal mol^{-1} in relation to the starting tetrahedral tetramer structure at **A** (Fig 2.12). From the metadynamics simulation, the estimated free energy barrier for the dissociation from the tetramers to dimers illustrates that, the tetrahedral tetramer is likely more stable in THF than in Et_2O. This study show the existence of a possible intermediate structure which was made visible from the use of the explicit solvent. The transformation from the tetrahedral tetramer to dimers involves a joint process of dissociation and solvation.

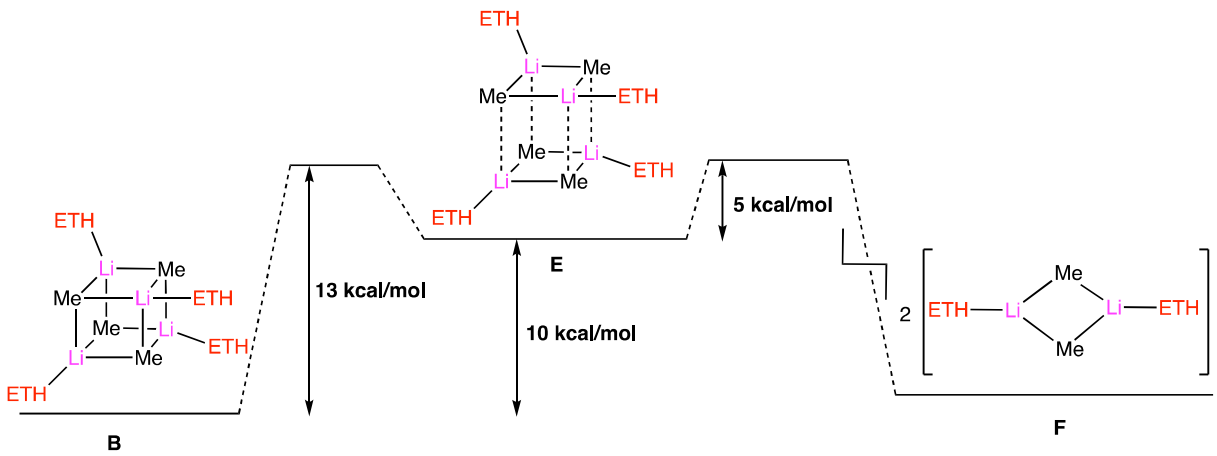

Fig. 2.11: Dissociation pathway from tetrahedral tetramer to dimers in diethyl ether solvent

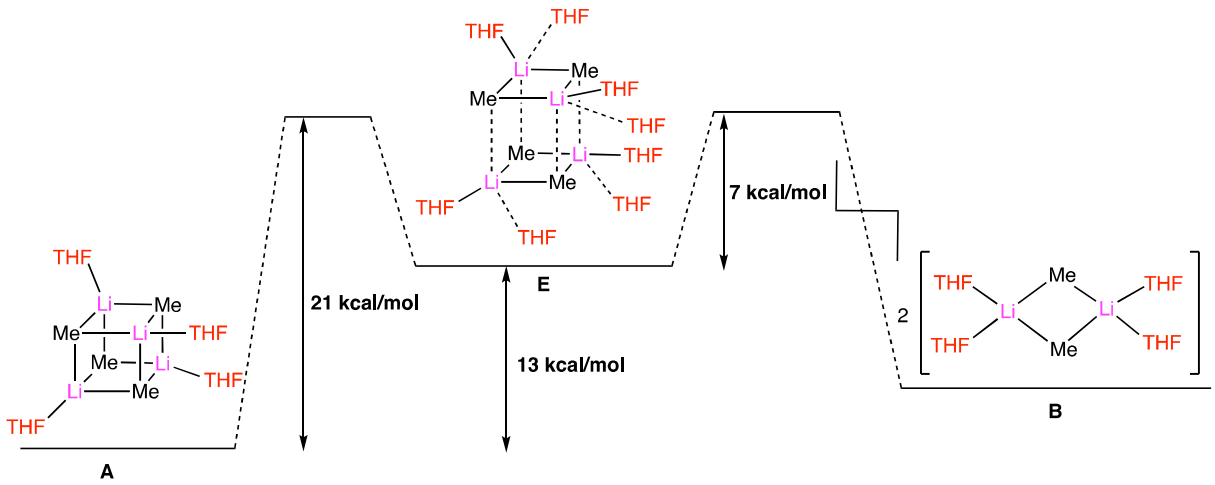

Fig. 2.12: Dissociation pathway from tetrahedral tetramer to dimers in THF solvent

2.7 Conclusion

It was found in general that the polyhedral structures of the MeLi clusters are more stable than the ring and ladder structures. The tetrahedral structures were found to be the most stable of the optimized aggregates in both diethyl ether and THF solvents. The solvent coordination number is higher with THF than with diethyl ether especially in the ring structures. This higher coordination number observed for THF solvated aggregates is mainly due to steric repulsion pose by the alkyl chains of the diethyl ether with themselves or with the bonded γ-chloroketone. This repulsion is minimal in the ring-structured THF. The common aggregates in ethereal solvents, ring dimer and tetrahedral tetramer were found to be fairly stable with minor fluctuations in their intermolecular bond distances. Elongation of the bond distances varies directly with the number of coordinated solvent. Likewise, the intermolecular interaction energy between solvents or ketone and the MeLi clusters are proportional to the number of coordinated solvent per Li^+. It was possible to unveil the pathway for the dissociation of tetrahedral MeLi tetramer to dimers by explicit solvation of the aggregate and through metadynamics simulation. The transformation of the tetrahedral MeLi tetramer cluster to MeLi in diethyl ether dimers was found to occur at a lower free energy of activation than in THF solvent. This therefore suggest that, the tetrahedral MeLi tetramer is likely more stable in THF than in diethyl ether solvent.

CHAPTER THREE

3 Organometallic Addition to Sulfinyl Ketimines

Nitrogen containing compounds of amide and amine functionalities have drawn interest due to their applications as drug candidates obtained both by synthesis and from natural products. For instance, biphenyl tetrazole *tert*-butyl Cl-amidine **1** (Fig. 3.1) was found to be effective in protein arginine deiminase (PAD4) inhibition and also blocks the formation of neutrophil extracellular traps, which is a promising step in selective treatment of inflammatory diseases resulting from dysregulated PAD activity.[84] By hybridization of tetrazole with some known pharmacophores as azoles, benzochromenes, imines, pyrimidines, quinolones or steroids, Xu, Zhang and co-workers reported promising synthesized anticancer candidates.[85]

Amines with chiral centre bore by tertiary carbon are found in a number of biologically active compounds used as drugs. For example, Tipifarnib (Zarnestra) **2** an antitumor, is used in the treatment of leukemia. It was found to exhibit selective inhibition against farnesyl protein transferase with disinhibiting selectivity towards non-target cytochrome P450-dependent enzymes.[86] In other examples, aminomethylpiperidine **3** was reported to be effective against mixed lineage leukemia by inhibiting its protein-protein interaction with menin[87] and 7-amino-7,8-dihydro-α-bisabolene **4** isolated from marine sponge was found to inhibit *Candida albicans*.[88]

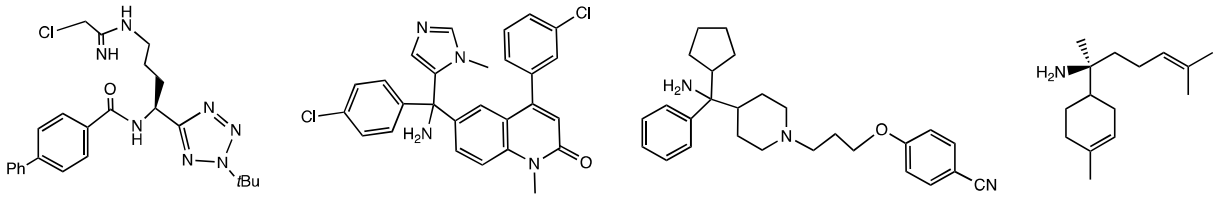

1 **2** **3** **4**

Fig. 3.1: potential drug candidates with amide and amine functionality

Despite their biological activities and therapeutic used, no efficient methodology exists for the synthesis of these chiral amines. For instance, Grembecka *et al* recorded only 2% yield of racemic mixture of the aminomethylpiperidine **3**.[87] It is in the quest to find an improved methodology for the synthesis of these chiral amines bore by tertiary carbon that Chukuka Achuenu in his doctoral studies under the supervision of Dr. Florian Berthiol of the organic synthesis group, SERCO of the "Département de Chimie Moléculaire" of Université Grenoble

Alpes devised an alternate route (unpublished as at the time of this report). The scheme (scheme 3.1) involves first the synthesis of thionoester from commercially available esters with phosphorus pentasulphide in the presence of hexamethyldisiloxane. To introduce chirality, a chiral auxillary, *t*-butylsulfinamide is added to the thionoester in the presence of a strong base and a methylating agent to obtain sulfinyl thioimidate. This is followed by alkylation. Then using Leibeskind Srogl type cross-coupling reaction, sulfinyl imine is obtained. Organometallic 1,2-addition on the sulfinyl imines gave rise to amines beared by chiral tertiary carbon.

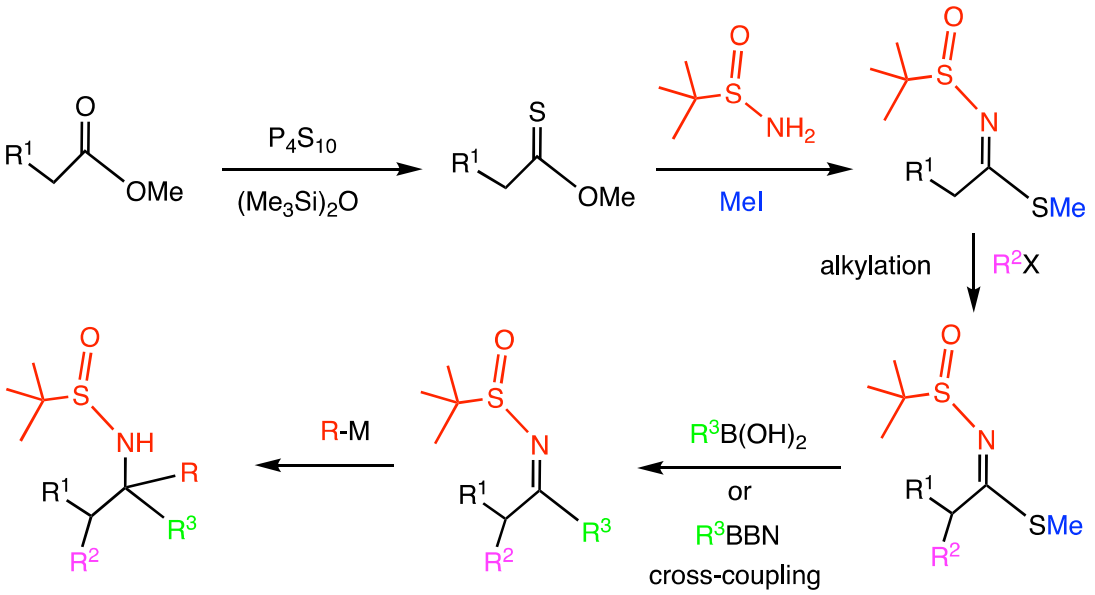

Scheme 3.1: Novel route for accessing a wide range of chiral amines beared by tertiary carbon

Among the organometallic compounds they used are the Grignard reagents of allyl-, vinyl- and methylmagnesium bromide and organolithiums of phenyl-, methyl- and *n*-butyl lithium. The sulfinyl ketimines used are given in Fig. 3.2a. The allylation of the sulfinyl imines with allylmagnesium bromide was predominantly reported (Table 3.1). Sulfinyl imines with dissimilar substituents on the imine-carbon such as those used in the synthesis (Fig. 3.2) are said to exist as mixtures of *E* and *Z* isomers in equilibrium with high capacity to undergo interconversion and are difficult to separate.[89] Davis and Kluger established through spectroscopy study (dynamic NMR, IR and mass spectra), that *p*-toluenesulfinyl ketimines are in rapid equilibrium between *E* and *Z* isomers with Gibbs free energy barriers between 13 and 19 kcal.mol^{-1}.[90] In a like vein, Eisentein *et al* calculated by DFT at B3LYP/cc-pVTZ level, the isomerization Gibbs energy barrier of 19.6 kcal.mol^{-1} for the interconversion of the aldimine *N*-Benzylidene-2-methylpropane-2-sulfinamide.[91] But interestingly, in their studies, Achuenu and Berthiol recorded the nucleophilic additions with moderate to very good diastereoselectivities (Table 3.1). It is these interesting results that brought us into the picture.

We therefore, sort to gain insight into this stereoselectivity observed, compare experimental observations with calculated results and study the effect of substituents on the addition.

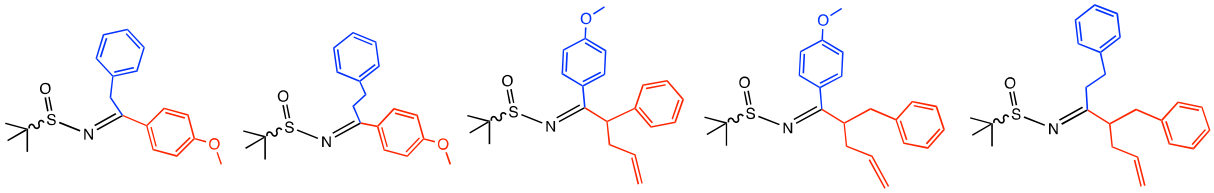

Fig. 3.2: sulfinyl ketimines for organometallic addition

Table 3.1: Experimental yield and diastereomeric ratio of organometallic addition of sulfinyl ketimines

Compound	R	Metal	Solvent	Yield (%)	d.r
5a	Allyl	MgBr	CH_2Cl_2	72	>98:2
5a	Phenyl	Li	Toluene	72	>98:2
5a	Phenyl	Li + $AlMe_3$	Toluene	81	>98:2
5a	Me	MgBr	THF	n.r	—
5a	Me	Li	THF	n.r	—
5a	*n*-Bu	Li	THF	30	>98:2
5b	Allyl	MgBr	CH_2Cl_2	83	>98:2
5b	Vinyl	MgBr	CH_2Cl_2	41	>98:2
6a	Allyl	MgBr	THF	traces	62:38
6b	Allyl	MgBr	THF	53	>98:2
6c	Allyl	MgBr	THF	23	>98:2

In pursuance of this study, we adapted the proposed mechanism by Ellman *et al* in which the reaction is said to proceed via a concerted six-membered ring transition state (Fig 3.3a). For the allylation, at the transition state, the imine is activated by the coordination of the metal of the organometallic reagent to the imine nitrogen, forming a four-membered ring with the sulfur and the sulfinyl oxygen. In addition, a six-membered ring is formed by the allyl group and the imine nitrogen and the metal (Fig. 3.3b). In the presence of a Lewis acid as $AlMe_3$, the acid is coordinated to the imine nitrogen at the transition state. [89]

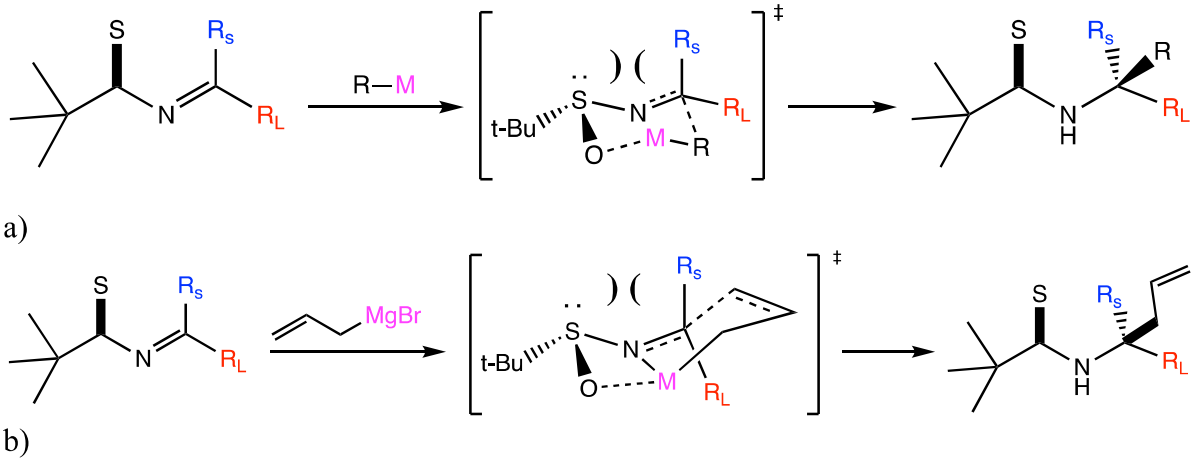

Scheme 3.2: proposed mechanism of 1,2-addition of sulfinyl ketimines a) addition with RLi or RMgBr through concerted six-membered ring b) addition with allylMgBr through four- and six-membered ring transition structure

For clarity, we labelled the ketimines as (S) or (L), depending, respectively, on whether the small (S) or bulky (L) substituent group is at the position axial to the sulfoxide group (Fig 3.3). They are further labelled according to the position of the highest ranked substituent on the imine-carbon according to Cahn-Ingold-Prelog (CIP) priority rules with respect to the position of the sulfoxide group. They are tag as either ***E*** or ***Z*** isomers when the highest ranked substituent is in *trans* or *cis* position to the sulfoxide group, respectively.

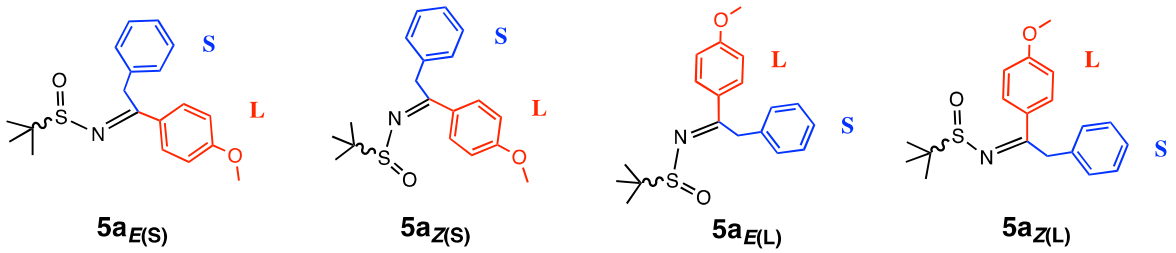

Fig. 3.3: using **5a** as an example to show the labelling of the sulfinyl ketimines diastereomers

The calculations were performed by the DFT method. In choosing a suitable level of theory for treating our system, optimization and energy calculation for geometries corresponding to the reactant and TS of the addition of allyl magnesium bromide on **5a**$_{E(S)}$ and **5a**$_{Z(S)}$ were first carried out by the hybrid-GGA functional, B3LYP with 6-31+G (d,p) basis. A second calculation was done at the same level but with the introduction of a dispersion correction, D3BJ. The free energy barrier from the two calculations were compared. The addition of the dispersion correction lowered the free energy barrier. For instance, from 24.6 to 21.4 kcal mol^{-1} for the **5a**$_{E(S)}$ addition. A further calculation with a change of basis sets was made (B3LYP/def2-SVP D3BJ) which resulted in a further decrease in the calculated free energy barrier (18.3 and 16.3 for the addition on **5a**$_{E(S)}$ and **5a**$_{Z(S)}$, respectively). Next, the DFT calculated energy is compared

with the energy from the benchmark domain based local pair natural orbital coupled-cluster method, DLPNO-CCSD(T) with the extended basis def2-TZVP for the allyl magnesium bromide addition on $\mathbf{5a}_{E(S)}$. The calculated energy barrier, $\Delta E^{\ddagger}$ from the DFT calculation at B3LYP/def2-SVP with D3BJ dispersion correction differ from the brenchmark coupled-cluuster calculation by only about 1.9 kcal mol^{-1} which is an acceptable value of error. On the other hand, a comparison of the B3LYP/6-31+G(d,p) level calculation with the coupled-cluster calculation yielded an energy barrier difference of 2.9 kcal mol^{-1}. Therefore, as a good compromise between accuracy and cost, the calculations were performed by DFT with the B3LYP functional and def2-SVP basis with dispersion correction added by the Becke-Johnson Grimme's dispersion correction, D3BJ. To include solvent effects, an implicit solvation was added by the conductor-like polarizable continuum model, CPCM by single point calculation of the optimized geometries. The calculation with the introduction of coordinated solvent will be discussed in section 3.4 of this chapter.

3.1 Stability and Interconversion of Diastereomers of ketimines, 5a

With the different possible conformations for the ketimines, their stabilities with respect to one another was calculated by DFT method at the B3LYP/def2-SVP level with D3BJ dispersion correction. Examining the energies of ketimine **5a** diastereomers, the calculated energies of the optimized diastereomers showed the *E* isomers to be more stable than the *Z* isomers. The diastereomer, $\mathbf{5a}_{E(S)}$ (Fig. 3.3) was found to be the most stable diastereomer and its electronic and Gibbs free energy relative to the other diastereomers is given in Table 3.2. The difference in Gibbs free energy between the most stable diastereomers, $\mathbf{5a}_{E(S)}$ and the least stable diastereomers, $\mathbf{5a}_{Z(L)}$ is 4.9 kcal.mol^{-1}. The next favoured diastereomer, $\mathbf{5a}_{E(L)}$ differ in free energy from $\mathbf{5a}_{E(S)}$ by only 0.3 kcal.mol^{-1}. The order of stability of the diastereomers from the calculated energies is: $\mathbf{5a}_{Z(L)} < \mathbf{5a}_{Z(S)} < \mathbf{5a}_{E(L)} < \mathbf{5a}_{E(S)}$. The favouring of stability of the *E* isomers over the *Z* isomers is due to the steric repulsion between the phenyl ring of the large group (substituents in red, Fig 3.3) and the sulfoxide group.

Table 3.2: Energies of ketimine 5a diastereomers

Ketimine	ΔE (kcal/mol)	ΔG (kcal/mol)
$\mathbf{5a}_{E(S)}$	0.00	0.00
$\mathbf{5a}_{E(L)}$	0.78	0.28
$\mathbf{5a}_{Z(S)}$	4.23	3.76
$\mathbf{5a}_{Z(L)}$	5.04	4.87

Interconversion between the *E* and *Z* isomers occurs through rotation about the C=N bond (scheme 3.3) yielding transition structure with CNS angle approaching linearity (Fig. 3.4). Isomerization from $\mathbf{5a}_{E(S)}$ to $\mathbf{5a}_{Z(S)}$ yielded transition structure with CNS angle of 166° opening from 127° for $\mathbf{5a}_{E(S)}$ and 119° for $\mathbf{5a}_{Z(S)}$. Similarly, $\mathbf{5a}_{(L)}$ interconverts through TS with CNS angle of 154° from 127° and 119° for *E* and *Z* isomers, respectively (Table 3.3). The rotation about the C=N bond resulted in moving the sulfoxide group, S=O from being closely in the plane of the C=N for the *E* isomer (with CNSO dihedral angles of 28° and -29°, for $\mathbf{5a}_{(S)}$ and $\mathbf{5a}_{(L)}$, respectively) to being completely out-of-plane on converting to the *Z* isomer with CNSO dihedral angles of -89° and -107°, for $\mathbf{5a}_{(S)}$ and $\mathbf{5a}_{(L)}$, respectively (Table 3.3). The elongation of the N-S bond in the Z isomers from 1.70 and 1.71 Å to 1.75 and 1.76 Å for $\mathbf{5a}_{(S)}$ and $\mathbf{5a}_{(L)}$, respectively is a further indication of the impact of repulsion between the phenyl ring of the large substituent group and the sulfoxide group.

The isomerization from $\mathbf{5a}_{E(S)}$ to $\mathbf{5a}_{Z(S)}$ and from $\mathbf{5a}_{E(L)}$ to $\mathbf{5a}_{Z(L)}$ occurs with a Gibbs free energy barrier, $\Delta G^{\ddagger}$ of 17.8 kcal.mol^{-1} and 18.2 kcal.mol^{-1}, respectively. Conversely, isomerization from $\mathbf{5a}_{Z(S)}$ to $\mathbf{5a}_{E(S)}$ and from $\mathbf{5a}_{Z(L)}$ to $\mathbf{5a}_{E(L)}$ occurs with a Gibbs free energy barrier of 13.6 kcal.mol^{-1} and 12.4 kcal.mol^{-1}, respectively (scheme 3.4). These barriers support the existence of the ketimines as mixtures of both diastereomers in equilibrium under room temperature with interconversion as the energy barriers are feasible to overcome at room temperature. The results are consistent with reported interconversion barrier of 19.6 kcal.mol^{-1} by Eisentein *et al,* for the isomerization of aldimine *N*-Benzylidene-2-methylpropane-2-sulfinamide.[91]

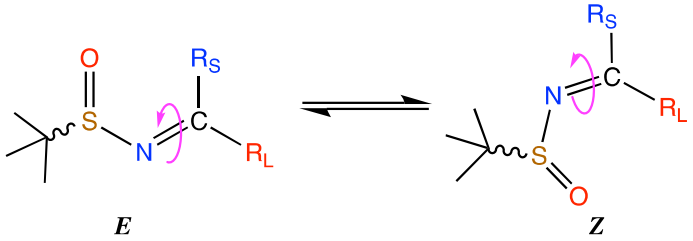

Scheme 3.3: Interconversion through rotation about C=N bond

Table 3.3: Geometric parameters of ketimine 5a isomerization

	5a$_E$			TS			**5a$_Z$**		
	CNS °	**CNSO °**	**NS Å**	**CNS °**	**CNSO °**	**NS Å**	**CNS °**	**CNSO °**	**NS Å**
5a$_{(S)}$	127.4	27.6	1.70	165.6	142.5	1.63	119.3	-89.3	1.75
5a$_{(L)}$	126.5	-29.4	1.71	154.1	-108.3	1.63	119.4	-107.9	1.76

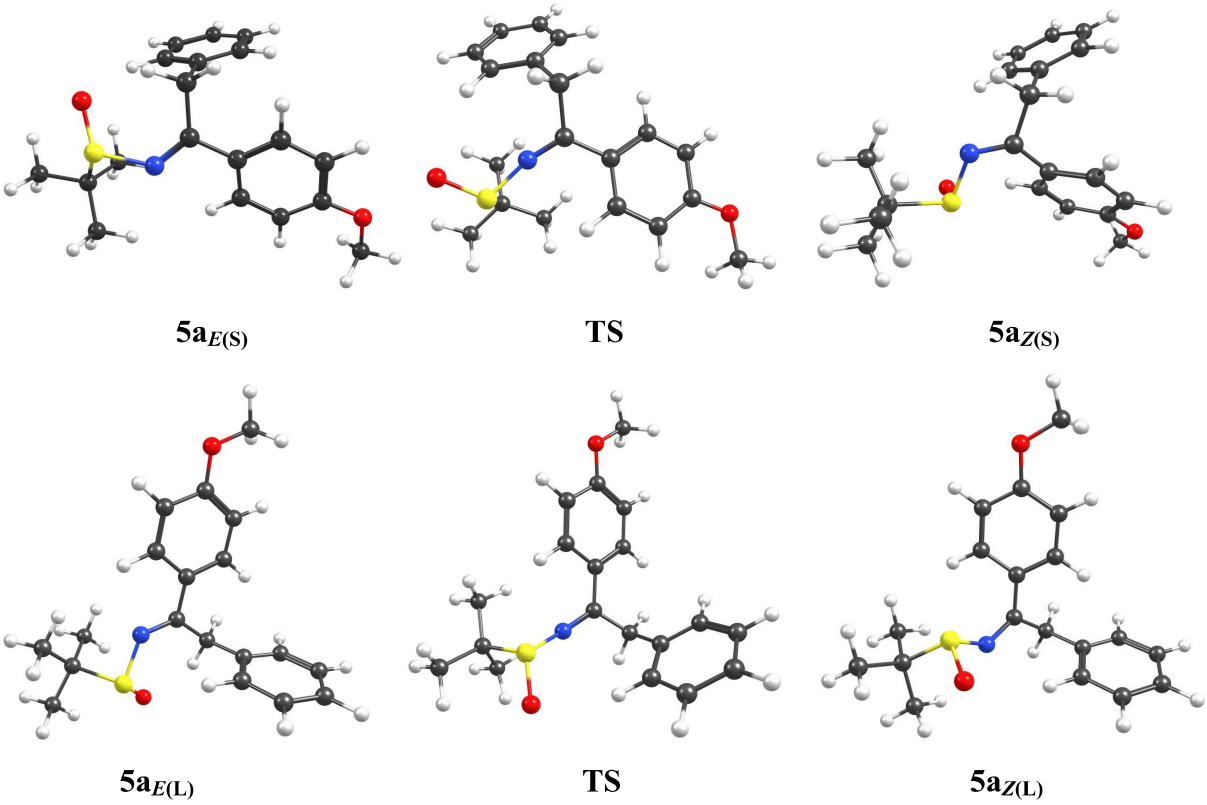

Fig. 3.4: E and Z diastereomer structures and their isomerization transition states

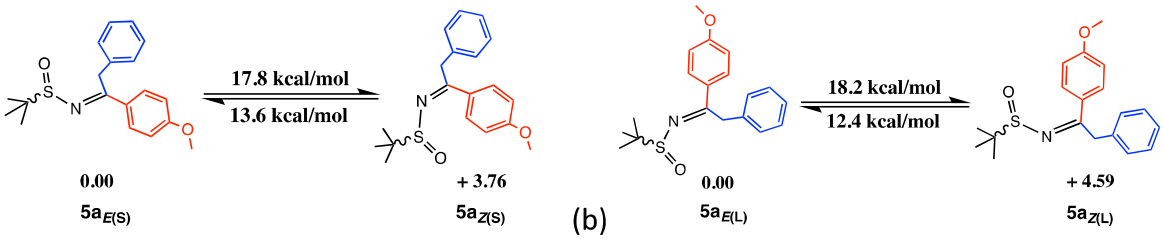

Scheme 3.4: equilibrium equation with interconversion Gibbs free energy barrier for a) **5a$_{E(S)}$** to **5a$_{Z(S)}$** and b) **5a$_{E(L)}$** to **5a$_{Z(L)}$**

3.2 Mechanism and Diastereoselectivity of Nucleophilic Addition of Allylmagnesium bromide to 5a

The nucleophilic addition reaction of the sulfinyl ketimines can occur from either the *re* face or *si* face of the chiral carbon of the ketimine. The allylmagnesium bromide (allylMgBr) addition to **5a** starts in a first step, with the coordination of the Mg of the Grignard reagent to the sulfoxide oxygen of the ketimine, forming a ketimine—allylMgBr complex. In the *Z* isomers of **5a**, the completely out-of-plane S=O group defined by the CNSO dihedral angle of -89.3° and 107.9° for $\mathbf{5a}_{Z(S)}$ and $\mathbf{5a}_{Z(L)}$ ketimines, respectively, moves toward planarity with CNSO dihedral angles of 148.7° and -169.4° for addition at the *re* face and 156.9° and 158.7° for addition at the *si* face. In the *E* isomers, however, an inversion at S atom is pronounced with their dihedral angles changing from 27.6° and -29.4° for S and L, respectively, to 151.7° and 151.2° for addition at the *re* face and 147.8° and -144.2° for addition at the *si* face. The complexation of the ketimine with the allylMgBr occurs via an exothermic process with the energy of formation given in Table 3.4.

From the ketamine—allylMgBr complex, subsequent attack either at the *re* or *si* face of the ketimine follows to form the transition state. Altogether, a total of eight possible route for the addition is seen with emerging transition states of: $\mathbf{5a}_{E(S)\text{-}re}\mathbf{TS}$, $\mathbf{5a}_{E(S)\text{-}si}\mathbf{TS}$, $\mathbf{5a}_{E(L)\text{-}re}\mathbf{TS}$ and $\mathbf{5a}_{E(L)\text{-}si}\mathbf{TS}$ from the *E*-isomer and $\mathbf{5a}_{Z(S)\text{-}re}\mathbf{TS}$, $\mathbf{5a}_{Z(S)\text{-}si}\mathbf{TS}$, $\mathbf{5a}_{Z(L)\text{-}re}\mathbf{TS}$ and $\mathbf{5a}_{Z(L)\text{-}si}\mathbf{TS}$ from the *Z*-isomer (scheme 3.5). An important Mg—N bond is formed at the transition state that is maintained in the structure of the product formed. The coordination of the Mg to N helps in bringing the allyl group and the imine carbon closer for bonding and also help in stabilizing the transition structure. The resulting transition structure is a four- and six-membered ring from the bonding of the Mg with the N and the coordination of the allyl group to the imine carbon (scheme 3.5).

Table 3.4: Enthalpy and free energy of formation of ketamine—allylMgBr complex

Ketimine	ΔH_f	ΔG_f
$5a_{E(S)\text{-}re}$	-45.13	-30.01
$5a_{E(S)\text{-}si}$	-44.44	-29.68
$5a_{E(L)\text{-}re}$	-45.08	-29.44
$5a_{E(L)\text{-}si}$	-44.31	-28.85
$5a_{Z(S)\text{-}re}$	-49.54	-33.56
$5a_{Z(S)\text{-}si}$	-48.30	-32.68
$5a_{Z(L)\text{-}re}$	-49.10	-32.74
$5a_{Z(L)\text{-}si}$	-49.07	-33.90

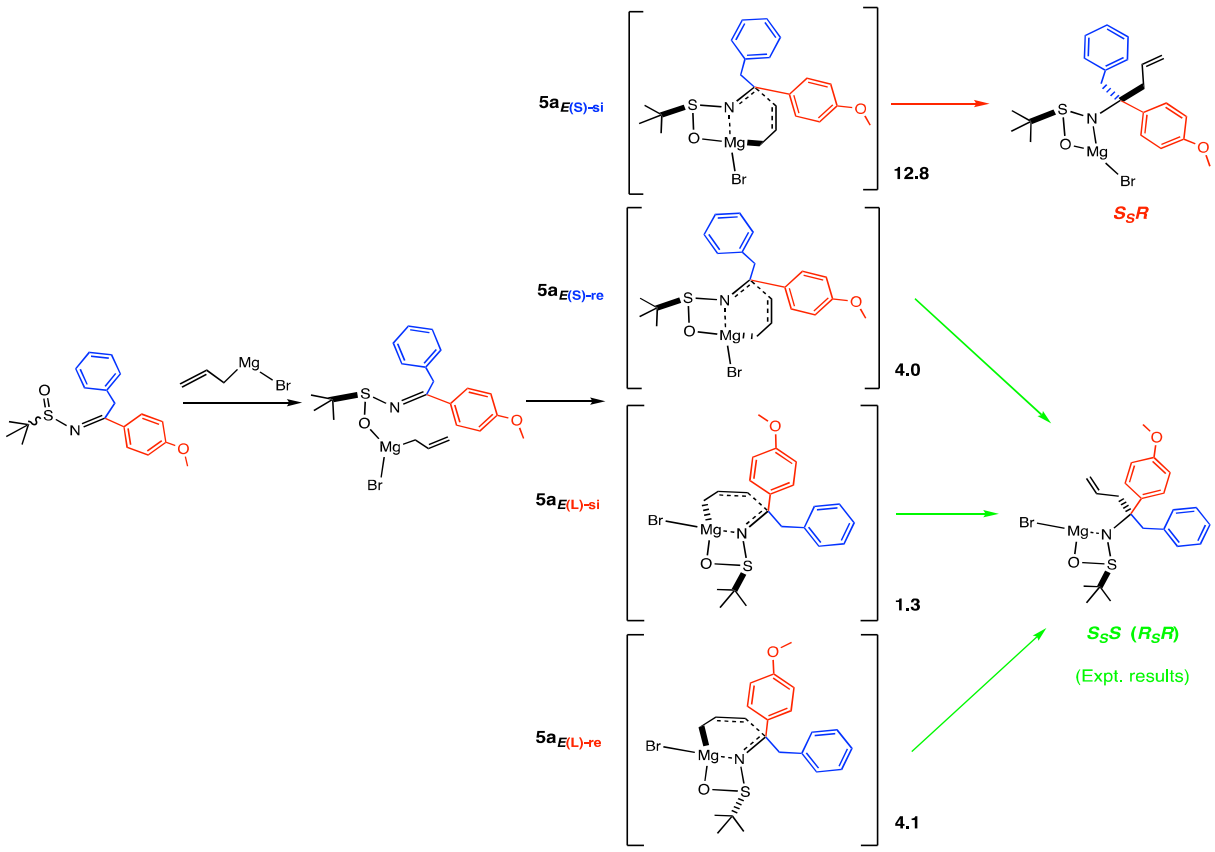

a)

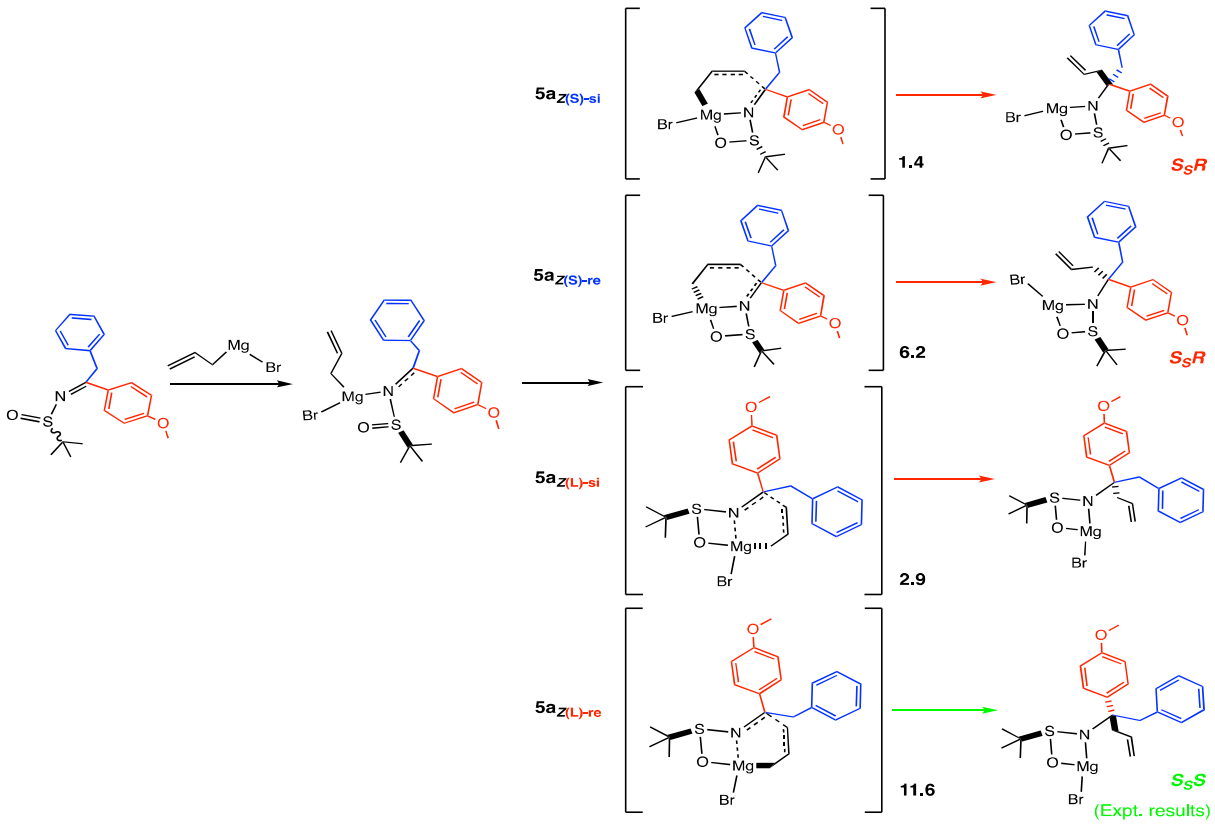

b)

Scheme 3.5: Gibbs free energy profile for the addition of allyMgBr to **5a** (energies in kcal/mol)

With the chiral centre at the imine-carbon, a number of stereoisomer products are possible to obtain. However, not all of the possible products were observed experimentally. The reaction was found to be highly stereoselective (Table 3.1) as performed by Berthiol and Achuenu (unpublished) yielding product with ***S*$_S$*S*** (or ***R*$_S$*R***) conformation. Our results showed four of the eight transition states yielded products corresponding to experimental product, of which three are from the *E*-isomer. The experimental product (***S*$_S$*S*** or ***R*$_S$*R*** conformation) proceeds from reactions involving **5a**$_{E(S)\text{-}re}$**TS, 5a**$_{E(L)\text{-}re}$**TS, 5a**$_{E(L)\text{-}si}$**TS** and **5a**$_{Z(L)\text{-}re}$**TS** transition states with Gibbs energy barrier, $\Delta G^{\ddagger}$ of 4.0, 4.1, 1.3 and 11.6 kcal.mol^{-1}, respectively (Fig. 3.5). The reaction paths that did not yield experimental products were also found to proceed with low $\Delta G^{\ddagger}$ ranging from 1.4 to 12.8 kcal.mol^{-1}, hence the question of the reason for the high stereoselectivity of this reaction. Looking at the stability of the *E* and *Z* isomers, the *E* isomers as previously mentioned are more stable than the *Z* isomers. And despite their existence in equilibrium under room temperature, their Gibbs energy barrier of interconversion from *E* to *Z* isomer (17.8 and 18.2 kcal.mol^{-1} for **5a**$_{(S)}$ and **5a**$_{(L)}$, respectively) are higher than the barriers for the formation of the addition product (Scheme 3.6). This suggests that the mixture with

presumably higher *E*-isomers have higher tendency of going into the addition product than interconverting. A lesser *Z* to *E* interconversion barriers of 13.6 and 12.4 kcal.mol^{-1} for **5a$_{(S)}$** and **5a$_{(L)}$**, respectively, further supports the preference of the *E* isomers over the *Z* isomers. The formation of the products is thermodynamically favoured with the process irreversible as seen by the high negative Gibbs free energy change, ΔG (shown in black digits in scheme 3.6).

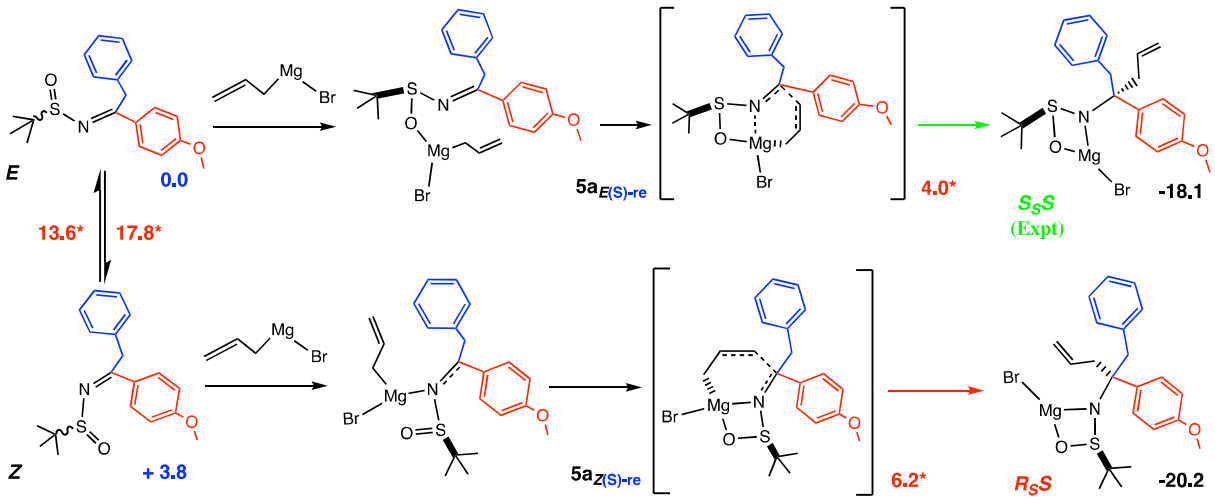

a)

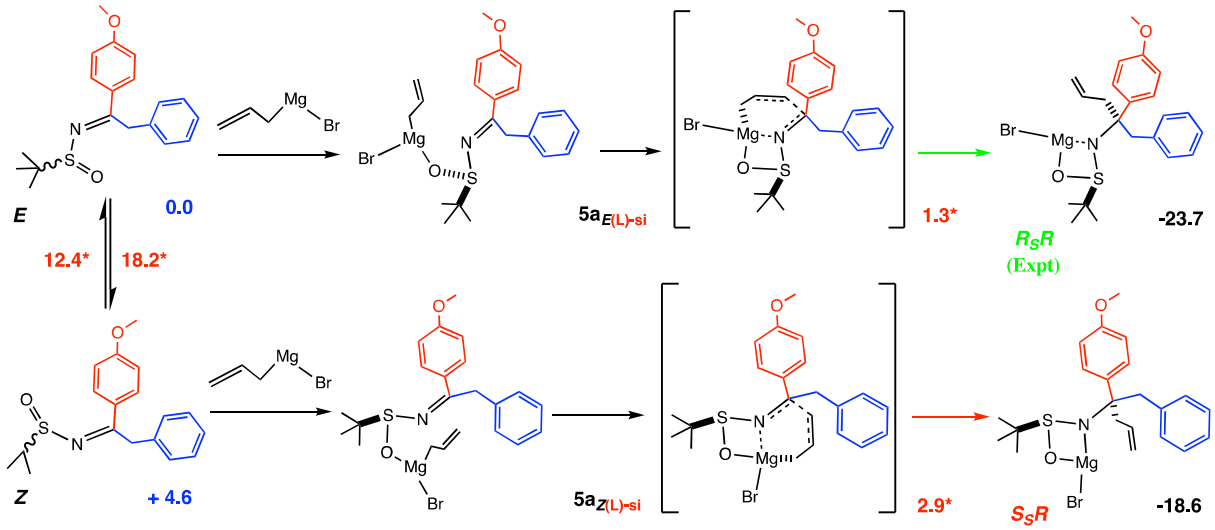

b)

Scheme 3.6: competition of diastereomers interconversion against nucleophilic addition for the reactions of a) **5a$_{(S)}$** and b) **5a$_{(L)}$**; *(all values of are Gibbs free energies in kcal/mol)*

3.3 Nucleophilic Addition of PhLi, MeMgBr to 5a and AllylMgBr, VinylMgBr to 5b

Nucleophilic addition on **5a** with other organometallic compounds such as phenyl lithium (PhLi) and methylmagnessium bromide (MeMgBr) were also calculated. As with allylMgBr, addition proceeds first, by coordination of the metal to the sulfoxide oxygen, then subsequent alkyl or aryl addition to the imine-carbon. A six-membered ring transition structure results as proposed in scheme 3.2. The addition of PhLi in the presence of a Lewis acid, trimethylaluminium ($AlMe_3$) was also calculated with similar six-membered ring transition state and the Lewis acid coordinated to the imine-nitrogen. The PhLi addition with the more stable *E* isomer was found to be favoured than the corresponding *Z* isomer. Reaction with attack on the *re* face (**5a**$_{E(S)\text{-}re}$**TS**) gave the experimental product having an ***S*$_S$*R*** conformation with $\Delta G^{\ddagger}$ of 4.6 kcal.mol^{-1} while attack from the *si* face (**5a**$_{Z(L)\text{-}si}$**TS**) accorded an ***S*$_S$*S*** conformer with a Gibbs barrier of 6.1 kcal.mol^{-1}. The ***S*$_S$*S*** isomer was not obtained experimentally. Addition with MeMgBr recorded high $\Delta G^{\ddagger}$ of 27.9 kcal.mol^{-1} in agreement with the poor experimental yield of only traces of product obtained.

Allyl addition of **5b** followed similar pattern as **5a**. For instance, reactions through **5b**$_{E(S)\text{-}re}$**TS** and **5b**$_{Z(L)\text{-}re}$**TS** paths yielded ***S*$_S$*R*** products corresponding to experimental product with $\Delta G^{\ddagger}$ of 4.9 kcal.mol^{-1} and 10.1 kcal.mol^{-1}, respectively for the *E* and *Z* isomers. Other paths such as through **5b**$_{Z(S)\text{-}si}$**TS** and **5b**$_{E(S)\text{-}si}$**TS** also yielded product with Gibbs energy barriers of 7.4 and 17.7 kcal.mol^{-1}, respectively and products with ***S*$_S$*S*** conformation different from that obtained experimentally. The reasoning for the stereoselectivity obtained in the experimental synthesis instead of a mixture given the low barriers and feasibility of both paths, is similar to that seen in the reaction with **5a**.

A summary of the calculated free energy barriers, $\Delta G^{\ddagger}$ for the nucleophilic reactions discussed thus far is given in Table 3.5. To include solvent effect in our systems a single point calculation was done on the optimized structures with CPCM implicit solvation. The added solvent correction showed an increase in the energy barriers as shown in Table 3.5 (column 5), while maintaining the same trend in the results. This gives an indication of a non-negligible contribution of solvents in the reactions. The high calculated $\Delta G^{\ddagger}$ recorded for vinylMgBr addition (Table 3.5 row 7) despite recorded experiment product is unclear (still under investigation).

Table 3.5: Gibbs free energy for the nucleophilic addition to 5a and 5b

Ketimines	Reagent	Solvent	Barrier kcal.mol^{-1} (Vacuum)	Barrier kcal.mol^{-1} (Solvent)	Product Conf.	Exptal. Yield (%)
5a$_{E(S)\text{-}re}$	AllylMgBr	CH_2Cl_2	4.0	8.1	***S*$_S$*S***	72
5a$_{E(S)\text{-}re}$	PhLi	Toluene	4.6	5.0	***S*$_S$*R***	72
5a$_{E(S)\text{-}re}$	PhLi + $AlMe_3$	Toluene	7.3	8.3	***S*$_S$*R***	81
5a$_{E(S)\text{-}re}$	MeMgBr	THF	27.9	31.4	***S*$_S$*S***	n.r
5b$_{E(S)\text{-}re}$	AllylMgBr	CH_2Cl_2	4.9	8.4	***S*$_S$*R***	83
5b$_{E(L)\text{-}re}$	VinylMgBr	CH_2Cl_2	37.1	42.6	***S*$_S$*R***	41

3.4 Nucleophilic Addition of Allylmagnesium bromide to 6a, 6b and 6c

In this class of α-alkylated sulfinyl imines, **6a**, **6b** and **6c**, the Gibbs free energy difference between the *E* and *Z* isomers is small. **6a**$_Z$ was found to differ in Gibbs energy from **6a**$_E$ by +1.1 kcal.mol^{-1} and **6b**$_Z$ is 2.2 kcal.mol^{-1} higher in Gibbs energy than **6b**$_E$ while **6c**$_Z$ and **6c**$_E$ are nearly equal in energy, about 0.001 kcal.mol^{-1} difference (Table 3.6). These isomers interconvert with ease and exist in equilibrium as in **5a** and **5b** isomers. For instance, the Gibbs energy barrier between **6a**$_E$ and **6a**$_Z$ is 18.6 kcal.mol^{-1} (Table 3.6). But unlike the non-alkylated ketimines **5a** and **5b**, not all faces of these α-alkylated sulfinyl imines are accessible for the nucleophilic addition due to steric hindrance posed by their bulky substituents. Their reaction was also found to favour the path with TS in which the bulky group is in the equatorial position to the sulfoxide group, avoiding 1,3-diaxial interaction (Fig. 3.5). Therefore, in this class of ketimines, the major controlling factor for the addition is steric effect. Paths from **6a**$_{Z(S)\text{-}si}$**TS**, **6b**$_{Z(S)\text{-}si}$**TS** and **6c**$_{E(S)\text{-}re}$**TS** yielded products corresponding to experimental ones with calculated Gibbs energy barriers, $\Delta G^{\ddagger}$ of 4.9, 7.6 and 4.3 kcal.mol^{-1} for **6a**, **6b** and **6c**, respectively. These low barriers however, do not correlate with the low yields obtained experimentally which are traces, 53% and 23% for **6a**, **6b** and **6c**, respectively (Table 3.6). By adding solvent correction by single point calculation with CPCM implicit solvent model, an increase in the Gibbs energy barrier were observed for the ketimines with values of 6.9, 10.4 and 6.9 kcal.mol^{-1} for **6a**, **6b** and **6c**, respectively. Having seen a non-negligible solvent effect by implicit solvation,

inclusion of an explicit THF molecule in addition to the polarizable continuum solvent correction was done (implicit-explicit solvent model) and up to 10 kcal.mol^{-1} increase in energy was recorded (Table 3.7). This huge difference is not surprising given the solvent used in the synthesis, THF, is a highly coordinating solvent. Therefore, the solvent effect in these reactions cannot be underestimated. In solution, up to three THFs can coordinate to the Grignard reagent, allylMgBr resulting in a penta-coordinated Mg atom. As established, the addition reaction involves first the coordination of the Grignard reagent to the sulfoxide oxygen of the ketimine before subsequent nucleophilic attack on the imine-carbon. Therefore, the organometallic reagent will need to have vacant coordination site to allow for the coordination with the sulfoxide oxygen. This may require dissociation of an already coordinated solvent from the organometallic compound (scheme 3.7). The dissociation of the THF solvent molecules is given by the following equilibrium equations:

$$[(C_3H_5)3THF] \rightleftharpoons [(C_3H_5)2THF] + THF \qquad 3.1$$

$$[(C_3H_5)2THF] \rightleftharpoons [(C_3H_5)THF] + THF \qquad 3.2$$

The calculated free energy of dissociation, ΔG of one THF from the tri-solvated allylMgBr (eq 3.1) is 2.3 kcal.mol^{-1}. Dissociation of a second THF occurs with a ΔG of 9.4 kcal.mol^{-1}. But since the energies were calculated in gas-phase at standard state corresponding to 1 atm and the THF molecules is as both solvating and solvated specie (seen from the RHS of equations 3.1 and 3.2), there is need to add the standard state correction for solution (taken as 1M) and the correction for solvent in solvent (same as discussed in Chapter two, section 2.2). The corrected free energy of dissociation, ΔG* of one THF from the tri-solvated allylMgBr is calculated to be 5.6 kcal.mol^{-1} and dissociation of a second THF occurs with ΔG* of 12.8 kcal.mol^{-1}. This suggests that the low yield recorded for this class of sulfinyl imines, **6a**, **6b** and **6c** is due to the effect of the highly coordinating solvent used in this synthesis.

Table 3.6: Energy difference and energy barriers for the isomerization between E and Z isomers of the α-alkylated ketimines

ketimine	Energy Barrier (*E* to *Z*) $\Delta G^{\ddagger}$ (kcal/mol)	Energy Difference ΔG_{Z-E} (kcal/mol)
6a	18.60	1.12
6b	15.20	2.17
6c	18.54	0.00

Table 3.7: Gibbs free energy for the nucleophilic addition to the α-alkylated ketimines

Ketimines	Solvent	Barrier kcal.mol^{-1} (Vacuum)	Barrier kcal.mol^{-1} (Solvent)	Barrier kcal.mol^{-1} (explicit THF)	Product Conf.	Exptal. Yield (%)
6a$_{Z(S)\text{-si}}$	THF	4.9	6.9	9.7	***S*$_S$*RR***	traces
6b$_{Z(S)\text{-si}}$	THF	7.6	10.4	18.0	***S*$_S$*RR***	53
6c$_{E(S)\text{-re}}$	THF	4.3	6.9	12.8	***S*$_S$*RR***	23

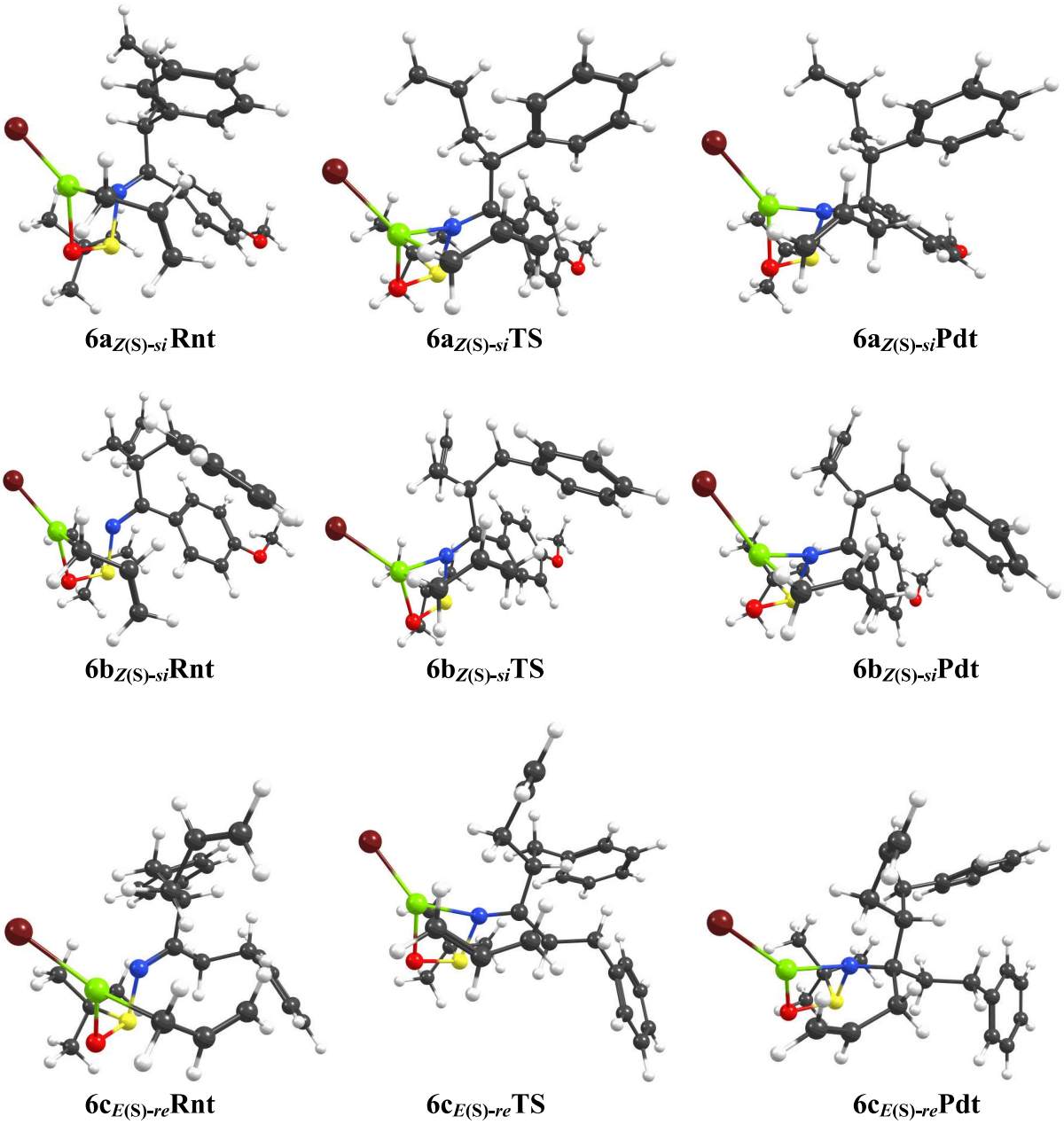

Fig. 3.5: structures of a-alkylated ketimines, **6a**, **6b** and **6c**, showing reactant, TS and product geometries

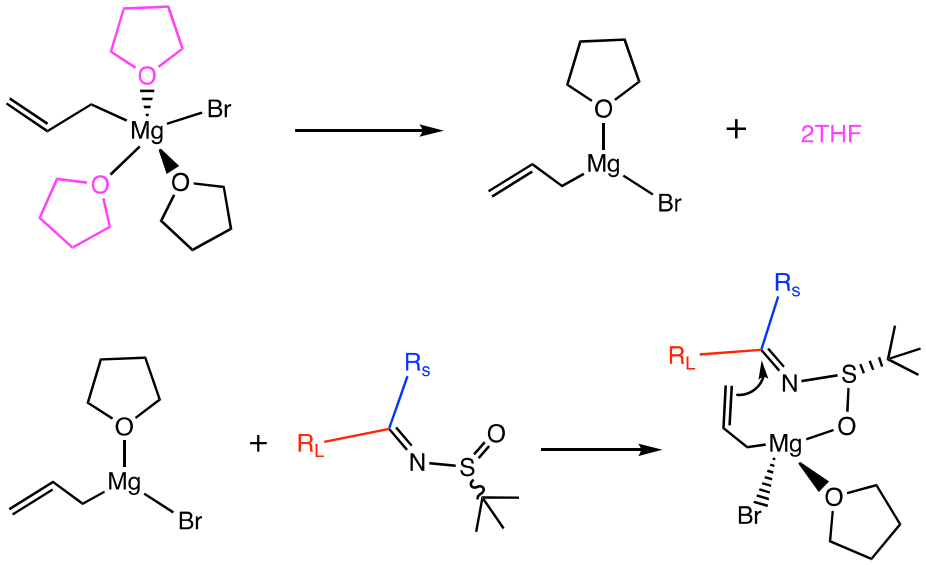

Scheme 3.7: dissociation of coordinated THF on allyMgBr and subsequent complexation with the α-alkylated ketimine

Looking at the addition with **6a**, only traces of the product were obtained far lower than the yield gotten for **6b** and **6c** and given that the same solvent was used for their synthesis, we try to get explanation for the cause of this poor yield with **6a**. On a closer look at the structure of **6a**, the α-proton is more acidic than the α-protons of **6b** and **6c**, therefore there could be competitive α-deprotonation reaction to form azaenolate. A Gibbs free energy barrier, $\Delta G^{\ddagger}$ of 6.8 kcal.mol^{-1} was calculated for the α-deprotonation in **6a**. This shows that the deprotonation reaction is in competition with the addition reaction (energy barrier of 4.9 kcal.mol^{-1}), hence, the poor yield obtained for the addition product of **6a**.

3.5 Conclusion

Here we study by DFT calculations, the nucleophilic addition of polar organometallic compounds to sulfinyl ketimines with chiral centers. We see from the organometallic addition to sulfinyl ketimine that the addition proceeds via first, the coordination of the metal of the organometallic reagent with the sulfoxide oxygen of the ketimine followed by subsequent alkylation at the imine carbon. The sulfinyl ketimines exist as *E* and *Z* isomers in equilibrium with interconversion feasible at room temperature. Despite a wide possible reaction pathways and varied product conformers, stereoselectivity was observed for these reactions from the experimental work. We were able to attribute this selectivity to the stability difference between *E* and *Z* isomers and the favouring of addition over competitive

interconversion between the *E* and *Z* isomers. In the class of α-alkylated sulfinyl ketimines, small energy difference was noted between the *E* and *Z* isomers but yet their reactions also proceeded with good stereoselectivity. For this class of sulfinyl ketimines, the effect of steric repulsion posed by the bulky substituent groups is responsible for the direction of the phase of the nucleophilic attack. The low yield of the product for the α-alkylated sulfinyl imines addition was found to be mainly due to the effect of the highly coordinating THF solvent used in the synthesis. Another, contributing factor to the low yield especially in **6a**, is the competition of addition with the α-deprotonation reaction. With these findings, we keep in perspective the need for explicit solvation for better understanding of the effect posed by the solvent especially while dealing with highly coordinating solvents.

CHAPTER FOUR

4 Nucleophilic Addition of Methyl lithium to Ketones

In an attempt to understand the accomplished reaction of some *s*-block organometallic addition in unconventional media, that is, in the presence of water and at room temperature under air, it is necessary as a first step to understand the mechanism of the reaction in the conventional controlled condition.

With the tendency of MeLi to exist in different aggregate forms, different predominant reactive species have been reported for different reactions. For instance, the addition of MeLi to 2,4-dimethyl-4′-methylmercaptobenzophenone was said to predominantly proceed via the monomeric specie which is in rapid equilibrium with the tetrameric specie in diethyl ether solvent. The mechanism of the reaction was proposed to follow through a four-membered ring transition state (scheme 4.1).[92,93] The reaction of *sec*-butyllithium and n-butyllithium with series of substituted phenyl *sec*-butyl ketones in hydrocarbon solvents were said to proceed predominantly via the tetrameric and hexameric species, respectively.[94]

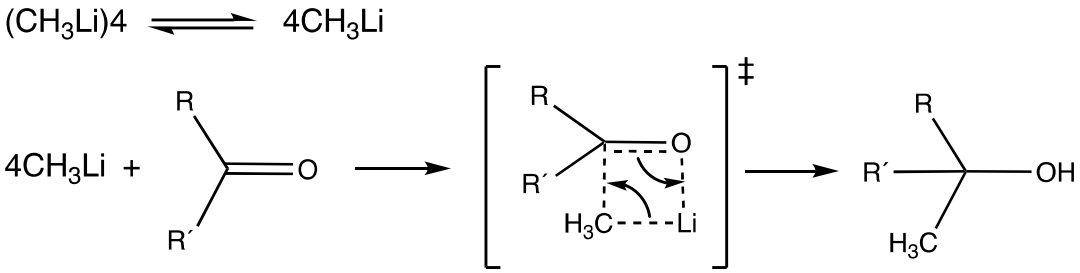

scheme 4.1: proposed mechanism of MeLi monomer addition[92,93]

On the other hand, in THF, McGarrity and co-workers through the use of rapid injection NMR reported that, butyllithium dimer reacts about 10-fold faster than the tetramer with benzaldehyde.[95] This was preceded by a high-field proton NMR study that showed that butyllithium exist in THF predominantly as a tetramer in equilibrium with dimeric specie. No evidence of monomeric specie was found even at low concentration of 10^{-4} M, therefore, ruling out the possibility of the butyllithium addition via a monomer in ether solvents.[96] Dimeric and tetrameric crystals structures of *n*-bityllitium in *N,N,N′,N′*-tetramethylethylenediamine, dimethoxyethane and THF solutions have also been reported.[97] On similarly note, in the study of the reactions of acetone and thioacetone with MeLi, Bailey and Wiberg *et al* noted that DFT calculated low activation free energies for the reaction involving the monomer of MeLi does

not agree with the slow experimental reaction observation, therefore, suggesting the reaction with the monomeric MeLi is not a feasible manner of the addition. Rather, the addition via a dimeric MeLi was found to be more viable. The reaction was said to proceed ionically via a six-membered ring transition state with the carbonyl carbon well aligned for the methyl addition with a Li—O—C angle of 169.7°.[98]

In another DFT study, Giessner-Prettre *et al* reported the reaction of formaldehyde and acetaldehyde with monomeric and dimeric MeLi. They concluded in the study that the reaction followed first by the formation of a stable complex from coordination of the lithium on the carbonyl oxygen with the aldehyde and organolithium coplanar. A transition state follows an out-of-plane rotation of the aldehyde, placing it perpendicular to the C—C forming bond to form a four-membered transition structure. In the dimer, the resulting alcoholate forms part of the MeLi dimer cluster (scheme 4.2).[99] Reaction of the formaldehyde with monomeric unsaturated organolithiums such as vinyl- and phenyllithium, like with MeLi also proceed via rotation of the aldehyde at the transition structure with the unsaturated organolithiums having slightly higher barriers than their counterpart sp^3 MeLi nucleophile. On intermediate bonding of the vinyllithium dimer with the aldehyde, the internuclear angle of the aldehyde and vinyl showed the planes of the vinyl and aldehyde to be fully perpendicular, a pattern similar to the MeLi dimer reported by Giessner-Prettre *et al.* In so doing the proton of the aldehyde is made to interact directly with the π-plane of the vinyl.[100]

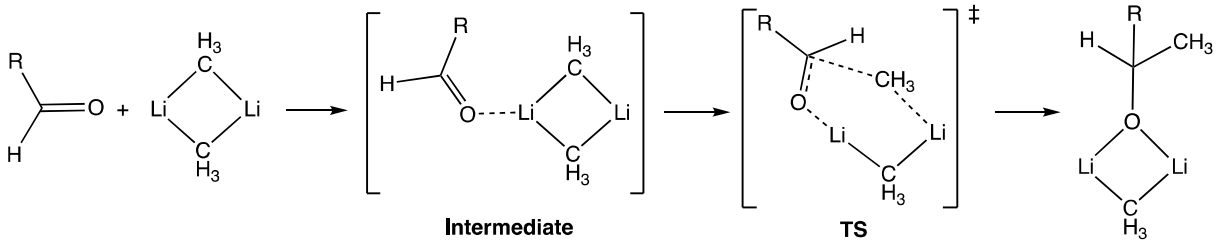

scheme 4.2: proposed mechanism of MeLi dimer nucleophilic addition[99]

Aside from the tendency of organolithium to exist in multiple aggregate forms, another challenge in the understanding of their reactivity is their strong interactions with ethereal solvents, especially diethyl ether and THF. In an early work in trying to account for explicit solvation in MeLi addition, Nakamura *et al* studied by Hartree-Fock calculation with 6-31+G* basis the reaction of a MeLi dimer with aldehyde in the presence of a coordinated water molecule. The solvent is coordinated to the Li ion bearing the formaldehyde. The reaction follows the cleavage of the Li—CH_3 bond assisted by the coordination of the water, resulting in opening of the MeLi dimer and then subsequent attack of the methyl to the carbonyl carbon

forming a six-membered ring transition state.[101] Also, Hæffner and co-workers carried out *ab initio* study at MP2/6-31+G* and HF/6-31+G* the addition of methyl from homo-dimeric MeLi, hetero-dimeric MeLi and NH_2Li as well as hetero-trimer of MeLi and two NH_2Li, to formaldehyde. Water molecule or methanol is coordinated to the Li ions. But unlike the study by Nakamura *et al,* the reported mechanism for the homo-dimer followed a concerted close-dimeric path with the polar solvents. In considering the effect of the coordinated solvent in the reaction, addition involving the hetero-dimer with the water bonded to the aldehyde-coordinated lithium proceeds via an open-dimer (non-concerted) mechanism with the water molecule stabilizing the Li ion allowing for cleavage of the methyl. On the other hand, the reaction with the water coordinated to the Li ion not bonded to the formaldehyde (homogeneous Li ion coordination) follows a concerted mechanism (close-dimer mechanism). The energy barrier for concerted mechanism was said to be 5 kcal mol^{-1} lower than the nonconcerted mechanism. Similar pattern was also noted with the hetero-trimer. They also reported that the homo-dimer MeLi structure with water molecule coordinated to the aldehyde-coordinated lithium is about 3.2 kcal mol^{-1} higher in energy than the corresponding structure with the water on the other lithium. This suggested that the homogeneous coordination of the Li ions and therefore the concerted mechanism is more probable. [102]

The effect of solvation especially highly coordinating solvent such as diethyl ether (Et_2O or simply referred as ETH) and THF in our case cannot be neglected. Therefore, we studied the mechanism of the MeLi nucleophilic addition to 4-chlorobutyrophenone (herewith, referred to as γ-chloroketone or simply chloroketone) with explicit solvent molecules by the hybrid QM/MM molecular dynamics with the well-tempered metadynamics enhanced-sampling method. We as a preliminary step performed the mechanism study on the simple ketone molecule, acetone to make comparison with our bulkier ketone and also as a first step in choosing a well representative collective variable(s) for the metadynamics. With the understanding of the mechanism of the reaction and the effect and role of solvents in our reaction we will be able to proceed in studying the unconventional "on water" reaction.

4.1 Mechanism of Nucleophilic Addition of MeLi on Ketone in Implicit Solvent

The nucleophilic addition reaction mechanism was studied by the DFT method using the combined Becke exchange and Lee-Yang-Parr functional, BLYP with def2-TZVPP basis set. The dispersion effects were accounted for by the D3BJ correction. Solvent effects were added

via implicit solvation with solvation model based on quantum mechanical charge density of the molecular system interacting with a continuum definition of the solvent (referred to as the SMD model). Explicit solvent molecules are coordinated to the Li^+ ions of the ketone—MeLi complexes based on established solvation state of the complexes in solvents as discussed in Chapter two (Fig 4.1). Intrinsic reaction coordinate calculation was performed on the optimized TS structures to confirm the reaction pathway ensuring the minimum energy reaction pathway was followed.

The addition first involves the complexation of the ketone with the methyl lithium aggregate by docking of the ketone on the aggregate through CO—Li bonding. The resulting complex undergoes geometrical transition leading to the addition of the methyl on the carbonyl carbon. In describing the manner of approach between the methyl group and the carbonyl compound, the interplanar angle between the plane of the methyl lithium and the plane of the ketone is measured (Fig 4.2). An interplanar angle around 90° indicate a parallel approach between the ketone and methyl lithium while an interplanar angle around 0° indicates the nucleophilic attack of the methyl lithium is in the direction perpendicular to the plane of the ketone. According to the Bürgi-Dunitz trajectory,[103–105] nucleophilic attack to carbonyl compound occurs through a trajectory perpendicular to the π-plane of the carbonyl group. In a typical Bürgi-Dunitz trajectory, along the reaction pathway, the bond angle C^1C^2O is about 105 ± 5° and the dihedral angle $C^1C^2OC^3$ is about 90°.

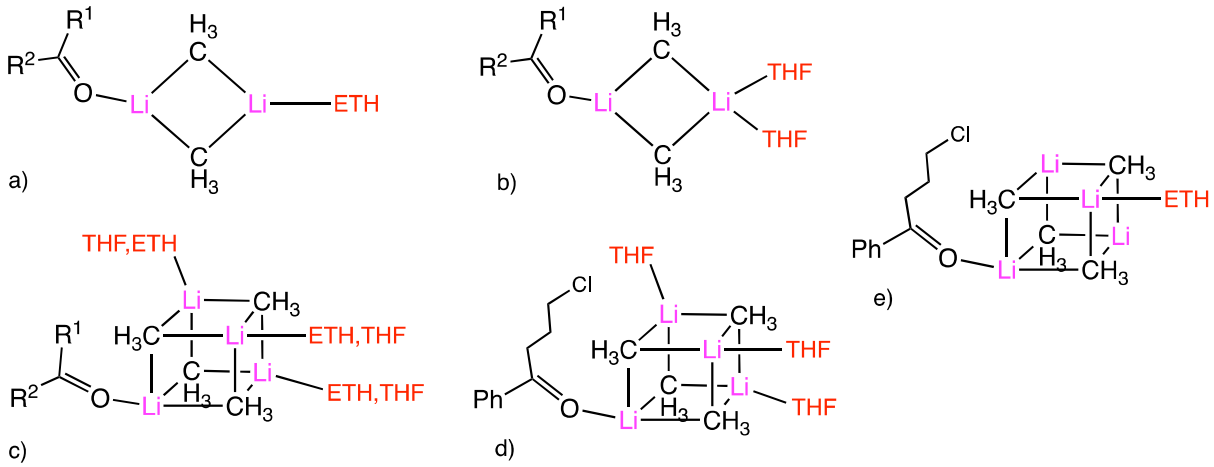

Fig. 4.1: Solvation of a) ketone—$(MeLi)_2$ in diethyl ether (R^1=CH3, R^2=CH3 for acetone and R^1=Ph, R^2=*(CH2)$_3$Cl for γ-chloroketone*) b) ketone—$(MeLi)_2$ in THF (R^1=CH_3, R^2=CH_3 for acetone and R^1=Ph, R^2=$(CH2)_3Cl$ for γ-chloroketone) c) ketone—$(MeLi)_4$ in diethyl ether and THF (R^1=CH_3, R^2=CH_3) d) γ-chloroketone—$(MeLi)_4$ in THF e) γ-chloroketone—$(MeLi)_4$ in diethyl ether

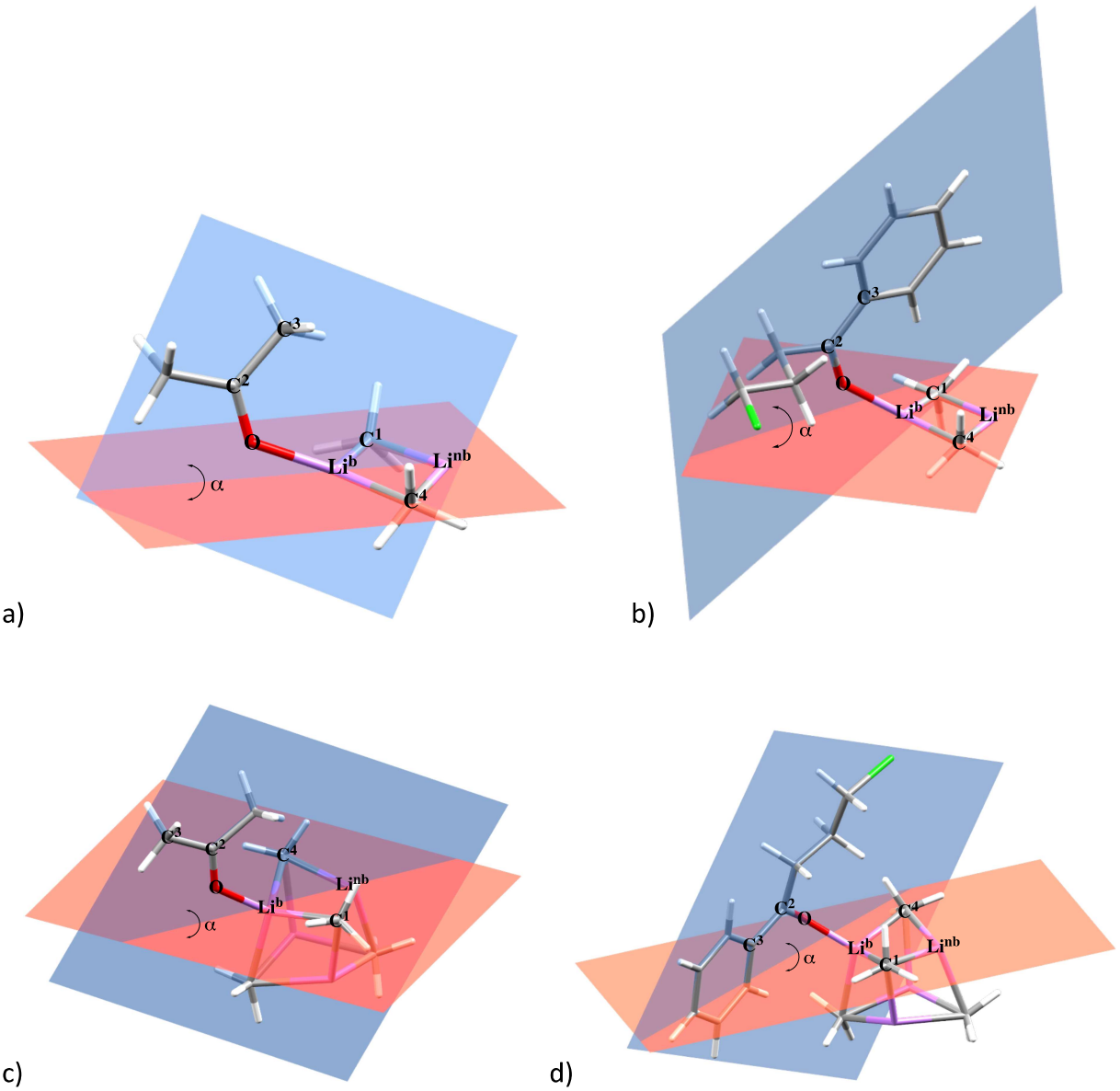

Fig. 4.2: structures of ketone—MeLi complexes showing the planes of the ketone and the MeLi aggregate with the labels of the atoms defining the geometric parameters

4.1.1 Nucleophilic Addition of MeLi Dimer on Acetone and 4-chlorobutyrophenone

As already established, the reaction starts with the docking of the ketone on the methyl lithium dimer to form the ketone—dimer complex. The complexation occurred along the carbonyl oxygen. For the acetone addition, the complexation occurred with complexation angle, C^2—O—Li^b of about 127° and 129° for the reaction with coordinated diethyl ether solvent and THF solvent, respectively (Table 4.2). The complexation occurred in the plane of the acetone, indicated by the $C^3C^2OLi^b$ torsional angle of 2 and 4° for the addition in diethyl ether and THF, respectively. The carbonyl group of the acetone is out-of-plane with the bonding MeLi unit of the methyl lithium dimer aggregate. This is defined by the $C^2OLi^bC^1$ dihedral angle. In diethyl

ether, the $C^2OLi^bC^1$ dihedral angle is measured to be about 74° and similarly a value of 74° was also measured for the reaction in THF. The interplanar angle (α) between the plane of the acetone defined by the carbons and oxygen of the acetone, and the plane of the methyl lithium dimer defined by the methyl carbons and lithium ions was measured. The values of the interplanar angle for the acetone addition reaction in diethyl ether and THF are 85 and 82°, respectively. This showed that the plane of the acetone is about perpendicular to the plane of the methyl lithium aggregate. The interaction energy between the acetone and the methyl lithium aggregate through the C=O—Li bond was calculated by SAPT method to be 14.6 kcal mol^{-1} in Et_2O and 14.2 kcal mol^{-1} in THF (Table 4.1). The complexation was found to be dominated by electrostatic attraction between the acetone and MeLi aggregate which is partially cancelled by the repulsive exchange interaction. Other minor contribution to the interaction are from the induction and dispersion interaction energies.

The addition reaction followed through a transition state resulting from the rotation of the acetone about the carbonyl group (C=O) in the MeLi—acetone complex and simultaneously from the bending of the C^2—O—Li^b bonding angle (Fig. 4.3). The rotation can be seen from the change in the $C^3C^2OLi^b$ dihedral angle from 2 and 4° in the MeLi—acetone complex (reactant) to 106 and 103° at the TS for the reaction in diethyl ether and THF, respectively. In the same vein, the C^2—O—Li^b angle decreases from 127 and 129° at the reactant to 92 and 92° at the TS for the reaction in diethyl ether and THF, respectively. At the TS, the carbonyl group of the acetone reorients to be in-plane with the bonding MeLi unit shown by the $C^2OLi^bC^1$ dihedral angle of about 2° for both reactions in diethyl ether and THF. The value of the interplanar angle, α between the plane of the acetone and the plane of the methyl lithium dimer for the reaction in diethyl ether and THF, respectively, are measured to be 52 and 65°. This indicates that the attack of the methyl on the carbonyl carbon occurred in a direction somewhat parallel to the plane of the acetone (from the value of α) and perpendicular to the carbonyl plane (from the value of $C^2OLi^bC^1$ dihedral). This is direction of attack is consistent with that reported for the dimeric MeLi addition on formaldehyde by Hæffner and co-workers.[102] The parameters C^1—C^2—O bond angle and $C^1C^2OC^3$ improper torsional angle defining the Bürgi-Dunitz trajectory for nucleophilic additions were measured. The values of 109 and 106° were measured for the C^1—C^2—O bond angle in diethyl ether and THF reactions. This is in agreement with the expected value of 105 ± 5° for a typical Bürgi-Dunitz trajectory for nucleophilic additions. The $C^1C^2OC^3$ dihedral angles of 104 and 101° were measured for the diethyl ether and THF reactions, respectively, which is higher than the ideal value of 90°. The geometric parameters

for the TS are given in Table 4.3. The addition product has the carbonyl oxygen bonded to the two Li^+ ions, taking the initial bonding site of the added methyl group. The C^1—C^2—O angle has a value of 109 ± 1° expected for an sp^3 tetrahedral carbon. The calculated free activation energy, $\Delta G^{\ddagger}$ for the nucleophilic MeLi dimer addition on acetone in diethyl ether is 9.58 kcal mol^{-1} while in THF, the calculated $\Delta G^{\ddagger}$ value is 8.69 kcal mol^{-1}. The lower free energy barrier in the THF reaction might be attributed to the coordination of two THF molecules on the lithium ion not bonded to the acetone (Li^{nb}) in comparison to one diethyl ether molecule. The two oxygen molecules of the THF solvents increase the crowdedness at the Li^{nb} resulting in elongation of the Me—Li bond thereby enhancing ease of cleavage of the leaving methyl nucleophile for the addition. This is evident in the longer Li—Me bond of about 2.62 Å in the THF solvated MeLi—acetone complex compared to 2.28 Å in the diethyl ether complex (Table 4.4).

The methyl lithium dimer addition to γ-chloroketone follow similar pattern to the acetone addition. Like with acetone, the complexation of the γ-chloroketone occurred through the carbonyl oxygen with C^2—O—Li^b angle of 140° and 132° for the reaction with coordinated diethyl ether and THF solvent, respectively. Also, the carbonyl group of the ketone is not in-plane with the bonding MeLi unit of the dimer ($C^2OLi^bC^1$ of 94 and 98° for diethylether and THF addition, respectively). But unlike in acetone, the complexation of the γ-chloroketone does not occurred in the plane of the ketone as seen from a $C^3C^2OLi^b$ torsional angle of 27 and 170° for the addition in diethyl ether and THF, respectively. The interaction energy between the ketone and the MeLi aggregate calculated by SAPT is given in Table 4.1. The interaction energy of the aggregate with the γ-chloroketone was found to be higher than with acetone (about 17 and 16.2 kcal mol^{-1} in Et_2O and THF, respectively for γ-chloroketone against 14.6 and 14.2 kcal mol^{-1} for acetone). A lower interplanar angles, α between the plane of the γ-chloroketone (defined by all its heavy atoms) and the plane of the methyl lithium dimer was recorded in comparison to that in the acetone system. The values of α here are 66 and 79°, respectively, for diethyl ether and THF solvated systems compared to 82 and 85° for acetone addition.

Like in the acetone reaction, the TS occurred via the bending of the C^2—O—Li^b bonding angle and the rotation about the C=O bond of the γ-chloroketone. The C^2—O—Li^b angle decreasing from 140 and 132° at the reactant to 95 and 91° at the TS while the π-plane of the carbonyl group of the ketone becomes in-plane with the bonding MeLi unit of the dimer ($C^2OLi^bC^1$ dihedral of 8 and 1° for the reaction in diethyl ether and THF, respectively). The interplanar angle, α measured for reaction in diethyl ether is 18° much lower than that observed in the THF

reaction ($\alpha = 67°$). The direction of the nucleophilic attack in diethyl ether leans towards a perpendicular direction while the attack occurs in a more parallel direction to the plane of the γ-chloroketone in THF. The Bürgi-Dunitz angles C^1—C^2—O and $C^1C^2OC^3$ have values of 108 and 100° for the addition in diethyl ether and values of 106 and 97° for the THF reaction. Like with acetone, the γ-chloroketone addition follows via the Bürgi-Dunitz trajectory with regards to the C^1—C^2—O angle but a higher $C^1C^2OC^3$ torsional angle compared to the ideal Bürgi-Dunitz trajectory in both solvents. A lower $\Delta G^{\ddagger}$ for the THF reaction in comparison to the diethyl ether reaction may be expected due to higher coordination number on the Li^{nb} from solvent coordination which facilitates the release of the methyl group from the aggregate for addition on the ketone. However, a very low value of $\Delta G^{\ddagger}$ for the reaction in THF was obtained (5.83 kcal mol^{-1}) compared to 12.04 kcal mol^{-1} in Et_2O reaction. It is not clear why such very low value was obtained for the THF reaction. This is still under investigation.

The geometric parameters for the γ-chloroketone — dimer complex and TS are given is Table 4.2 and Table 4.3.

Table 4.1: Interaction energy (kcal/mol) of MeLi dimer and ketone through O—Li bond forming $(MeLi)_2$—ketone complex

Complex	Elst.	Exch.	Ind.	Disp.	Total
Acetone—$(MeLi)_2$ in ETH	-22.05	11.23	-1.05	-2.69	-14.57
Acetone—$(MeLi)_2$ in THF	-23.22	11.40	1.08	-3.43	-14.16
Chloroketone— $(MeLi)_2$ in ETH	-23.63	12.89	-1.67	-4.55	-16.96
Chloroketone— $(MeLi)_2$ in THF	-21.60	12.99	-2.60	-5.04	-16.24

Table 4.2: Geometric parameters in the $(MeLi)_2$—ketone complexes

Complex	C^2OLi^b (°)	$C^2OLi^bC^1$ (°)	$C^3C^2OLi^b$ (°)	α (°)
Acetone—$(MeLi)_2$ in ETH	127	-74	2	85
Acetone—$(MeLi)_2$ in THF	129	-74	-4	82
Chloroketone— $(MeLi)_2$ in ETH	140	-94	27	66
Chloroketone— $(MeLi)_2$ in THF	132	-98	170	79

Table 4.3: Geometric parameters of the TS for the MeLi dimer addition on the ketones

System	C^2OLi^b (°)	$C^2OLi^bC^1$ (°)	$C^3C^2OLi^b$ (°)	α (°)	C^1C^2O (°)	$C^1C^2OC^3$ (°)	$\Delta G^{\ddagger}$ kcal/mol
Acetone—$(MeLi)_2$ in ETH	92	2	-106	52	109	104	9.58
Acetone—$(MeLi)_2$ in THF	92	2	-103	65	106	101	8.69
Chloroketone—$(MeLi)_2$ in ETH	95	-8	107	18	108	-100	12.04
Chloroketone—$(MeLi)_2$ in THF	91	-1	-97	67	106	97	5.83

A closer look at the correlation of the C—C bond distances at TS for the addition with the Li—C distances and the O—Li distance defining the complexation of the ketone with the MeLi aggregate is given in Table 4.4 for the dimer addition on acetone and γ-chloroketone in both Et_2O and THF solvents. As expected the TS is marked with the elongation of the Li^{nb}—C^1 distance indicating the concurrent cleavage of the Me—Li bond with the C—C bond formation. The complexation bond, O—Li^b remains unbroken at the TS.

Table 4.4: C—C, O—Li and Li—C bond distances (in Å) at TS

System	C^1-C^2	O-Li^b	Li^b-C^1	Li^{nb}-C^1	Li^b-C^4	Li^{nb}-C^4
Acetone—$(MeLi)_2$ in ETH	2.43	1.82	2.18	2.28	2.13	2.09
Acetone—$(MeLi)_2$ in THF	2.57	1.85	2.13	2.62	2.11	2.14
Chloroketone— $(MeLi)_2$ in ETH	2.34	1.82	2.21	2.42	2.11	2.11
Chloroketone— $(MeLi)_2$ in THF	2.64	1.86	2.14	2.70	2.11	2.13

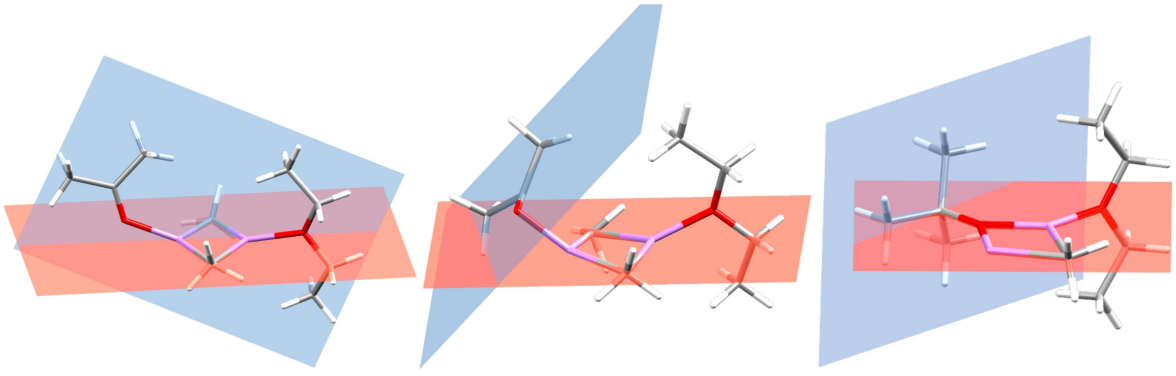

Reactant **TS** **Product**

Fig. 4.3: geometrical transition and interplanar angle of MeLi dimer addition on acetone

4.1.2 Nucleophilic Addition of MeLi Tetramer on Acetone and 4-chlorobutyrophenone

The nucleophilic addition of MeLi tetramer follows similar path as the dimer addition. First the docking of the ketone on the MeLi aggregate. Like with the dimers, the complexation was found to be dominated by electrostatic attraction between the acetone and MeLi aggregate with contributions from the induction and dispersion interactions. The repulsive exchange interaction only partially cancelled out these interactions (Table 4.5). With the bending of the C^2—O—Li^b angle and the rotation about the carbonyl group, the methyl nucleophile is added unto the carbonyl carbon of the ketone.

In the acetone addition reaction, the complexation of the acetone on the tetramer occurred in the plane of the acetone. The complexation angle, C^2—O—Li^b and torsional angle, $C^3C^2OLi^b$ defining the plane of complexation of the acetone on the Li^+ ion were measured to be 129 and 1°, respectively in diethyl ether solvated system and 130 and 0° in the THF solvated acetone—$(MeLi)_4$ complex. Measurement of the $C^2OLi^bC^1$ dihedral angle showed the reactive carbonyl group of the acetone is not in the plane of the MeLi unit that will come to participate in the methyl addition. The $C^2OLi^bC^1$ dihedral angle is 58 and 62° in diethyl ether and THF reaction, respectively. The plane of the acetone is nearly perpendicular to the plane of the MeLi aggregate (defined by atoms Li^b, C^1, Li^{nb} and C^4, Fig 4.2c) in the THF solvated acetone—$(MeLi)_4$ complex (α = 88°) while in diethyl ether, the interplanar angle is 43° (Table 4.6). The approach of the methyl nucleophile to the carbonyl carbon is in the direction nearly parallel to the plane of the acetone. This is observed from the measured α of 60 and 67° for reactions in diethyl ether and THF, respectively at the TS. At the TS, the reactive carbonyl group and MeLi unit move towards planarity ($C^2OLi^bC^1$ = 2 and 12° in diethyl ether and THF, respectively). Like in the dimer addition, the C^1—C^2—O angle (values of 109° in both solvents) is consistent with the Bürgi-Dunitz trajectory for the nucleophilic approach while the recorded $C^1C^2OC^3$ dihedral angles of 108 and 109° for diethyl ether and THF reactions, respectively, are higher than the ideal expected values (90°) in the Bürgi-Dunitz trajectory. The measured geometric parameter at the TS are given in Table 4.7. The TS reveals concurrent cleavage of the Me—Li bond with the C—C bond formation. This is marked with the elongation of the Li^{nb}—C^1 distance (Table 4.8).

The MeLi tetramer addition on γ-chloroketone exhibit somewhat different geometrical parameters from the acetone addition in the MeLi—ketone complex and the TS. Here, the carbonyl group of the ketone is nearly in-plane with the bonding MeLi unit in the ketone—$(MeLi)_4$ complex ($C^2OLi^bC^1$ = 17 and 7° for the diethyl ether and THF addition, respectively).

The ketone—$(MeLi)_4$ complexation angle, C^2—O—Li^b is 142 and 134° respectively, in diethyl ether and THF. The complexation of the Li^+ ion on the ketone does not occur in the plane of the ketone ($C^3C^2OLi^b$ dihedrals of 125 and 86° in diethyl ether and THF, respectively). Similar to the acetone addition, the methyl nucleophile approach the γ-chloroketone from a nearly parallel direction to the plane of the ketone (α = 73 and 75° for diethyl ether and THF reaction, respectively). At TS, the π-plane of the carbonyl group of the ketone remains in-plane with the bonding MeLi unit of the tetramer ($C^2OLi^bC^1$ = 11 and 2° for the diethyl ether and THF addition, respectively). The nucleophilic addition in diethyl ether does not follow the typical Bürgi—Dunitz trajectory (C^1—C^2—O = 113° and C^1C^2OC = 100°) and the geometric transformation leading to the addition is mainly by rotation about the C=O bond. This is drawn from the fact that the C^2—O—Li^b angle is 142° at the reactant and 144° at the TS while the $C^3C^2OLi^b$ dihedral is 125° at reactant and 87° at the TS. The case is different in THF. The C^2—O—Li^b bending is the major geometric transformation. The C^2—O—Li^b is 134° at reactant and 93° at TS while $C^3C^2OLi^b$ dihedral is 86° at reactant and 98° at the TS. The interplanar angle, α is 45° in diethyl ether reaction and 55° in THF reaction.

Like in the acetone addition, the complexation bond, O—Li^b remains unbroken at the TS. As expected, the TS geometry is marked with the elongation of the Li—C distance indicating the concurrent cleavage of the Me—Li bond with the C—C bond formation (concerted mechanism). In the tetramer addition of the γ-chloroketone in Et_2O, the cleavage occurred at the Li^b—C^1 bond instead of at the Li^{nb}—C^1 bond observed in the other additions. The correlation of the C—C bond distances at TS for the addition with the Li—C distances and the O—Li distance is given in Table 4.8 for the tetramer addition in both Et_2O and THF solvents.

The calculated free energy barrier of this MeLi tetramer addition is given in Table 4.7. For the addition on acetone the calculated free energy barrier is 14.70 kcal mol^{-1} in diethyl ether and 14.05 kcal mol^{-1} in THF. The similar barriers exhibited for the reaction in both solvents correlates with the homogeneous coordination number of the Li^+ ions of the tetramer in both diethyl ether and THF solvents. Each Li^+ ions other than the lithium bonded to the acetone (Li^b) is bonded a solvent molecule. For the MeLi tetramer addition on γ-chloroketone on the other hand, the MeLi tetramer are solvated differently in the diethyl ether and THF (Fig 4.1). For the diethyl ether-solvated reaction in which only one diethyl ether molecule is coordinated to the MeLi tetramer cluster, the calculated free energy barrier, $\Delta G^{\ddagger}$ is 14.72 kcal mol^{-1} while the free energy barrier for the reaction in THF where the Li^+ ions are homogeneously solvated is calculated to be 10.40 kcal mol^{-1}. The lower energy barrier in the THF solvated tetramer

addition may be attributed to the higher solvent coordination in comparison to the diethyl ether solvated tetramer. A loss of methyl group leaves the Li^+ with a coordination number of 3 in the THF solvated aggregate contrary to the diethyl ether solvated aggregate which will leave a coordination number of 2. Therefore, an ease of loss of methyl in the THF solvated system than the diethyl ether system.

Table 4.5: Interaction energy (kcal/mol) of MeLi tetramer and ketone through O—Li bond forming $(MeLi)_4$—ketone complex

Complex	Elst.	Exch.	Ind.	Disp.	Total
Acetone—$(MeLi)_4$ in ETH	-19.52	11.90	-1.05	-5.39	-14.07
Acetone—$(MeLi)_4$ in THF	-20.91	12.98	-0.58	-5.60	-14.10
Chloroketone— $(MeLi)_4$ in ETH	-19.24	11.87	-0.98	-6.30	-14.65
Chloroketone— $(MeLi)_4$ in THF	-18.20	11.22	0.07	-7.21	-14.12

Table 4.6: Geometric parameters and interaction energy of the $(MeLi)_4$—ketone complexes

Complex	C^2OLi^b (°)	$C^2OLi^bC^1$ (°)	$C^3C^2OLi^b$ (°)	α (°)
Acetone—$(MeLi)_4$ in ETH	129	58	-1	43
Acetone—$(MeLi)_4$ in THF	130	-62	0	88
Chloroketone— $(MeLi)_4$ in ETH	142	-17	125	73
Chloroketone— $(MeLi)_4$ in THF	134	-7	-86	75

Table 4.7: Geometric parameters of the TS for the MeLi tetramer addition on the ketones

System	C^2OLi^b (°)	$C^2OLi^bC^1$ (°)	$C^3C^2OLi^b$ (°)	α (°)	C^1C^2O (°)	$C^1C^2OC^3$ (°)	$\Delta G^{\ddagger}$ kcal/mol
Acetone—$(MeLi)_4$ in ETH	93	-2	-106	60	109	108	14.70
Acetone—$(MeLi)_4$ in THF	92	-12	-98	67	109	109	14.05
Chloroketone—$(MeLi)_4$ in ETH	145	-11	-87	45	113	103	14.72
Chloroketone—$(MeLi)_4$ in THF	93	-2	-98	55	109	100	10.40

Table 4.8: C—C, O—Li and Li—C bond distances (in Å) at TS

System	C^1-C^2	O-Li^b	Li^b-C^1	Li^{nb}-C^1	Li^b-C^4	Li^{nb}-C^4
Acetone—$(MeLi)_4$ in ETH	2.46	1.88	2.21	2.95	2.25	2.14
Acetone—$(MeLi)_4$ in THF	2.45	1.88	2.21	2.89	2.29	2.14
Chloroketone— $(MeLi)_4$ in ETH	2.38	1.81	3.90	2.41	2.19	2.16
Chloroketone— $(MeLi)_4$ in THF	2.50	1.89	2.24	2.47	2.28	2.18

4.2 Nucleophilic Addition of MeLi in Explicit Solvation

To study the mechanism of the nucleophilic addition in solvents, molecular dynamic simulation was carried out. The hybrid QM/MM method was employed where the reactive methyl lithium cluster and the ketone (acetone, γ–chlorophenone) are embedded in a solvent box (diethyl ether or THF) with period boundary condition and treated at the DFT level with BLYP functional and DZVP-MOLOPT basis. The solvent molecules are treated at the classical level with their force potential defined using the generalized AMBER forcefield, GAFF. Since the formation of the C—C bond is a rare event and cannot be attained in practical time by the simple molecular dynamics, a well-tempered metadynamic enhanced- sampling method was used to study these reactions in the explicit solvent box and the free energy surface in the direction of the selected collective variable was constructed from which the free energy barrier for the C—C bond formation is calculated. The parameters for the metadynamics Gaussian bias potential, biasfactor for the well-tempered, and the selected collective variables are detailed in section 2.7 of Chapter one.

To follow the mechanism of this addition reaction, the evolution of some specific geometrical parameters and solvent coordination were studied. The evolution of C^1OLi^b angle was measure. This angle is an important geometrical parameter for the approach of the methyl to the carbonyl carbon as seen from the previous DFT calculation in section 4.1, therefore, it was chosen as a second collective variable in addition to the C^1—C^2 bond distance. Here, C^1 is the methyl carbon, C^2 is the carbonyl carbon and Li^b denotes the lithium ion coordinated to the carbonyl oxygen, O while Li^{nb} represents the lithium(s) not bonded to the ketone but rather to the solvent in most cases as will be discussed (Fig 4.4). The bond angle C^1C^2O and the improper dihedral angle $C^1C^2OR^1$ defining the Bürgi-Dunitz trajectory that shows the plane of the carbonyl group with respect to the plane of the methyl group were also measured. Other measured geometrical

parameters are the $R^1C^1OLi^b$ and $C^2OLi^bC^1$ dihedral angles. Reactions in diethyl ether are denoted by ETH while those in tetrahydrofuran are tag with THF.

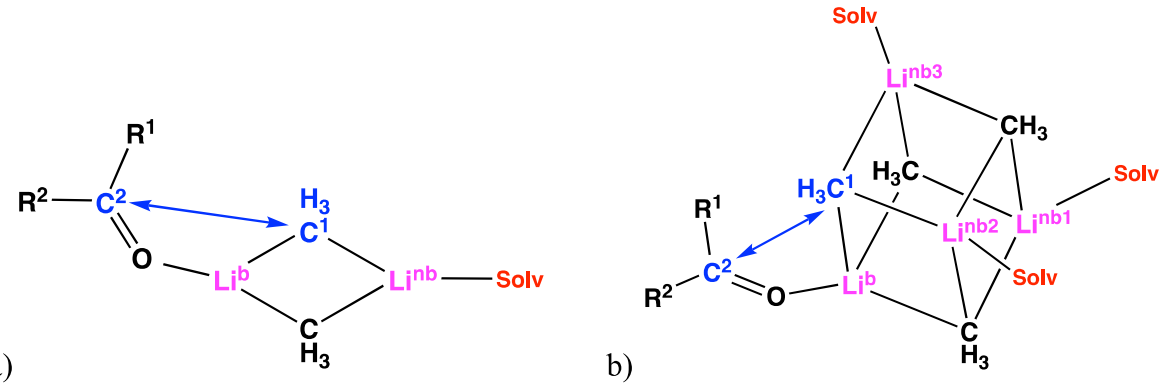

Fig. 4.4: labelling in the a) $(MeLi)_2$—ketone and b) $(MeLi)_4$—ketone clusters

4.2.1 Addition of MeLi Dimers on Ketones in Diethyl ether and THF

The reactions were followed in Et_2O and THF for addition of the MeLi dimer to acetone and 4-chlorobutyrophenone. First, the addition in Et_2O will be discussed and subsequently the addition in THF.

In the addition of the dimer to acetone in Et_2O, the acetone—$(MeLi)_2$ complex was coordinated to an Et_2O solvent molecule at the lithium ion, Li^{nb} through the oxygen of the ether, leaving both lithium ions tri-coordinated. The solvation state of the Li^{nb} ion is maintained through-out the reaction with a partial cleavage of the Li^{nb}— OEt_2 bond for short period that recombined before the transition state (Fig 4.5a). The C^1—C^2 addition is facilitated by the contraction of the C^2—O—Li^b bond angle bringing the electrophilic carbonyl carbon in proximity to the nucleophilic methyl group. The C^2—O—Li^b angle decreases from around 160° at the start of the reaction to up to around 70° just before the transition state (Fig 4.5b). At the transition state, the angle increases to around 149 ± 8°. The TS has a C^1—C^2 bond distance around 2.42 ± 0.41Å. The angle of attack of the methyl group to the carbonyl carbon defined by C^1—C^2—O was around 94 ± 12° at the transition state. This is slightly lower than the generally expected values of 105 ± 5° for nucleophilic addition to carbonyl carbon according to the Bürgi-Dunitz trajectory. It is however, in agreement with the values of 93-96° for addition of homogeneous and heterogeneous dimers of methyl lithium and dimethylamide to formaldehyde from DFT calculation, as reported by Maddaluno *et al* [100]. The C^1—C^2 bond formation is also facilitated by the rotation of the acetone about the C^2=O carbonyl bond which can be seen from the evolution of the dihedral angle $R^1C^2OLi^b$ (Fig 4.5c). The improper torsional angle $C^1C^2OR^1$

has a value of -111 ± 12°. The resulting addition product has C—C bond distance value of about 1.59 ± 0.1Å. At the product, the C^1—C^2—O angle is maintained around 108 ± 6° as expected for an sp^3 hybridized carbon (109°). The snapshot of the reaction at reactant, "TS" and product is given in Fig 4.5d. The nucleophilic addition occurred with a free activation energy, $\Delta G^{\ddagger}$ of about 11 kcal mol^{-1}.

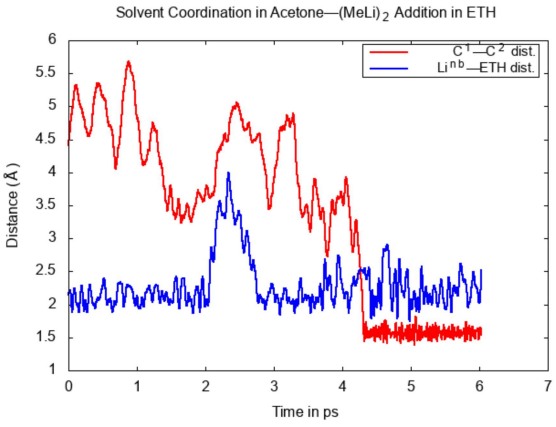

a)

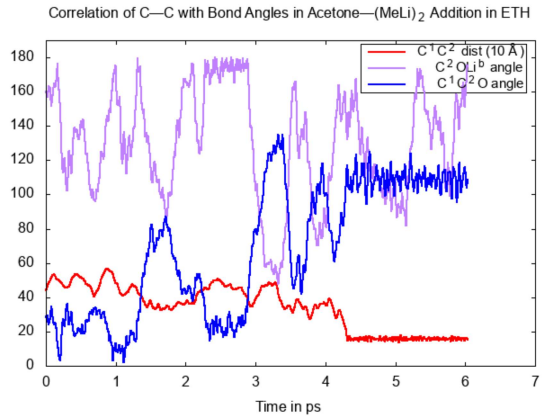

b)

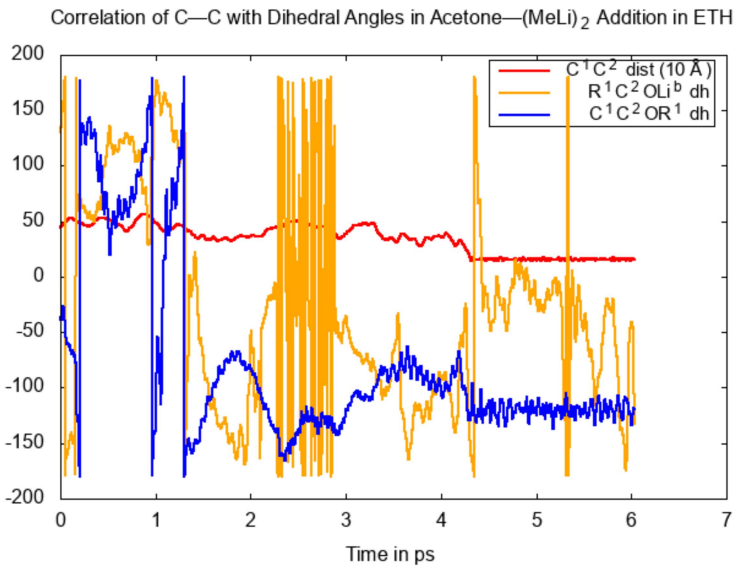

c)

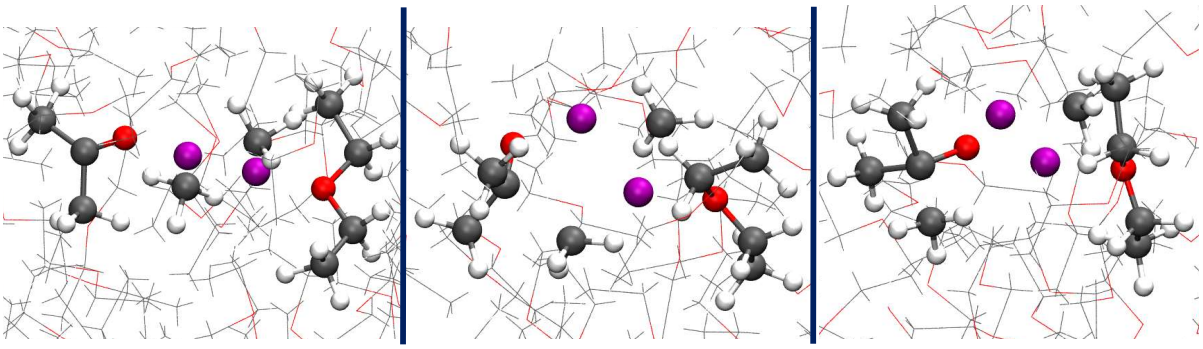

d) **Reactant** **"TS"** **Product**

Fig. 4.5: nucleophilic addition of $(MeLi)_2$ on acetone in explicit Et_2O solvent: a) graph showing solvent coordination in relation to C^1—C^2 bond distance b) the evolution of the C^2OLi^b angle and the C^1C^2O angle defining the Bürgi-Dunitz trajectory leading to the C^1—C^2 bond formation c) evolution of the $R^1C^2OLi^b$ and $C^1C^2OR^1$ dihedral angles in relation to the C^1—C^2 bond distance d) snapshot of the reactant, "TS" and product in the nucleophilic addition of $(MeLi)_2$ on acetone in Et_2O solvent

In THF, the addition of $(MeLi)_2$ to the acetone occurred through a slightly different pattern. The dimer dissociates into monomers at the TS before recombining after the C—C bond formation. The splitting of the dimer can be attributed to the ease of the highly coordinating THF solvent to form multiple coordination with the Li ions with less steric hindrance (having cyclic structure) compared to the diethyl ether solvent with chain-like structure. Also, the ease of the solvent exchange at the course of the reaction offers flexibility in the solvation of the Li^+ ions (Fig 4.6a & b). At the initial state of the reaction, the acetone—$(MeLi)_2$ complex is coordinated to two THF molecules at the lithium not coordinated to the acetone, Li^{nb}. One of the coordinated solvent molecule undergoes exchanged with another at the reactant state. The dimer splits into monomers at the "TS" and in so doing, the lithium ion coordinated to the acetone, Li^b was solvated, making both lithium ions tri-coordinated. Solvent exchange also occurred at the Li^b ion. The C^1—C^2 bond distance at the "TS" is around 2.36 ± 0.4 Å. As with the reaction in diethyl ether, the C^1—C^2 bond formation is facilitated by the bending of the C^2—O—Li^b bond angle and the rotation about the C^2=O bond (Fig 4.6c and d). The C^1—C^2—O angle and $R^1C^2OLi^b$ dihedral angle defining the Bürgi-Dunitz trajectory have values around 108 ± 8° and 105 ± 8°, respectively. The C^1—C^2—O angle is consistent with the expected value of 105 ± 5° while the $R^1C^2OLi^b$ dihedral angle value is slightly higher than the expected value of around 90°. Similar to the Et_2O reaction, the value of the C^1—C^2—O angle at the product is 110 ± 6° which is consistent with the value expected for an sp^3 hybridized carbon. The calculated free energy barrier, $\Delta G^{\ddagger}$ for this acetone—$(MeLi)_2$ reaction is about 17 kcal mol^{-1}.

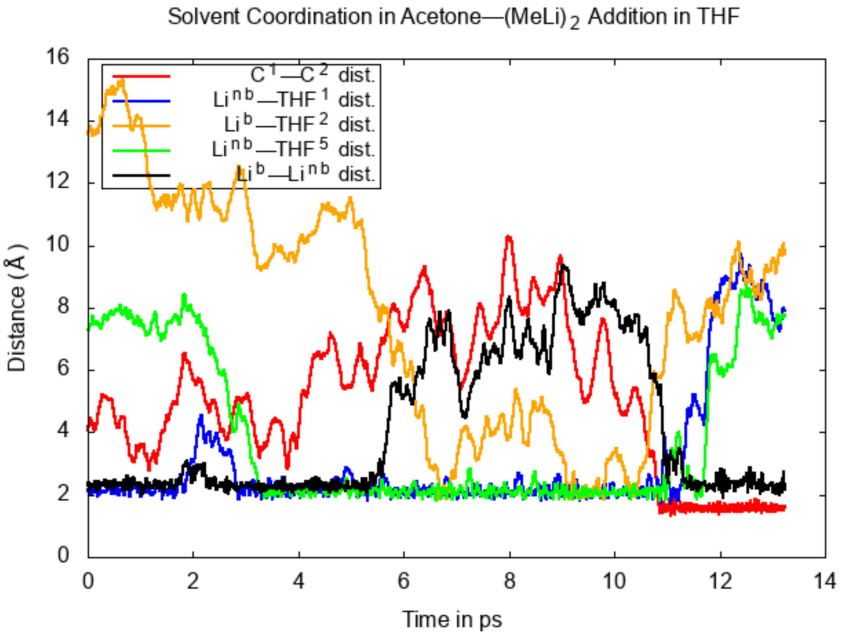
Solvent Coordination in Acetone—(MeLi)2 Addition in THF
C1—C2 dist.
Linb—THF1 dist.
Lib—THF2 dist.
Linb—THF5 dist.
Lib—Linb dist.
Distance (Å)
Time in ps

a)

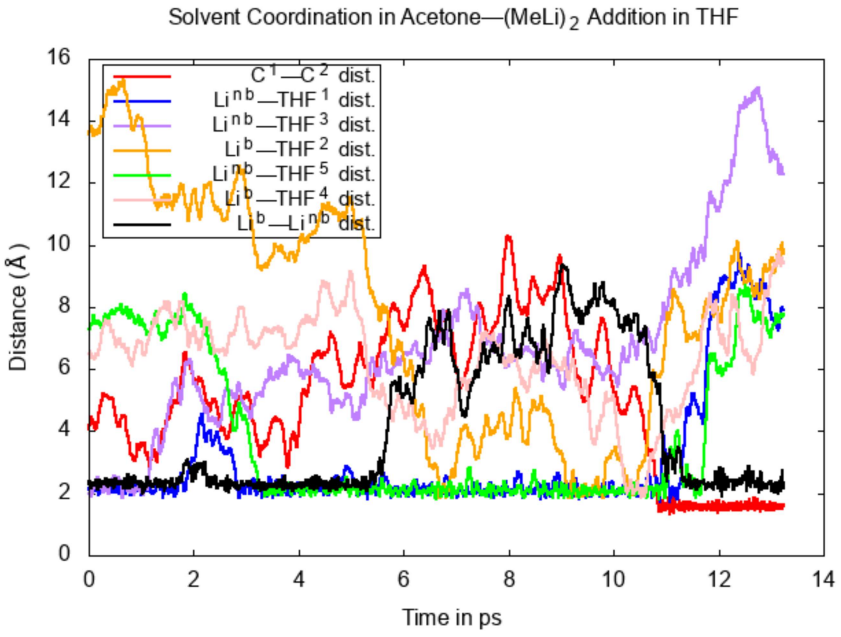
Solvent Coordination in Acetone—(MeLi)2 Addition in THF
C1—C2 dist.
Linb—THF1 dist.
Linb—THF3 dist.
Lib—THF2 dist.
Linb—THF5 dist.
Lib—THF4 dist.
Lib—Linb dist.
Distance (Å)
Time in ps

b)

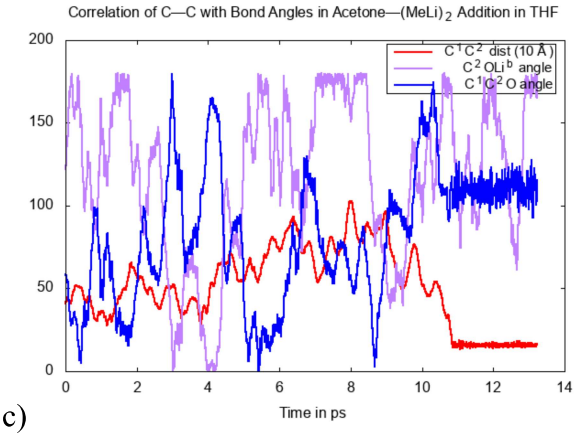
Correlation of C—C with Bond Angles in Acetone—(MeLi)2 Addition in THF
C1C2 dist (10 Å)
C2OLib angle
C1C2O angle
Time in ps

c)

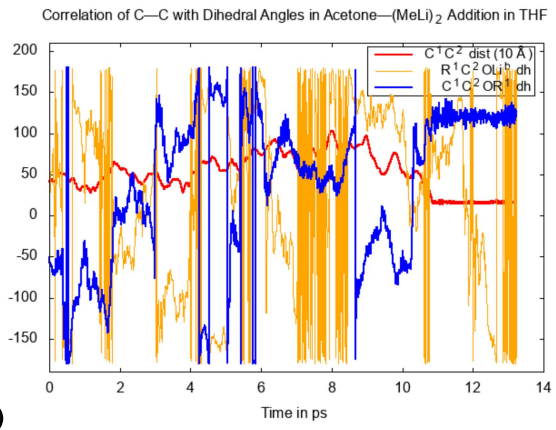
Correlation of C—C with Dihedral Angles in Acetone—(MeLi)2 Addition in THF
C1C2 dist (10 Å)
R1C2OLib dh
C1C2OR1 dh
Time in ps

d)

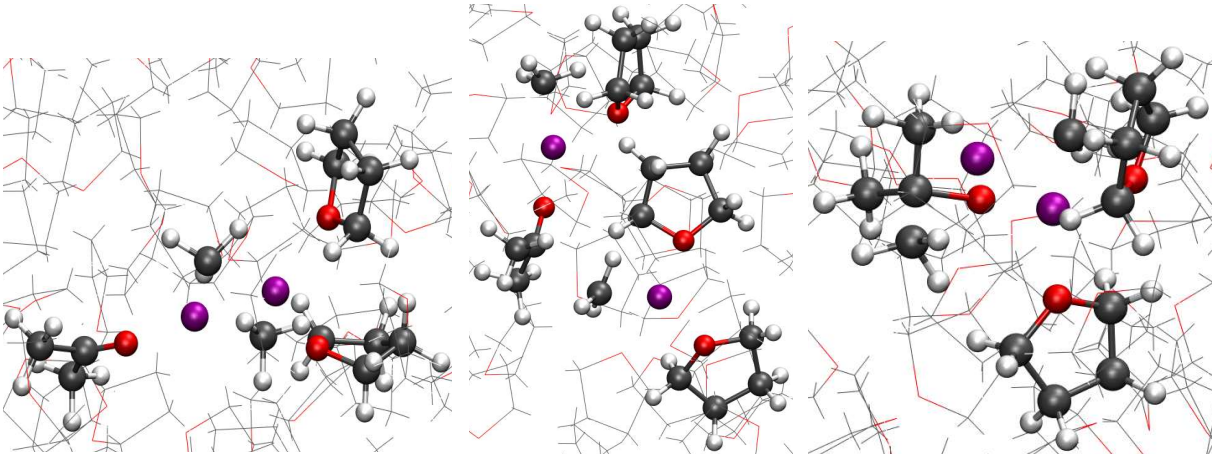

e) **Reactant** **"TS"** **Product**

Fig. 4.6: nucleophilic addition of $(MeLi)_2$ on acetone in explicit THF solvent: a) graph emphasizing solvent exchange with dimer splitting in $(MeLi)_2$—acetone complex in THF b) graph showing the full solvent coordination c) the evolution of the C2OLib angle and the C^1C^2O angle defining the Bürgi-Dunitz trajectory leading to the C^1—C^2 bond formation d) evolution of the $R^1C^2OLi^b$ and $C^1C^2OR^1$ dihedral angles in relation to the C^1—C^2 bond distance e) snapshot of the reactant, "TS" and product in the nucleophilic addition of $(MeLi)_2$ on acetone in THF solvent

The addition of the methyl lithium dimer on γ-chloroketone was also studied in the two conventional solvents, Et_2O and THF. For the addition in Et_2O, like with acetone, the Li^{nb} ion was coordinated to an Et_2O molecule at the early stage of the reaction. But unlike with acetone, the solvent molecule was lost from the Li^{nb} ion after about 2 ps, before attaining the transition state. The Li^{nb} ion was only re-solvated at the product (Fig 4.7a). In like manner to the acetone addition, the bending of the C^2—O—Li^b angle and the rotation about the carbonyl bond facilitated the approach of the nucleophilic methyl to the carbonyl carbon. The values of the C^1—C^2—O bond angle and $R^1C^2OLi^b$ dihedral angle defining the Bürgi-Dunitz trajectory are 95 ± 5° (lower than the general expected value of 105 ± 5) and 98 ± 8°, respectively (higher than the general expected values of about 90°). The calculated $\Delta G^{\ddagger}$ for this addition reaction is about 13 kcal mol^{-1}.

The addition reaction of the γ-chloroketone in THF occurred with similar solvation to the acetone addition. At the start of the reaction, the Li^{nb} ion was tetra-coordinated with two bonded THF molecules. One of the Li^{nb} solvent was lost while the Li^b ion gained a solvent molecule. On coordination of this solvent, the MeLi dimer partially dissociates with each Li ions homogeneously solvated with one THF. The Li^{nb} is tri-coordinated while Li^b is tetra-coordinated. Solvent exchange was observed at the Li^b ion. Here, the monomer entities

recombined into the dimer before the "TS" and the Li^{b} losses it solvation. At the "TS", the Li^{nb} ion is di-solvated (Fig 4.7c & d). The activation free energy, $\Delta G^{\ddagger}$ for this reaction is 19 kcal mol^{-1} higher than the value calculated for the reaction in Et_2O.

The summary of the geometric parameters for the nucleophilic addition of the methyl lithium dimer on acetone and γ-chloroketone in diethyl ether and THF is given in Table 4.9. The free energy surface for these reactions showing the metastable state for the reactant, A and the product, B are given in Fig 4.8a – d.

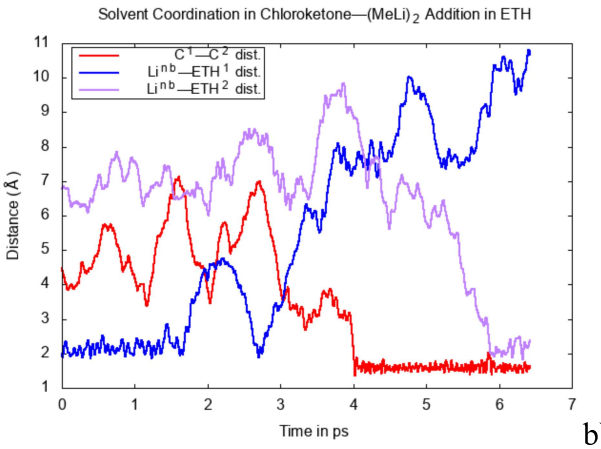

a)

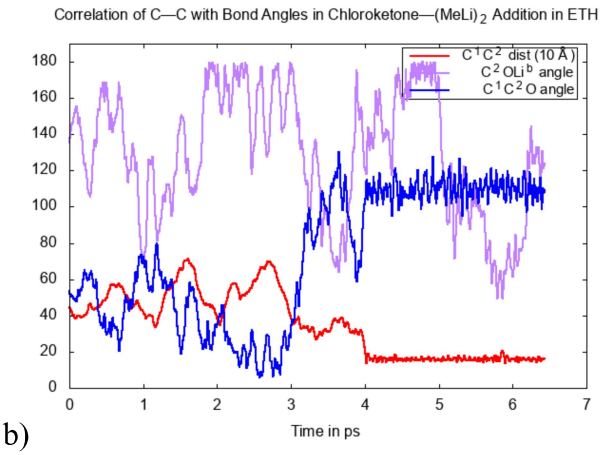

b)

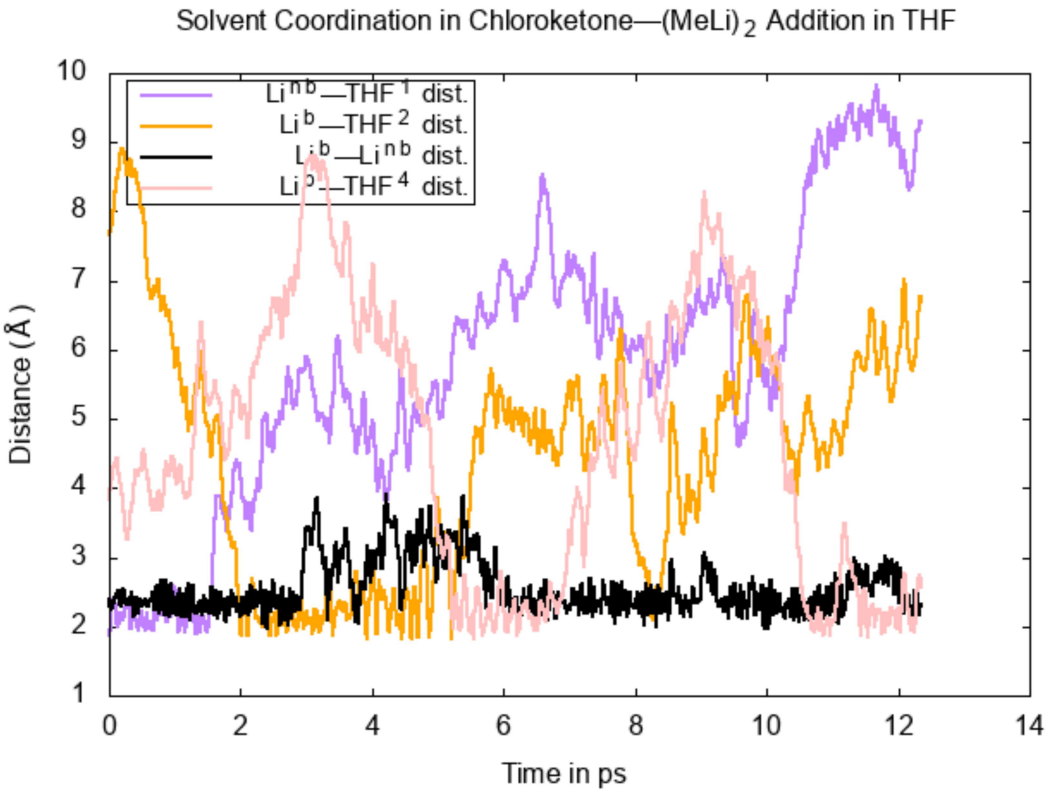

c)

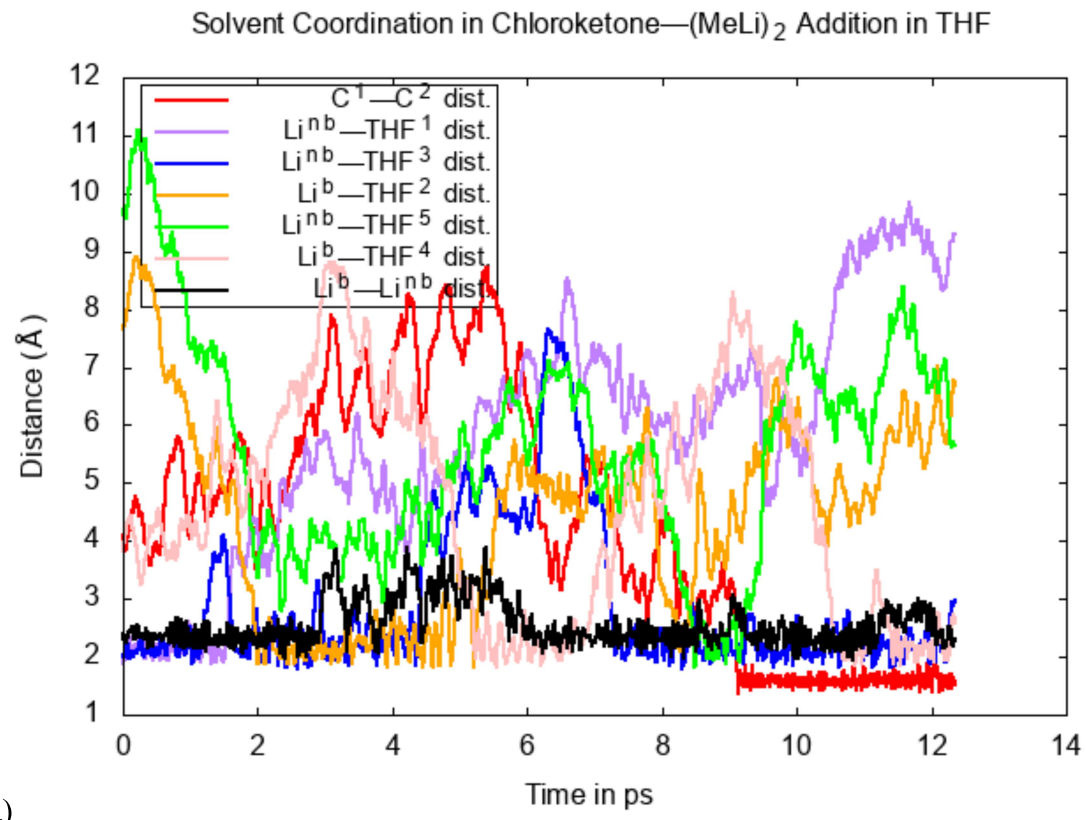

d)

Fig. 4.7: a) solvent coordination in dimer splitting in $(MeLi)_2$—chloroketone addition in Et_2O b) the evolution of the C^2OLi^b angle and the C^1C^2O angle defining the Bürgi-Dunitz trajectory in $(MeLi)_2$—chloroketone addition in Et_2O c) graph showing solvent exchange in $(MeLi)_2$—chloroketone addition in THF d) graph showing full solvent coordination in $(MeLi)_2$—chloroketone

Table 4.9: Geometric parameters for the addition of MeLi dimer on acetone and γ-chloroketone

System	TS				Product	
	C^2OLi^b (°)	C^1C^2O (°)	$C^1C^2OR^1$ (°)	C^1C^2 (Å)	C^2OLi^b (°)	C^1C^2O (°)
Acetone — $(MeLi)_2$ in ETH	149 ± 9	94 ± 12	-111 ± 12	2.42 ± 0.41	128 ± 24	109 ± 6
Acetone — $(MeLi)_2$ in THF	169 ± 4	108 ± 8	105 ± 8	2.36 ± 0.40	130 ± 33	110 ± 6
Chloroketone — $(MeLi)_2$ in ETH	129 ± 10	97 ± 8	117 ± 6	2.42 ± 0.42	121 ± 39	110 ± 6
Chloroketone — $(MeLi)_2$ in THF	154 ± 5	95 ± 5	98 ± 8	2.48 ± 0.42	120 ± 40	110 ± 5

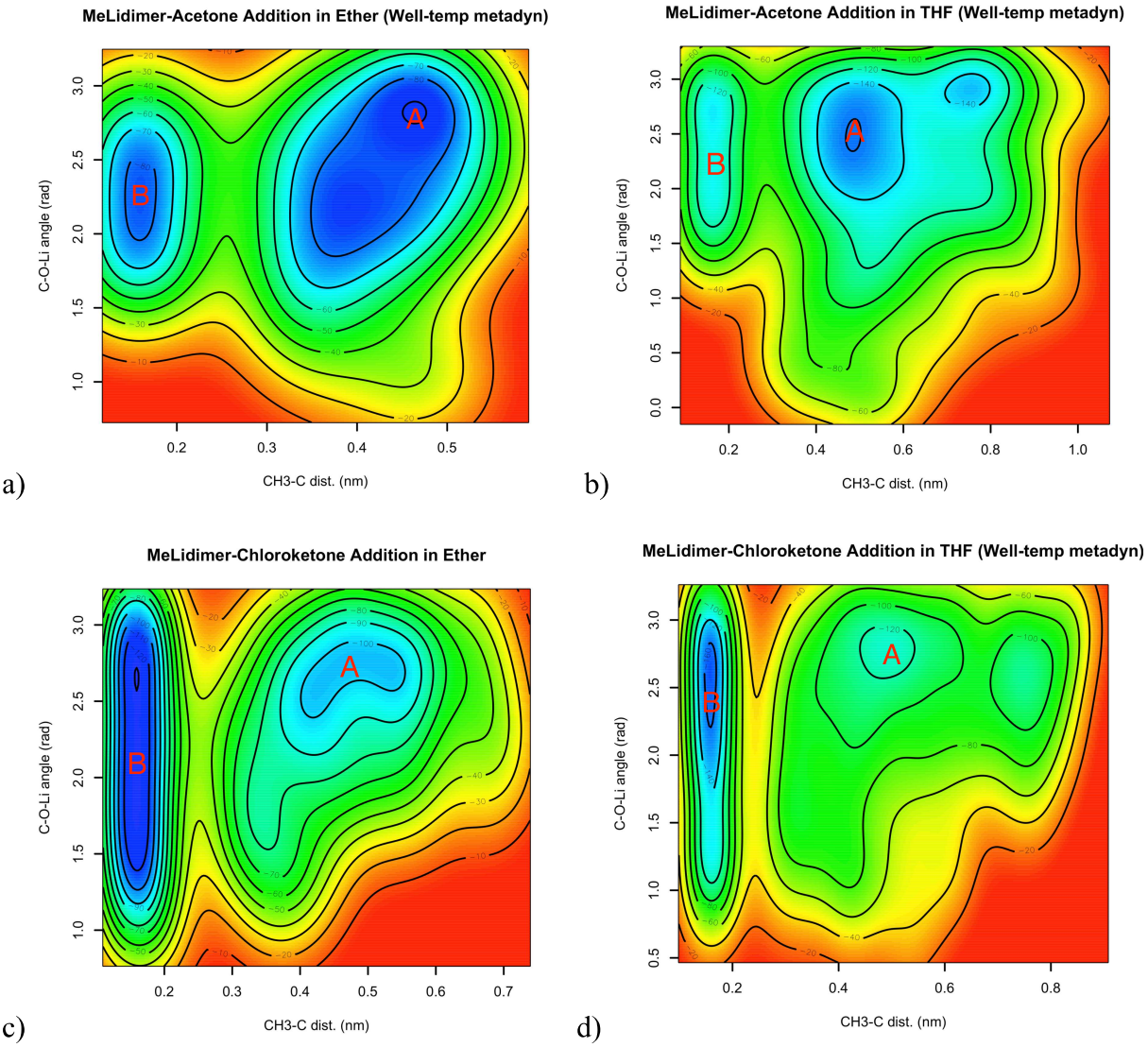

Fig. 4.8: Free energy surface showing metastable state of reactant, A going to product, B for the MeLi dimer addition on: a) acetone in Et_2O b) acetone in THF c) γ-chloroketone in Et_2O d) dimer addition on γ-chloroketone in THF

The intermolecular interaction between the solvents and the ketone—$(MeLi)_2$ is dominated by electrostatic attraction that is partially quenched by the exchange repulsion. Other contributions are from dispersion and induction attractions. The correlation of the solvent—cluster intermolecular interaction energy and the free energy barrier for the addition reaction is given in Table 4.10. The free energy barrier was found to decrease with increased interaction energy. The role of this interaction energy on lowering of the free energy barrier is not clear but rather, the lower interaction energy relates to the tendency for solvent exchange. This is manifested in the ease of solvent exchange observed in THF.

Table 4.10: Intermolecular interaction energy between solvent and (MeLi)2—ketone complex and the free energy barrier for the addition of MeLi dimer on acetone and γ-chloroketone

System	Interaction Energies (kcal/mol)					$\Delta G^{\ddagger}$ (kcal/mol)
	Elst.	Exch.	Ind.	Disp.	Total	
[Acetone—$(MeLi)_2$]—ETH	-18.70	13.12	-5.68	-4.69	-15.96	11
[Acetone—$(MeLi)_2$THF]—THF	-21.81	14.34	-1.53	-6.14	-15.14	17
[Chloroketone—$(MeLi)_2$]—ETH	-20.27	13.00	-4.22	-4.67	-16.17	13
[Chloroketone—$(MeLi)_2$THF]—THF	-16.68	13.29	-5.35	-5.67	-14.41	19

4.2.2 Addition of MeLi Tetramers on Ketones in Diethyl ether and THF

Like the methyl lithium dimer reactions, the methyl lithium tetramer addition was also studied in the conventional Et_2O and THF solvents. In the MeLi tetramer addition on acetone in Et_2O, the lithium atoms not bonded to the acetone (Li^{nb}) were initially each bonded to a Et_2O molecule. Within a few thousand steps, one of the lithium ion, Li^{nb1} lost it solvation. The other two Li^{nb} ions remained each coordinated to a solvent molecule through the reaction (Fig 4.9a). The TS is facilitated by the bending of the C^2—O—Li^b angle from a value of around 140° at the reactant state to a value of 104 ± 12° at TS (Fig 4.9b). The tetrahedral geometry of the Li^+ ions was maintained through the reaction with slight elastic distortions during the reaction. The nucleophilic carbon travels in a plane perpendicular to the plane of the carbonyl group. The reaction pass through an approximated "TS" with the angle, C^1—C^2—O with value 110 ± 11° and with improper dihedral angle C^1—C^2—O—R^1 with a value of 112 ± 14° both inconsistent with the Bürgi-Dunitz trajectory. The calculated free energy barrier from the free energy surface for this reaction going from the reactant A to the product B ((Fig 4.9e) is about 19 kcal mol^{-1}. The solvation in the acetone—$(MeLi)_4$ reaction in THF is slightly different. Here, the three Li^{nb} ions are each coordinated to a THF molecule up to just about the so-called transition state (Fig 4.9c). And like the reaction in Et_2O, the bending of the C^2—O—Li^b bond angle and the rotation about the carbonyl group is an important geometrical evolution for the addition reaction which enhances the approach of the nucleophilic methyl group and the electrophilic carbonyl carbon (Fig 4.9d). The values of the C^1—C^2—O bond angle and the C^1—C^2—O—R^1 dihedral angle are about 103 ± 14 and 102 ± 20°, respectively. The tetrahedral geometry of the lithium ions

was maintained up to the C—C bond formation. The free energy of activation, $\Delta G^{\ddagger}$ for this reaction going from A to B, calculated from the free energy surface (Fig 4.9f) is about 23 kcal mol^{-1}.

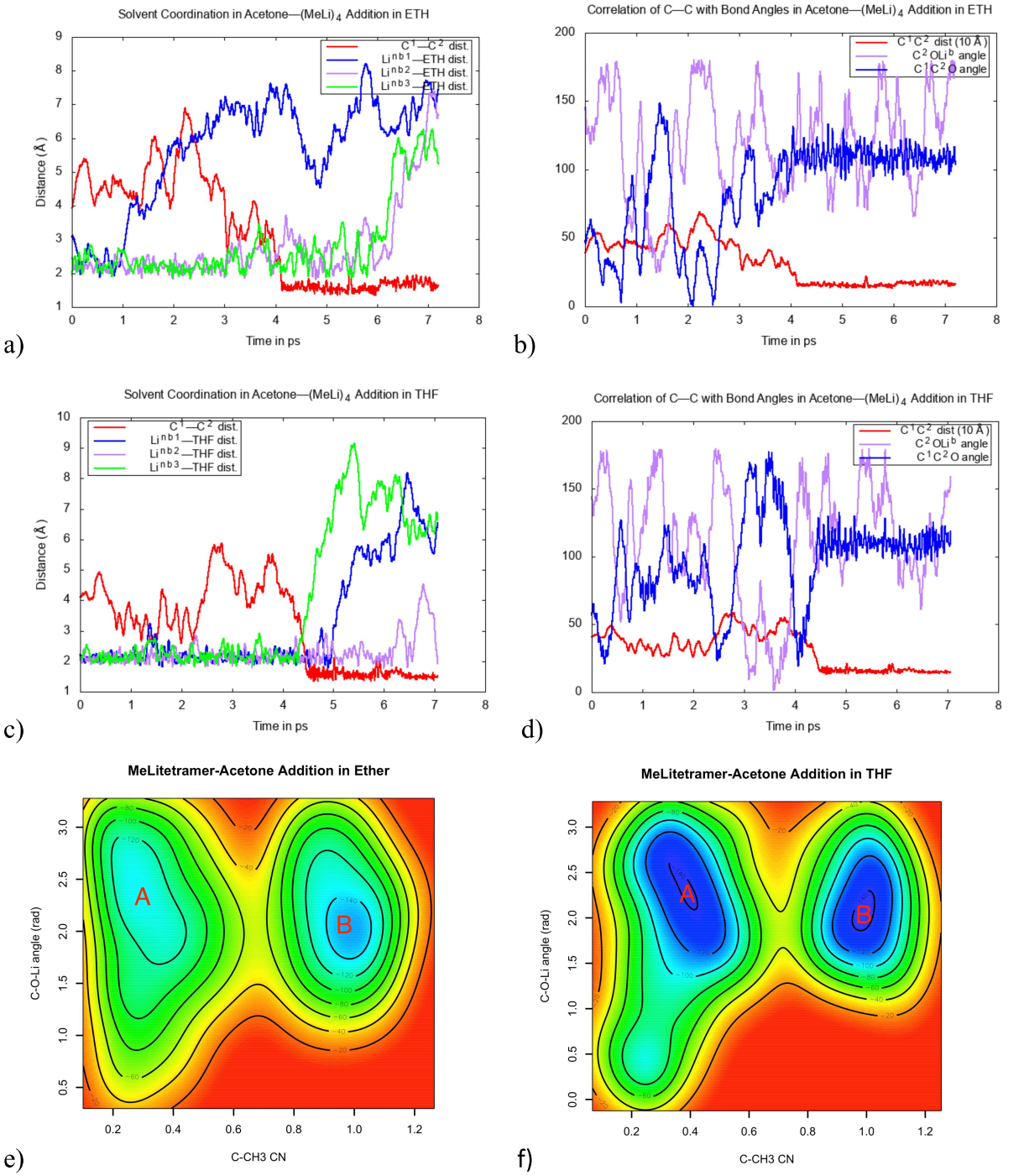

Fig. 4.9: MeLi tetramer addition on acetone: a) solvent coordination in the addition in Et_2O solvent b) evolution of the C^2OLi^b and C^1C^2O angles in relation to the C—C bond formation in the addition in Et_2O solvent c) solvent coordination in the addition in THF solvent d) evolution of the C^2OLi^b and C^1C^2O angles in relation to the C—C bond formation in the addition in THF solvent e) free energy surface showing metastable state of reactant, A going to product, B for the addition in Et_2O solvent f) free energy surface showing metastable state of reactant, A going to product, B for the addition in THF solvent

The MeLi tetramer addition on γ-chloroketone follows through similar route as the addition in acetone. The bending of the bending of the C^2—O—Li^b bond angle and the rotation about the C^2=O bond remain key in bringing the reactive sites close for the C^1—C^2 bond formation. The nucleophilic attack did not occur through the Bürgi-Dunitz trajectory for both reactions is Et_2O and THF. At "TS", the C^1—C^2—O angle for the reactions in Et_2O and THF are 96 ± 5 and 91 ± 9°, respectively, lower than the expected Bürgi-Dunitz trajectory angle. Also, the dihedral angle $C^1C^2OR^1$ in Et_2O and THF reactions are -103 ± 7 and -109 ± 10°, respectively, which are higher than the general value in the Bürgi-Dunitz trajectory. The geometric parameters for this reaction for both solvents are given in Table 4.11.

The solvation of the Li^+ ions in Et_2O and THF are quite different. In Et_2O, only one of the non-ketone-bonded lithium is coordinated to a solvent molecule. That is, only the Li^+ ion at the vertex of the tetrahedron of the lithium cluster (Li^{nb2}) is solvated. The ketone is bonded to one of the Li ions on the base of the tetrahedron. The observed limited solvation of the cluster can be attributed to the steric effect between the chain-like diethyl ether and the jiggling chloroalkyl group of the γ-chloroketone. On the contrary, in THF, all the three non-ketone-bonded lithium ions (Li^{nb1}, Li^{nb2} and Li^{nb3}) are each mono-solvated with the THF molecule (Fig 4.10). This methyl addition via the tetrameric cluster on γ-chloroketone in Et_2O and THF occurred with free activation energies, $\Delta G^{\ddagger}$ of 20 and 31 kcal mol^{-1}, respectively.

We next look at the intermolecular interaction between the solvent and the MeLi cluster. And like with the dimer clusters, the interaction is dominated by the electrostatic interaction. The second major interaction energy is the exchange repulsion energy which to a large extent cancel out the electrostatic interaction. Other contributing interaction results from induction and dispersion interaction energies. The total energy of interaction with all contributing energies and the energy barrier for the reactions are given in Table 4.12.

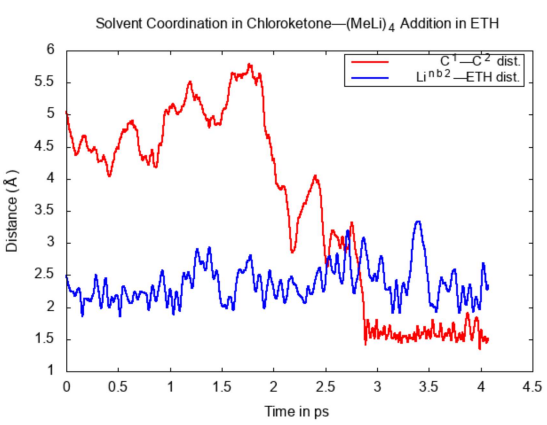

a)

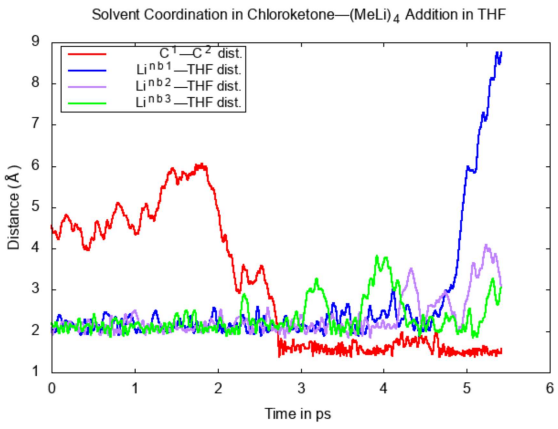

b)

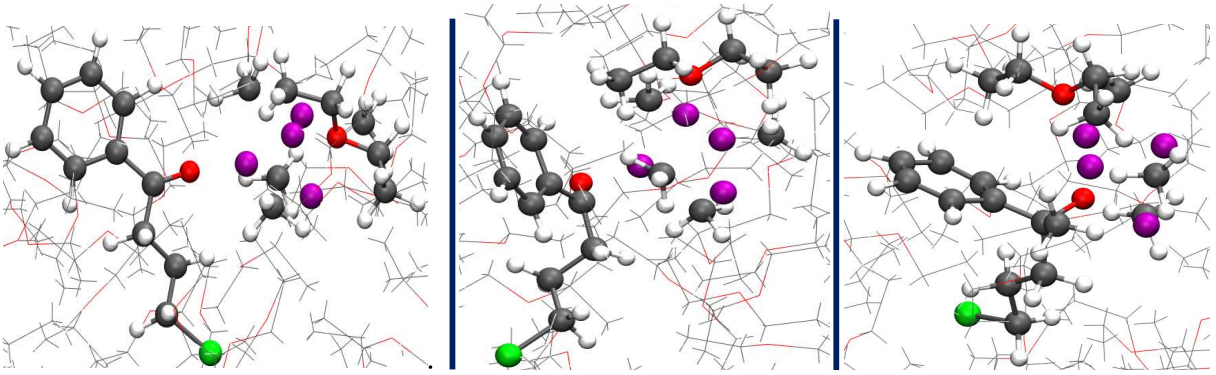

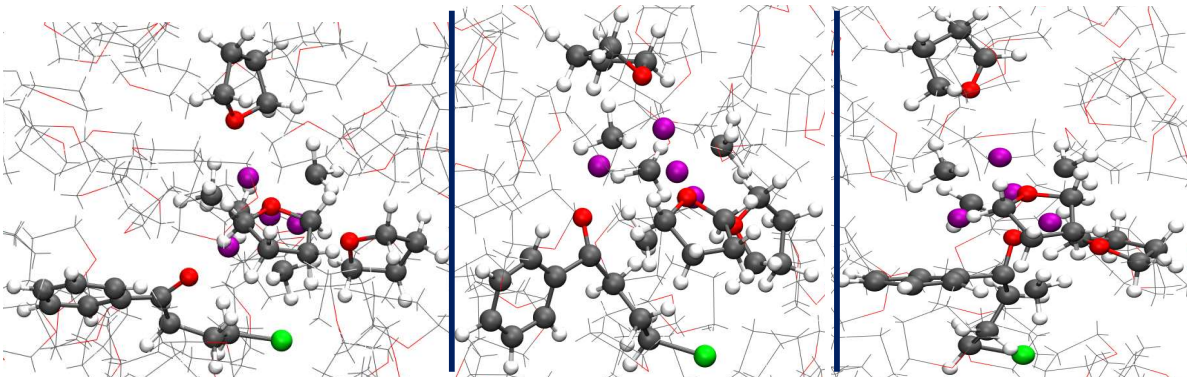

Fig. 4.10: : MeLi tetramer addition on γ-chloroketone: a) solvent coordination in the addition in Et_2O solvent b) solvent coordination in the addition in THF solvent c) snapshot of the reactant, "TS" and product in the nucleophilic addition in Et_2O showing the nature of solvation d) snapshot of the reactant, "TS" and product in the nucleophilic addition in THF showing the nature of solvation

Table 4.11: Geometric parameters for the addition of MeLi tetramer on acetone and γ-chloroketone

System	TS				Product	
	C^2OLi^b (°)	C^1C^2O (°)	$C^1C^2OR^1$ (°)	C^1C^2 (Å)	C^2OLi^b (°)	C^1C^2O (°)
Acetone — $(MeLi)_4$ in ETH	104 ± 12	110 ± 11	112 ± 14	2.39 ± 0.31	125 ± 30	110 ± 7
Acetone — $(MeLi)_4$ in THF	104 ± 12	103 ± 14	102 ± 20	2.21 ± 0.50	123 ± 28	110 ± 7
Chloroketone — $(MeLi)_4$ in ETH	128 ± 6	96 ± 5	-102 ± 7	2.49 ± 0.37	135 ± 23	108 ± 5
Chloroketone — $(MeLi)_4$ in THF	125 ± 11	91 ± 9	-109 ± 10	2.57 ± 0.35	126 ± 28	109 ± 5

Table 4.12: Intermolecular interaction energy between solvent and (MeLi)4—ketone complex and the free energy barrier for the addition of the MeLi tetramer on acetone and γ-chloroketone

System	Interaction Energies (kcal/mol)					$\Delta G^{\ddagger}$ (kcal/mol)
	Elst.	Exch.	Ind.	Disp.	Total	
[Acetone—$(MeLi)_4$ 3ETH]—ETH	-19.99	14.31	-1.99	-8.26	-15.93	19
[Acetone—$(MeLi)_4$ 3THF]—THF	-16.51	13.12	-4.91	-5.85	-14.16	23
[Chloroketone—$(MeLi)_4$]—ETH	-20.28	14.62	-3.47	-7.23	-16.35	20
[Chloroketone—$(MeLi)_4$ 3THF]—THF	-20.46	13.30	-1.59	-5.85	-14.60	31

4.3 Conclusion

In this chapter, the mechanism of the MeLi nucleophilic addition reaction on ketone was studied in the conventional solvents (Et_2O and THF). The conventional addition on acetone and γ-chloroketone both in implicit and explicit solvation with the MeLi dimer and tetramer aggregate were studied. The addition follows through first, the complexation of the ketone on the MeLi aggregate through O—Li bonding to form the $(MeLi)_n$—ketone complex (where n=2 or 4). On complexation, the bonded MeLi is in out-of-plane with the carbonyl group of the ketone except in the case of the addition of MeLi tetramer on γ-chloroketone. The interaction energy between the ketone and the methyl lithium aggregate was calculated by SAPT method. The complexation was found to be dominated by electrostatic attraction between the ketone and MeLi aggregate which was partially cancelled by the repulsive exchange interaction. Other minor contribution to the interaction are from the induction and dispersion interaction energies. Through the bending of the COLi bond angle and rotation about the carbonyl group, C=O, the methyl group approach the carbonyl carbon to form the corresponding alkylated adduct. The TS follows through a concerted mechanism with simultaneous cleavage of the Me—Li bond and C—C bond formation leading to a six-membered ring transition structure. The attack of the methyl group occurs in a direction perpendicular to the plane of the carbonyl group and the bonding MeLi group is in plane with the carbonyl group. In the implicit solvation study, this approach of the methyl group was observed to follow the typical Bürgi-Dunitz trajectory for neutral nucleophilic addition with respect to the CCO bond angle with values between 106 to 109° except in the tetramer addition on γ-chloroketone in Et_2O with value of 113°. But with

respect to the CCOC dihedral, the values here are a bit higher than the typically expected values of 90°. The adduct addition product results with the CCO angle consistent with the expected value (about 109°) for a typical sp^3 hybridized carbon. The free activation energy, $\Delta G^{\ddagger}$ for the nucleophilic addition correlates with the number of coordinated solvent. Higher solvent coordinated systems showed lower values of $\Delta G^{\ddagger}$ than their corresponding counterparts.

CHAPTER FIVE

5 On-Water Methyl Lithium Nucleophilic Addition

Until recently, the idea of deliberately introducing water in reactions of organometallic compounds especially those of polar *s* block metals will be considered preposterous. In fact, it is still surprising and unclear how water could be added in organic transformations involving organometallic compounds without the organometallic compound being completely consumed but rather, the reaction proceeding to the product and in some cases resulting in faster and/or better yield. An early reported work involving the presence of water in reactions of polar organometallic compounds is the preparation of tritiated arene **2** by the addition of *n*-BuLi to a mixture of bromoarene **1** and tritiated water-wetted (T_2O) sodium-dried diethyl ether (scheme 5.1). The halogen-lithium exchange intermediate was hydrolysed by the T_2O to give the tritiated arenes. [106]

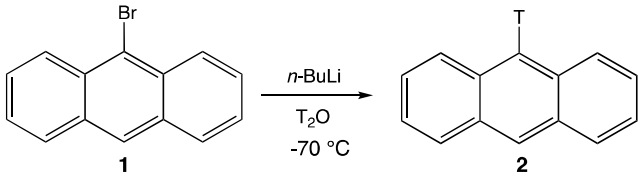

scheme 5.1: preparation of tritiated arene using wetted diethyl ether

Another early work on the role of water in organometallic reaction was noted in the reaction of equivalents of lithium carboxylates **3** with organollithium. Upon quenching the reaction with water after about 30mins of reflux, a mixture of ketone and tertiary alcohol (carbinol) **5** were produced (scheme 5.2). A decrease in the percentage of **5** and increase in the percentage of ketone was observed on increasing the reflux time. Only the ketone product was formed after 24hour reflux. This goes on to suggest that the excess organolithium reacts with part of the ketone formed by the hydrolysis of the intermediate **4**, faster than with the water to form the carbinol.[107]

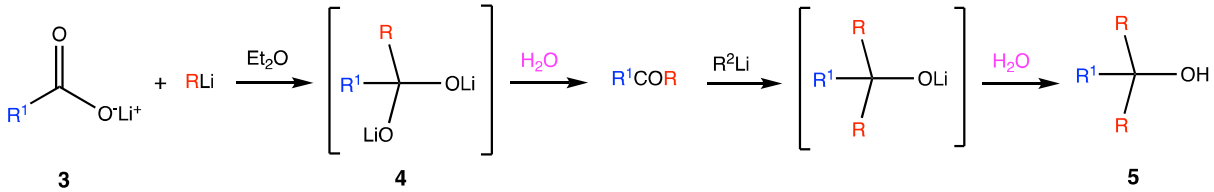

scheme 5.2: role of water in the synthesis of carbinol from lithium carboxylate

A pioneering work in which the term "on water" reaction was coined was performed by Sharpless and co-workers. The "on water" reaction entails reactions in which insoluble organic reactants are stirred in aqueous suspension, often leading to substantial rate acceleration and ease of product isolation. They studied the [2σ + 2σ + 2π] cycloaddition of quadicyclane **6** with dimethyl azodicarboxylate (DMAD, **7**) to yield 1,2-diazetidine **7** (scheme 5.3). The vigorous stirring of the **6** and **7** mixture "on water" (generating aqueous suspension) at room temperature yielded the product **8** in few minutes while on the other hand, the corresponding neat reaction takes about 48 hours to give the product. Adequate phase separation between the water and organic phase was said to be important for the rate acceleration and the homogeneity of the reaction lowers the rate. This does not however conclude that heterogeneity is solely responsible for the rate acceleration as only minor acceleration was observed when the reaction was conducted on perfluorohexane, a very water-insoluble compound. Isotope effect was observed in this class of reaction. Other reported reactions in their work that were also found to be accelerated by the "on water" process include the allylic animation of olefins by ene reaction of bis(trichloroethyl) azodicarboxylate **9** (scheme 5.4) and nucleophilic opening of epoxides and airidines.[108] Breslow and Rideout suggested that association of the insoluble organic reagents in water diminishing the organic-water interfacial area , the "hydrophobic effect", was responsible for the acceleration of Diel-Alder reaction of cyclopentadiene **10** with butenone **11** in water (700-fold increase compared to the reaction in 2,2,4-trimethylpentane) (scheme 5.5).[109] However, there might be more than just the hydrophobic effect that is responsible for the rate acceleration. Hydrogen bonding by water has also been thought of as an important property for the "on water" rate acceleration.[110,111] Engberts *et al* reported that the hydrophobic effect is not due to interfacial surface reduction as postulated by Breslow and Rideout but rather, due to the loss of the hydrophobic character near the activated reaction complex. [112]

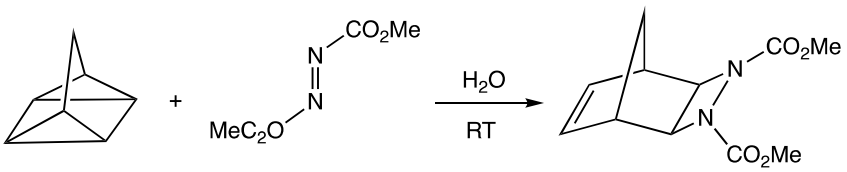

6 7 8

scheme 5.3: the [2σ + 2σ + 2π] cycloaddition of quadicyclane with DMAD

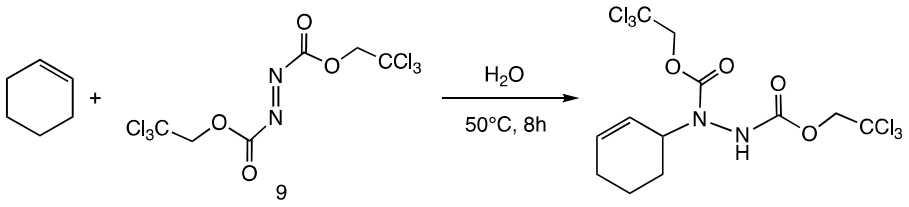

scheme 5.4: allylic animation of olefins by ene reaction of bis(trichloroethyl) azodicarboxylate

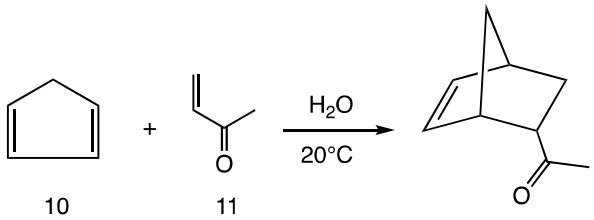

scheme 5.5: Diel-Alder reaction of cyclopentadiene with butenone

Though the role of water is not fully understood, recent developments on the use of water in organic synthesis involving polar organometallic compounds have continued to increase. In the use of tetrahydrofuran as an effective direct metalation group in the regioselective desymmetrization/functionalization of diaryltetrahydrofuran, Capriati and co-workers observed some interesting behaviour with the use of water in the transformation. They performed the lithiation of 2,2-diphenyltetrahydrofuran **12** with organolithium reagents such as *s*-BuLi (1.4 equiv. at 0°C) and *t*-BuLi (1.9 equiv. at 0°C) in diethyl ether and in cyclopentyl methyl ether (CPME) to yield the *ortho*-lithiated adduct **13**. Addition of 6 equiv. of acetone to the adduct in CPME afforded the expected hydroxylated compound **14** in 30% yield. The low yield was said to be probably due to the high competition of enolization with the nucleophilic addition. While no reaction was observed upon carrying out the addition of the acetone to dry-diethyl ether solution of **13** (direct addition), a yield of 30% of **14** was detected when the diethyl ether solution of **13** was added over acetone-water mixture (6 equiv. each) at room temperature. To check the possible role played by water in the reaction, a subsequent reaction of the diethyl ether solution of **13** was carried out in 6 equiv. of acetone alone (neat condition) and again a 30% yield of **14** was observed (scheme 5.6). This implied that the formation of the product is unrelated to any "rate acceleration" promoted by water but instead may be attributed to the "inverse addition". The water is simply thought of as acting as a bystander.[113]

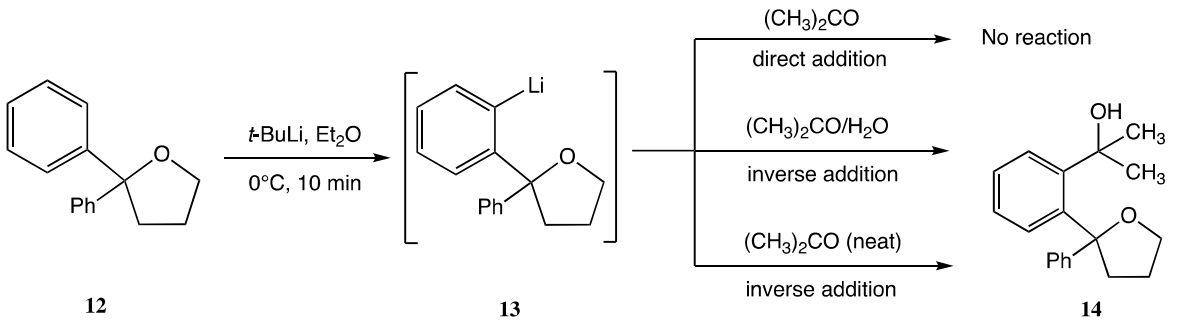

scheme 5.6: regioselective functionalization of 2,2-diphenyltetrahydrofuran via lithiation with *t*-BuLi and addition by acetone (comparing direct addition with inverse addition in water and in neat condition)

Madsen and Holm reported the addition of allylmagnesium bromide to some carbonyl compounds in the presence of protic reagents such as water. Their inspiration for the use of water as co-solvent was due to the fact that, the addition of allylmagnesium bromide to acetone was found to occur at an extremely fast rate thus suggesting a chance for a competition with the protonation of the Grignard reagent by the water. The reaction of diethyl ether solution of allymagnesium bromide with equimolar mixture of acetone and water in diethyl ether yielded the addition product in 90% yield suggesting that the addition occurred much faster than the protonation of the Grignard reagent. Addition with other carbonyl compounds as benzaldehyde, methyl benzoate and acetophenone were noted to be slower than the competitive protonation. They noted that the nucleophilic addition in the presence of alcohols or benzoic acid showed lower yield of addition product (52-63%). But using water as the proton source gave up to 75% yield of the addition product better than with methanol, phenol and benzoic acid (about 42-63%) suggesting the alcohols seem to be better proton source. In trying to explain this phenomenon of addition, they postulated that water coordinate to magnesium better than the alcohols therefore the water is scavenged by the Grignard reagent making it less available for protonation while on the other hand the alcohols are more available for protonation since they coordinate less effectively to the magnesium.[114]

The groups of Hevia and Garcia-Alvarez have worked on chemoselective addition of polar *s*-block organanometallic reagents (organolithiums and Grignard reagents) on ketones and nitriles under air and at room temperature which on the normal conventional methods are often carried out under controlled environment.[115,116] They employed the use of deep eutectic solvent (DES) in their reactions. DESs are a family of green solvents which are formed from a eutectic mixture of Lewis or Brønsted acids and bases which can contain a variety of anionic and/or cationic species. They are usually obtained by complexation of a quaternary ammonium salt with a metal

salt or hydrogen bond donor resulting to a mixture with decreased melting point relative to the melting point of the individual components.[117,118]

Among the reported work of the groups of Hevia and Garcia-Alvarez is the instantaneous chemoselective formation of the tertiary alcohol **16** by the addition of vinylmagnesium bromide to 2′-methoxy-acetophenone **15** in 1:2 choline chloride/glycerol mixture (1ChCl/2Gly) at room temperature, under air (scheme 5.7), not requiring the use of the Schlenk technique. The high heat capacity of the DES makes it not mandatory for cooling. A yield of up to 78% was obtained when 2 equiv. of the vinylmagnesium bromide was employed. Replacing the glycerol by hydrogen bond donors like ethylene glycol and urea resulted in lower yields (55% and 67%, respectively). An even lesser yield was recorded with replacement by lactic acid (30%). Interestingly, using water as a solvent in the reaction yielded 21% product.[115] Another work they reported is the one-pot synthesis of benzophenone **19** by the addition of phenyllithium to benzonitrile **17** in air, at ambient temperature (scheme 5.8) using in glycerol (Gly) as solvent and its choline-chloride-based eutectic mixture (1 ChCl/2 Gly). The resulting benzophenone imine **18** undergoes hydrolysis to give the ketone **19**. A yield of up to 83% was obtained in the reaction in Gly solvent and 71% with 1 ChCl/2 Gly solvent. The reagents are insoluble in the solvents thereby making the reaction of the type “on water”. Using water as the solvent (in which the reagents are also insoluble) yielded 79% product. The importance of stirring in the reaction was noted as only 51% product was obtained in the reaction in Gly without stirring. Only 8% product was obtained when the reaction was carried out in methanol where the reagents are completely soluble. Therefore, the reaction is of the “on water” type with insolubility and stirring as key for good yield.[116]

This is by no means an exhaustive example of the use of DES in reactions with polar organometallic compounds. But our focus here is not on DES but rather water. Extensive examples of the use of DES organic transformation can be found in the reviews by Capriati and co-workers.[14–16]

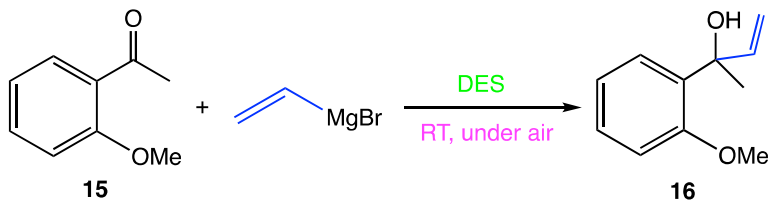

15 **16**

scheme 5.7: vinylmagnesium bromide addition to 2′-methoxy-acetophenone in DES

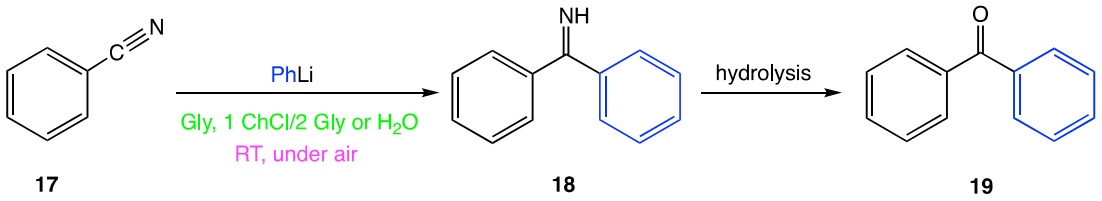

scheme 5.8: one-pot synthesis of benzophenone in unconventional solvent

Refocusing on the use of water in the reaction of polar organometallic compounds, one of the recent use of water is in the nucleophilic addition of polar organometallic compounds to imines and nitriles reported by Capriati and co-workers. 1.4 equiv. of *n*-BuLi was spread over a suspension of water-insoluble aldimine **20** (0.5 mmol) in water (1 mL), under air with vigorous stirring at room temperature ("on water" reaction). Up to 96% of the amine product **21** was recovered after dilution with CPME, filtration, evaporation and chromatography (scheme 5.9). Scaling up the reaction (5.5 mmol 20 nad 10 mL water) resulted in > 99% yield. In contrast, the reaction performed with minimal stirring resulted in drop of the product yield to 66%. Also, significant deuterium solvent effect was noted, with the yield dropping to 57%. Higher drop in yield was observed for the reaction in methanol (only 15% yield). This indicate the uniqueness of water in the effectiveness of the reaction which may probably be due to the stronger intermolecular hydrogen bonding in water than in methanol. In a bid to observe whether the protonolysis of the organolithium occurs instantaneously, 1.4 equiv. of *n*-BuLi was spread over 1 mL of water followed by the addition of imine **20** after 5 s. Interestingly a yield of 20% of **21** was obtained indicating that the consumption of the organolithium is not as instantaneous as it is thought of. They reported in the same paper the one-pot, two-step synthesis of tertiary alkyl primary amine (carbinamine) by the addition of organometallic compounds to nitriles which was generally challenging to achieve in a one-pot procedure. Sparingly water-soluble benzonitrile **22** was suspended in water and stirred vigorously with *s*-BuLi and allyl magnesium chloride (equal equiv.) to give tertiary carbinamine **23** in 95% yield and a trace of 2-methyl-1-phenylbutan-1-one (< 5%) (scheme 5.10). The reaction also performed well with PhLi and EtLi organolithiums and with MeCN, EtCN and PrCN nitriles.[110]

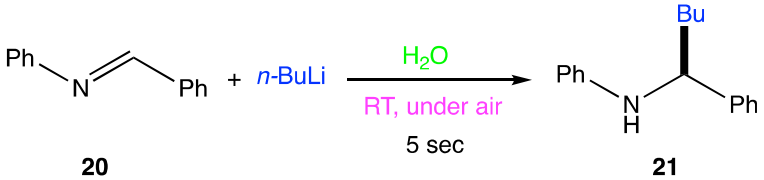

scheme 5.9: organometallic addition on imine to give amine

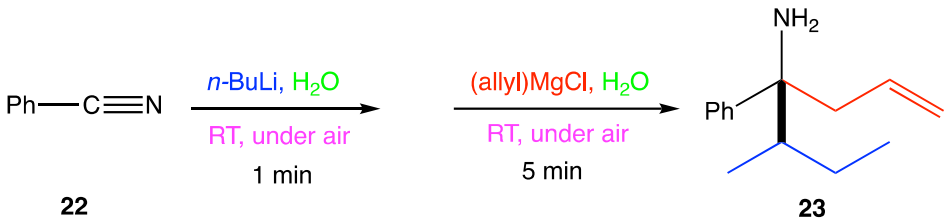

scheme 5.10: one-pot synthesis of carbinamine by the addition of organometallic compounds to nitriles

In another work, for which this project is centred on, Capriati and co-workers reported the synthesis of 2,2-disubstsituted tetrahydrofuran **26** by nucleophilic addition of polar *s*-block organometallic compounds (Grignard and organolithium reagents) to 4-chloro-1-phenylbutan-1-one **24** (4-chloro-butyrophenone or simply γ-chloroketone). The reaction was carried out "on water" where methyllithium (3 equiv.) or methyl magnesium chloride (3 equiv.) was rapidly spread over a suspension of **24** (0.5 mmol) in 1 mL water at room temperature under air. The nucleophilic addition proceeded via an intermediate chlorohydrin **25** (70 and 72% yield for MeMgCl and MeLi addition, respectively, after 10 mins) which on treatment with 10% aq. NaOH yielded the corresponding THF derivative **26** in up to 75% yield (scheme 5.11). The corresponding percentage conversion of the reactants in the conventional anhydrous THF solvent at -40 °C was 25% for MegMgCl reaction and 60% for MeLi reaction. A substantial decrease in yield of **26** (from 75 to 45%) was observed on increase of the water volume (from 1 mL to 2 mL). On drying, by removing most of the THF or hexane from the commercial solution of the organometallic compounds through passing under vacuum before the reaction, the addition product was still obtained but in reduced yield (30 - 35%). This pointed out that solvation and dilution of the organometallic reagent is essential for good yield. They proposed that especially with the MeLi addition, the reaction occur in the oil-water phase boundary with the ketone being insoluble in the aqueous medium. A small deuterium kinetic isotope effect was observed in the nucleophilic addition. The yield of **26** in D_2O showed decrease of up to about 8%. Trying the addition in another protic solvent, methanol, the disubstituted tetrahydrofuran product **26** was only obtained in traces. It is worthy of note that the γ-chloroketone is completely soluble in methanol. This result indicate that it is important that the reactant is insoluble in the protic solvent for the reaction to be favoured.[17]

The explanation for this unexpected reaction in the unconventional media and conditions remains by far not understood. Among some postulated explanations given in literature for this "on water" reaction include the trans-phase hydrogen bonding from dangling OH groups that stabilizes the reactants and TS proposed by Jung and Marcus and the hydrophobic effect

proposed by Breslow and Rideout. A review by Cartes-Clerget and co-workrs put together some postulates suggesting explanations for the "on water" reaction.[119] However, many puzzling aspects of the "on water" reaction remained poorly understood. It is for this that this thesis is focused, seeking to get a deeper understanding of the "on water" reaction which will prove very useful especially in moving away from volatile organic compounds as solvent to environmentally friendly, cheap and easy to handle water as solvent. Particular emphasis is placed on the MeLi addition to γ-chloroketone "on water" to yield 2,2-disubstituted tetrahydrofuran (scheme 5.11).

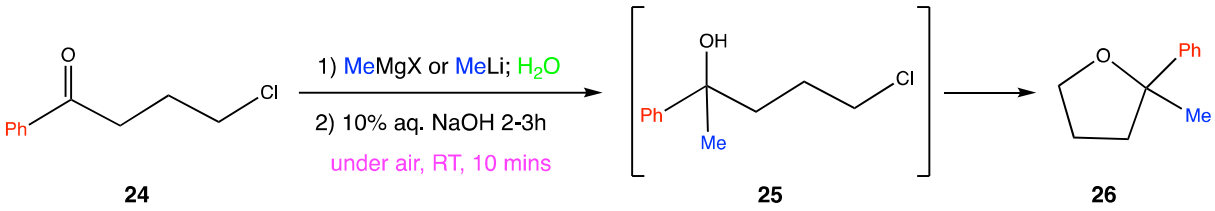

scheme 5.11: synthesis of 2,2-disubstsituted tetrahydrofuran by nucleophilic addition of polar *s*-block organometallic compounds (Grignard and organolithium reagents) to 4-chloro-1-phenylbutan-1-one

5.1 Implicit Solvation and Bulk Solvent Effect in On-Water Addition of γ-Chloroketone

In a first step, to investigate whether the water plays a role on a macroscopic level as a bulk or at the microscopic level, we calculated the energy barrier of the reaction in different implicit solvation with varied dielectric constants using the conductor-like ploarizable continuum model (CPCM) at the B3LYP/6-31+G(d,p) level. In the CPCM solvent model, the solvent is defined by a continuum that interact with the charges on the surface of the cavity which were generated by the solute that is placed in a created cavity. As this solvent model entails a continuous surface, a pronounced effect on the reaction by the varying of the dielectric constant may suggest the solvent plays a role in the reaction by acting as a reaction surface rather than interfering on an explicit scale. To this, single point energy calculation of the optimized gas phase reactant and TS geometries of MeLi dimer addition on γ-chloroketone were performed with different dielectric constants of 1.89, 7.25, 32.63, 80.40 and 60.00 corresponding to hexane, THF, methanol, water and a dummy solvent, respectively. The calculated energy barrier from the single point energies were compared to the energy barrier from the gas phase calculation. The results showed no significant difference between the reaction in the gas phase and in the different solvents (Table 5.1). This suggest the water may be involved in the reaction in an explicit molecular level rather than as just a bulk charge surface.

Table 5.1: Free energy barrier for MeLi dimer addition on γ-chloroketone in different implicit solvation

Solvent	Dielectric Constant	$\Delta E^{\ddagger}$ (kcal/mol)
hexane	1.89	6.25
THF	7.25	6.29
methanol	32.63	6.32
dummy	60.0	6.33
Water	80.40	6.33
No solvent	—	6.33

5.2 Water Coordination and MeLi Stabilization in Droplet

From the experimental work, Capriati and co-workers reported that despite the fast formation of the addition product **26** (in 10 mins) with good yield (up to 83%) for the nucleophilic MeLi addition of the γ-chloroketone "on water", the reaction with methanol solvent was poor. Only traces of product were obtained in the reaction in methanol solvent. With this in mind, the free energy barrier of the dimer addition reaction with coordinated water molecules was calculated and compared with the reaction with coordinated methanol molecules. Different forms of solvent coordination were considered: the system with one water or methanol molecule coordinated to the non-ketone-bonded lithium ion; system with a second solvent molecule in hydrogen-bonding with the already lithium-bonded solvent; the system where two solvent molecules (water or methanol) are coordinated to the non-ketone-bonded lithium ion to make it tetra-coordinated (Fig. 5.1). The free energy barrier of the nucleophilic methyl addition in these systems were calculated at the B3LYP/6-31+G (d,p) level with D3BJ dispersion correction in the gas phase. The results are given in Table 5.2. A significant difference in the calculated free energy barriers for the systems were noted. For instance, the addition in **2-water_1-coord** occurs with a calculated free energy barrier of 6.5 kcal mol^{-1} while 14.2 kcal mol^{-1} was calculated for **2-methanol_1-coord** system. This goes to say that, the "on water" reaction results from some unique property of water other than it polarity.

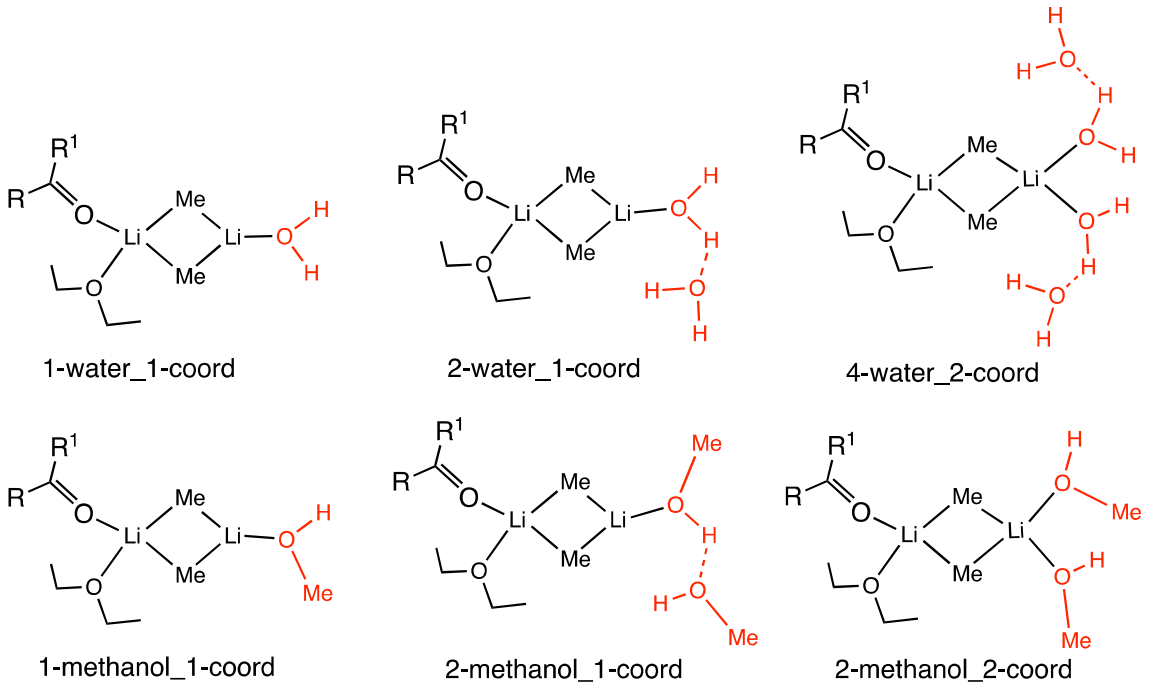

Fig. 5.1: water coordination and methanol coordination in $(MeLi)_2$—chloroketone

Table 5.2: Comparison of water coordinated and methanol coordinated MeLi dimer addition on γ-chloroketone

Water		**Methanol**	
system	**$\Delta G^{\ddagger}$ (kcal/mol)**	**system**	**$\Delta G^{\ddagger}$ (kcal/mol)**
1-water_1-coord	4.1	1-methanol_1-coord	2.7
2-water_1-coord	6.5	2-methanol_1-coord	14.2
4-water_2-coord	2.5	2-methanol_2-coord	3.4

The question arises of the existence and stability of these systems of coordinated solvent on the MeLi aggregate in the solvent media. Capriati and co-workers were able to point out that the solubility of the γ-chloroketone is important in the addition reaction. This they note by the poor yield (only traces) of the addition product when the reaction was carried out in methanol in which the ketone is soluble.[17] This is consistent with the Diel-Alder reaction in water reported by Breslow and Rideout where the reaction in methanol proceeded with small rate increment as compared with the high rate acceleration observed in the reaction in water.[109] Therefore, in modelling our reaction system in explicit solvent, it is important to maintain the insolubility of the ketone and also note that the achievement of the "on water" reaction is a function of some peculiar property of water. It is pertinent to note also, that the reaction involves vigorous stirring. To this we deemed probable that a water—emulsion surface is formed (the "on-water"

reaction, as named by Sharpless and co-workers) in this reaction. Yousung and Marcus proposed that the reaction rate acceleration observed in on-water reaction of cycloaddition of quadricyclane with dimethyl azodicarboxylate (scheme 5.4) results from a peculiar chemistry occurring between water and the reactant at the water—oil droplet interphase. The interfacial water molecules are said to have dangling OH group that protrudes into the oil (organic) phase and form hydrogen bonds with the reacting species. They suggested that stronger hydrogen bonds are formed with the transition state than with the reactant which is the reason for the rate acceleration obtained.[110]

To adequately model the "on water" reaction, a diethyl ether droplet containing the organic reactants (MeLi aggregate and the ketone) with surrounding water surface is constructed (Fig 5.2). In our case, protruding OH groups forming hydrogen bonds with the reacting species may not be feasible as only the carbonyl oxygen is the likely hydrogen-acceptor site in our ketone (γ-chloroketone). Because of the docking of the ketone on the MeLi through lone pair on the carbonyl oxygen, hydrogen bonding on the oxygen is a weak one. We further postulate the diffusion of few water molecules into the organic phase as a consequence of the vigorous stirring applied in the reaction.

Two scenarios were modelled. One in which a water molecule bonds to the lithium bonded to the ketone, Li^{b} (Fig 5.2a) and the second in which the water is coordinated to the lithium ion not bonded to the ketone, Li^{nb} (Fig 5.2b). In both scenarios, the MeLi aggregate was hydrolysed with the expulsion of a methane molecule as would be expected for reaction of water with polar organometallic compounds. The system with water coordinated to Li^{b} undergo hydrolysis in fewer steps than the corresponding Li^{nb}—water bonded system. On hydrolysis, the OH group from the water bonded to the two Li^{+} ions occupy the position previously occupied by the displaced methyl group. Next, we introduced a second water molecule to the systems in the same positions as the previous cases. Again, the systems were hydrolysed and methane was produced (scheme 5.12). This clearly shows that there is something more involved that is responsible for the stabilization against the consumption of the MeLi by hydrolysis. Our most probable guess is the formation of hydrogen bond network in water molecules diffusing into the organic layer. This is from taking into account that the reaction is far better in water which has stronger hydrogen bonding than in methanol with less hydrogen bonding capability.

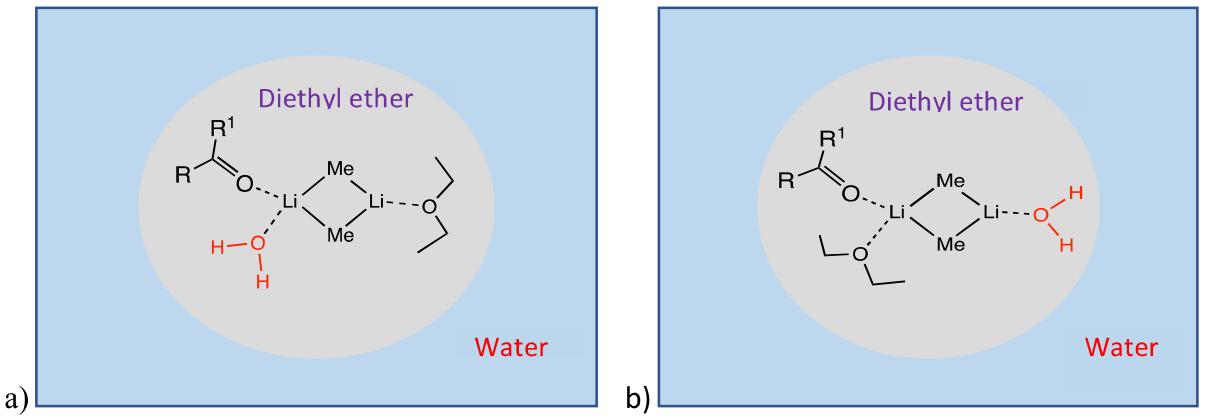

Fig. 5.2: oil—water droplet model with reactants in the diethyl ether phase (oil) surrounded by water surface: a) diffused water coordinated to Li^{b} b) diffused water coordinated to Li^{nb}

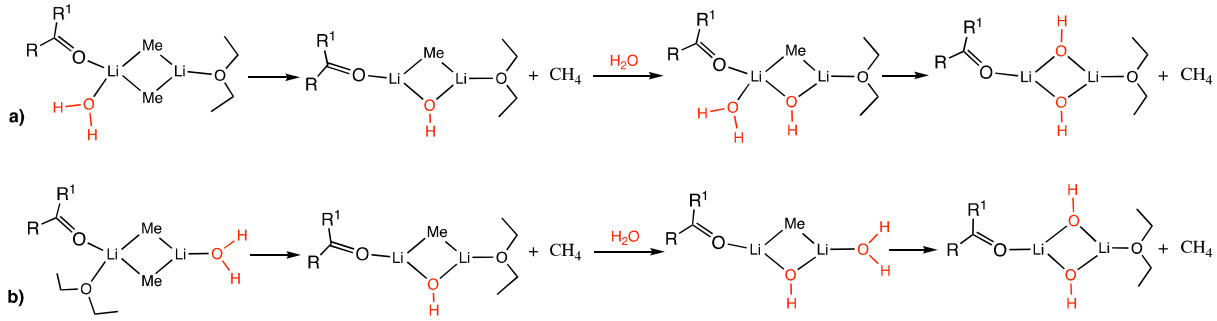

scheme 5.12: a) hydrolysis of $(MeLi)_2$—chloroketone system by diffusion of water molecule on Li^{b} b) hydrolysis of $(MeLi)_2$—chloroketone system by diffusion of water molecule on Li^{nb}

Since our immediate goal is to prevent the complete consumption of our organolithium reagent by the diffusing water, our next intuition is to create a hydrogen bond network with the diffused water molecules and the partially hydrolysed MeLi aggregate. Hydrogen bonding between hydrogen of coordinated water on the metal of organometallic complex and some ionic center have been reported, where the water act as a ligand rather than an acid. For instance, the complexation of 2-mercaptobenzoxazole with *N,N,N′,N′*-tetramethylethylenediamine in the presence of water showed hydrogen bonding between the proton and the polarised sulphur centre as reported by Wright and co-workers (Fig 5.3) .[120] In a DFT calculation at B3P86/6-31+G(d,p) and by mass spectrometry Gimbert *et al* noted the aggregation of water molecules (up to four) with strongly polar partner such as LiCl, LiBr or MeLi protected against hydrolysis of the lithium amide of lithium benzyhydryl(1-benzylpyrrolidin-3-yl)amide **23** (scheme 5.13). The protection was said to rely probably on the repulsion of the molecules away from the amide nitrogen by the presence of the polar LiX (X=Cl, Br or Me) partner, thereby making its protonation more difficult.[121]

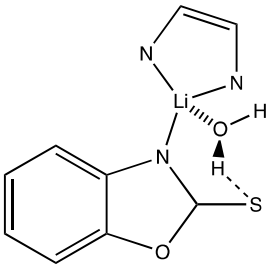

Fig. 5.3: hydrogen bonding in the complexation of 2-mercaptobenzoxazole with *N,N,N′,N′*-tetramethylethylenediamine in the presence of water

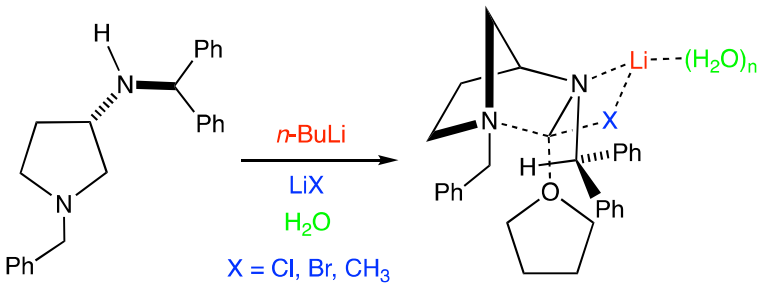

23

scheme 5.13: hydrogen bonding from LiX protecting against hydrolysis of lithium benzyhydryl(1-benzylpyrrolidin-3-yl)amide

In our system, we consider two cases of hydrogen bond network for a partially hydrolysed $(MeLi)_2$—ketone system. On the one case, one or two molecules of water form a hydrogen-bond network with the OH group in the partially hydrolysed system and a bonded water molecule on Li^{b+} ion. And on the other case, one or two molecules of water form a hydrogen-bond network with the OH group in the partially hydrolysed system and a bonded water molecule on Li^{nb+} ion (Fig 5.4). The relative stability of the systems with respect to one another was calculated by DFT at BLYP/def2-TZVPP level with the Becke-Johnson damped Grimme's dispersion correction, D3BJ. The result showed that the structures with the hydrogen-bond network at Li^{nb} (that is, **2wat-Eth_HB_B** and **3wat-Eth_HB_B** (Fig 5.4) are more stable than their counterparts with the hydrogen-bond network involving Li^{b} (Table 5.3). The free activation energy for the nucleophilic addition in these systems were calculated at the same DFT level. The **3wat-Eth_HB_B** system showed the lowest energy barrier and the highest barrier was observed for **3wat-Eth_HB_A** (Table 5.3 column 4) owing to the crowdedness around Li^{b} that tends to push the ketone away.

Molecular dynamic simulation of the hydrogen-bonding network systems in droplet were carried out by QM/MM with the systems treated at the quantum level and the surrounding diethyl ether and bulk water treated at the force field level. All the systems underwent hydrolysis of the MeLi except **2wat-Eth_HB_B**. This system remained stable for up to 52 ps

simulation time carried out. Its stability results from the strong hydrogen-bond network. On this stable system, further water coordination and hydrogen-bond network expansions were made. They include: a water molecule in hydrogen bond with the carbonyl oxygen (scheme 5.14a); one water molecule in hydrogen bond with the carbonyl oxygen and at the same time bonded to Li^b (scheme 5.14b); a new hydrogen-bond network involving Li^b, the carbonyl oxygen and two water molecules (scheme 5.14c) or three water molecules (scheme 5.14d). These systems either results in displacement of water molecule while maintaining the **2wat-Eth_HB_B** geometry (scheme 5.14 a and b) or lead to hydrolysis of the methyllithium in the cluster (scheme 5.14 c and d).

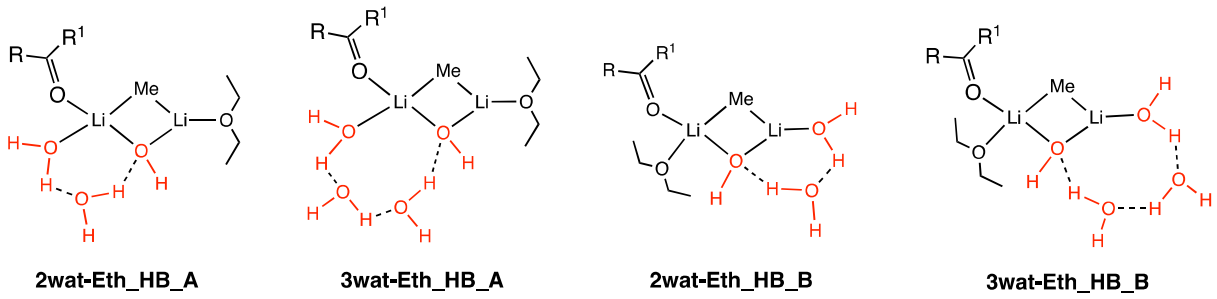

Fig. 5.4: hydrogen bond network in the partially hydrolysed MeLi dimer

Table 5.3: Comparison of stability of various hydrogen-bond network and free energy barrier for the MeLi addition

system	ΔE	ΔG	$\Delta G^{\ddagger}$ (kcal/mol)
2 water HB			
2wat-Eth_HB_A	+1.90	+2.40	3.55
2wat-Eth_HB_B	0.00	0.00	3.70
3 water HB			
3wat-Eth_HB_A	+0.35	+2.24	5.17
3wat-Eth_HB_B	0.00	0.00	3.33

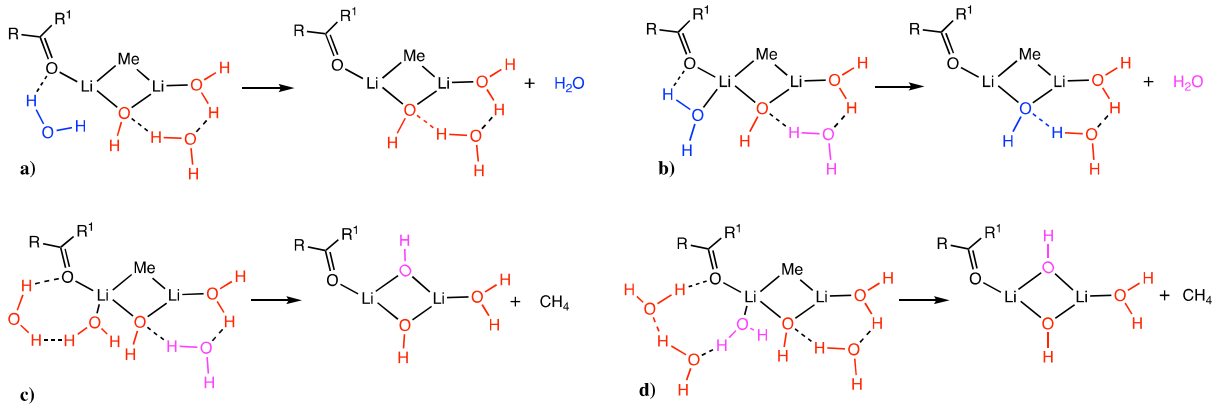

scheme 5.14: water coordination and hydrogen-bond network expansion of **2wat-Eth_HB_B**: a) added water in hydrogen bond with the carbonyl oxygen b) added water coordinated to Li^b and in hydrogen bond with the carbonyl oxygen c) expanded hydrogen bond network at Li^b with two water molecules d) expanded hydrogen bond network at Li^b with three water molecules

5.3 Nucleophilic Addition in Partially Hydrolysed MeLi Aggregates

Given the existence of **2wat-Eth_HB_B** in the droplet without hydrolysis, a well-tempered metadynamics study of the nucleophilic addition reaction was conducted on this system. Same parameters (collective variables, pace of Gaussian addition, Gaussian height and weight) used for the conventional system were set for the metadynamics. In the addition, the complex **2wat-Eth_HB_B** did not undergo solvation with diethyl ether molecule at the initial state of the reaction. Coordination with a diethyl ether molecule only occurred after the C—C bond formation (Fig 5.5a). As in the conventional case, the transition state is attained by the bending of the C^2OLi^b angle, from around 140° at the start to around 84 ± 9 at the TS (Fig 5.5b). Here also, the methyl group approach in a direction perpendicular to the plane of the carbonyl group. The C^1—C^2—O bond angle and the C^1C^2OR dihedral defining the Bürgi-Dunitz trajectory have values of 106 ± 6 and –106 ± 6, respectively. The C^1—C^2—O is consistent with the expected value for a typical Bürgi-Dunitz trajectory for nucleophilic addition while C^1C^2OR has value higher than the generally expected value. The free activation energy for this addition is 12 kcal mol^{-1} similar to the calculated value for the conventional reaction (13 kcal mol^{-1}). This however, does not explain the quick reaction observed in the on-water reaction in comparison to the reaction in the conventional THF as reported in the experimental work by Capriati and co-workers.[17] At the product, the carbonyl oxygen is protonated by one of the water molecule from the hydrogen-bond network and the Li^b ion is solvated by a diethyl ether (Fig 5.5c). The free

energy surface for this ether—droplet "on water" reaction is given in Fig 5.5d and the overall proposed mechanism is given in scheme 5.15.

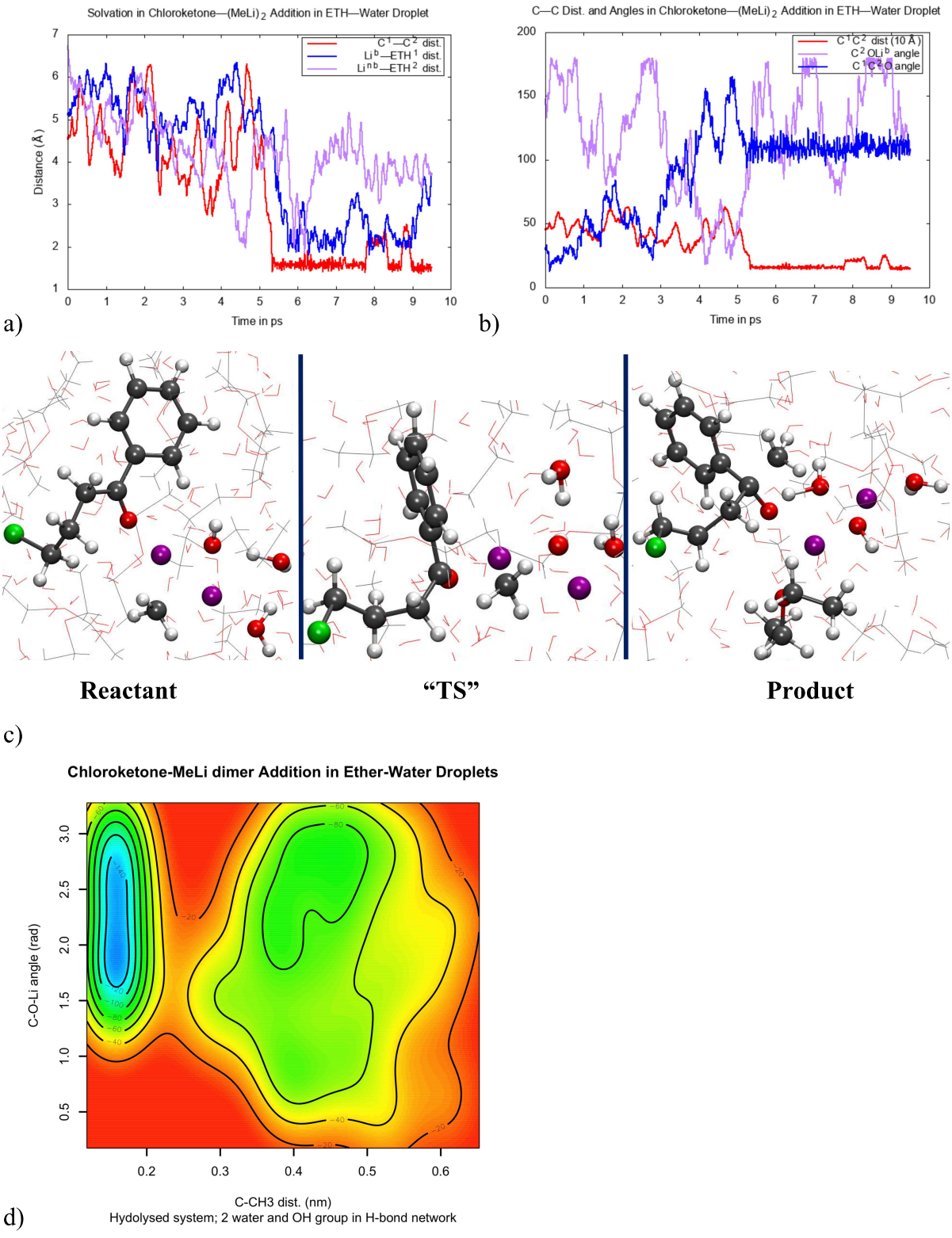

Fig. 5.5: "on water" MeLi addition in ether—water dropletfor **2wat-Eth_HB_B** system: a) Et_2O coordination in the addition in ether—water droplet b) evolution of the C^2OLi^b and C^1C^2O angles in relation to the C—C bond formation in the addition c) snapshot of the reactant, "TS"

and product in the nucleophilic addition in ether—water droplet d) free energy surface for the Methyl addition in the ether—water droplet

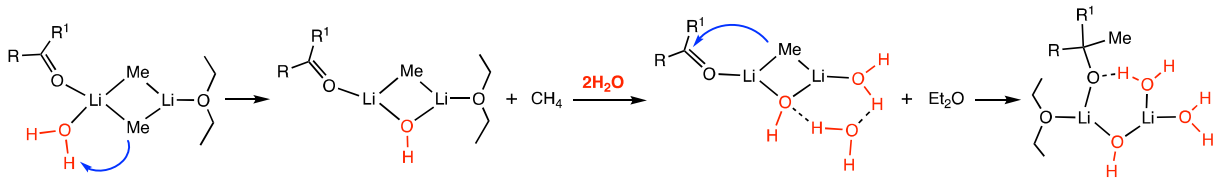

scheme 5.15: proposed mechanism of the "on water" nucleophilic MeLi dimer addition in wa

Next, the "on water" droplet addition with MeLi tetramer was considered. As earlier established, only one Li^+ ion is solvated with diethyl ether in $(MeLi)_4$—chloroketone, leaving the remaining three Li^+ ions more susceptible to coordination with the diffusing water into the oil phase (diethyl ether phase) of the droplet due to the less steric repulsion around these Li^+ ions. The energy of interaction between the coordinated diethyl ether and the $(MeLi)_4$—chloroketone cluster via Et_2O—Li bond was calculated by SAPT2/aug-cc-pvdz to be 16.4 kcal mol^{-1}. This is higher than the interaction energy between water and the cluster (H_2O—Li) with calculated value of 12.3 kcal $mol^{-1}$and also higher than the interaction energy between the γ-chloroketone and the MeLi tetramer cluster, with value of 14.7 kcal mol^{-1}. Pocker and Exner reported in their work that, in fact the rate determining step in the hydrolysis of diethyl ether solution of the organolithiums, PhLi and $PhCH_2Li$, is the displacement of the metal-coordinated solvent molecule by the water.[122] This suggest the more reason other than the steric repulsion from the diethyl ether why water may be reluctant to coordinate to the lithium bonded to the diethyl ether solvent as fast as it would to the non-solvated lithium ions in the aggregate. Therefore, diffusing water molecules are coordinated to the three Li^+ ions without coordinated solvent which then undergo hydrolysis of the Me—Li bonds, expelling methane and the OH groups occupying the methyl positions in the aggregate to give a partially hydrolysed tetramer cluster. To the partially hydrolysed system, metadynamics simulation was performed. The addition occurred with an intermediate opening of the tetrahedral structure leading to the TS before reverting back to the tetrahedral structure on product formation (scheme 5.16). The free energy barrier for the conversion to the intermediate ring structure is about 3 kcal mol^{-1} and the free energy of activation for the nucleophilic addition is 12 kcal mol^{-1}. At the initial state of the reaction, only one Li^+ ion is coordinated to a diethyl ether solvent. At the intermediate ring structure, the solvent coordination is lost. The solvent coordination at one Li^+ ion remerges at the TS (Fig 5.6a). A study of the diffusion of a water molecule from a distance of about 9Å to

a Li^+ ion in the partially hydrolysed tetramer, **C** showed the diffusion cost about 7 kcal mol^{-1} which further suggest that the complete hydrolysis of **C** may not occur rapidly. The values, respectively, of 111 ± 6 and 99 ± 10° were calculated for the C^1—C^2—O bond angle and C^1C^2OR dihedral defining the Bürgi-Dunitz trajectory.

It is worth noting that, the addition involving the partially hydrolysed MeLi dimer (one of the methyl group hydrolysed) without the hydrogen bond network was unattainable. Also, the tetramer with only two methyl lithium hydrolysed yielded addition with higher free activation energy of 19 kcal mol^{-1} (similar to the value of 20 kcal mol^{-1} calculated for the conventional reaction) and with a poor free energy surface without smooth transition from reactant to product.

Therefore, from the calculated free energy barrier for the addition involving the partially hydrolysed dimer system with hydrogen-bond network stabilizing it against complete hydrolysis (**2wat-Eth_HB_B**) and the calculated free energy barrier involving the partially hydrolysed tetramer **C**, it can be suggested that the "on water" reaction may be driven by a combination of more than one route all competing against hydrolysis. However, much still needs to be done to validate this proposed mechanism as well as explanation for the rate acceleration observed as reported in the experimental work.

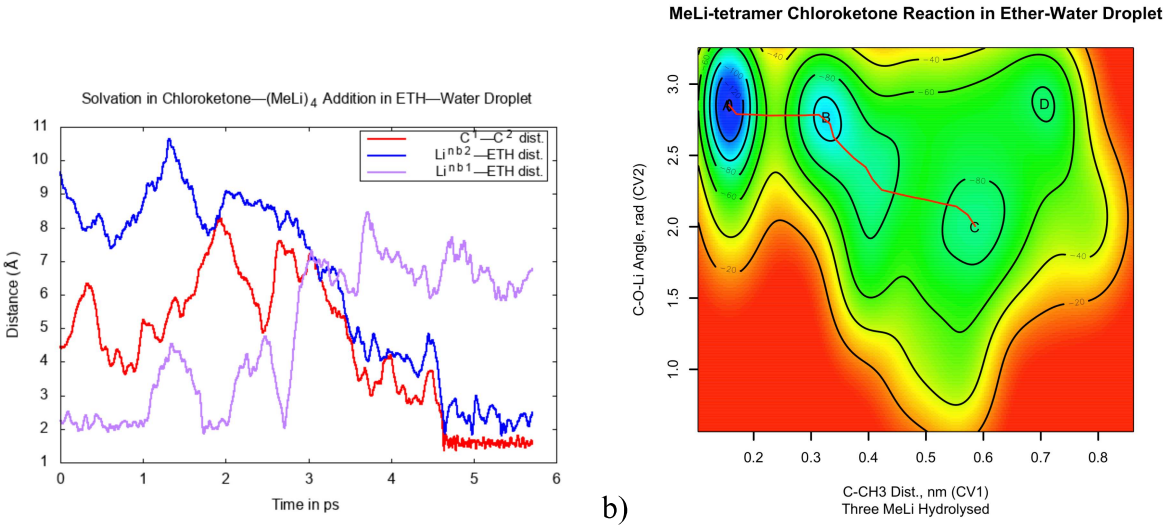

Fig. 5.6: "on water" MeLi addition in ether—water droplet for partially hydrolysed tetramer system, $[MeLi(LiOH)_3]$—chloroketone: a) nature of Et_2O solvent coordination in the partially hydrolysed tetramer cluster b) free energy surface for the methyl addition showing metastable state of partially hydrolysed tetramer, **C** going to product, **A** through an intermediate **B**

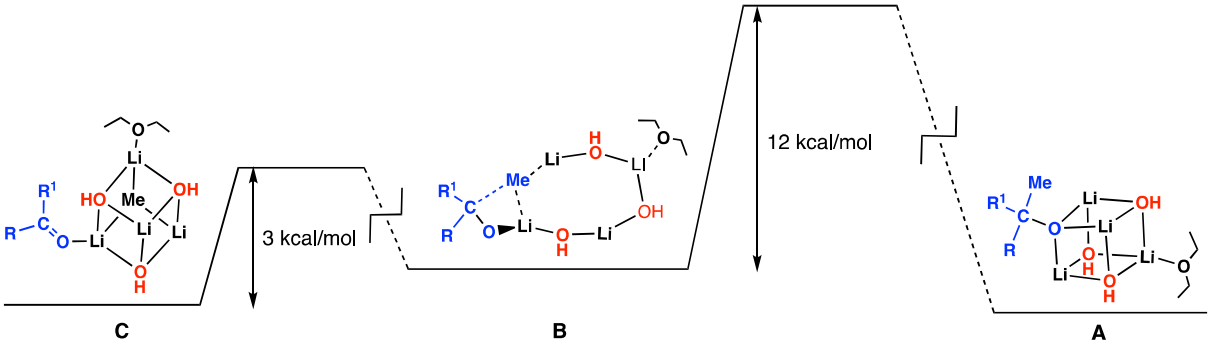

scheme 5.16: energy diagram and reaction path for "on water" nucleophilic addition involving partially hydrolysed tetramer system [MeLi(LiOH)$_3$]—chloroketone

5.4 Conclusion

The study of the mechanism for unconventional "on water" nucleophilic addition of MeLi to the γ-chloroketone is reported in this chapter. The system was modelled as a water—diethyl ether droplet with the organic reactants (MeLi aggregate and the ketone) in the organic phase surrounded by water surface. Hydrogen-bonding network was found to play a significant role against the complete consumption of the organolithium by hydrolysis. A strong hydrogen network was formed between diffusing water in the diethyl ether layer and the partially hydrolysed MeLi dimer. Like in the conventional reaction, the addition follows through the bending of the COLi bond angle and rotation about the carbonyl group, C=O. The free activation energy for the addition reaction of this stabilized partially hydrolysed dimer system in the droplet was found to be similar to the corresponding reaction in the conventional diethyl ether. In the case of the tetramer, rapid hydrolysis by the diffusing water molecules at the easily accessible Li^+ ions (the three Li^+ not coordinated to Et_2O solvent) were observed. The Li^+ ion coordinated to diethyl ether is less accessible for coordination with the diffusing water due to steric. This partially hydrolysed tetramer undergoes addition at a lower free activation energy, about 8 kcal mol^{-1} less than the corresponding conventional addition. The addition follows through an intermediate opening of tetrahedral structure into ring structure.

We therefore, proposed that the "on water" reaction may occur through a combination of these partially hydrolysed dimer and tetramer routes. However, more still need to be done to validate this proposed mechanism.

CONCLUSION AND PERSPECTIVES

After all that has been done and said, it is rewarding to take a step back and reflect on the key notes that have been established in this study. In pursuing the main objective of this thesis, which is to study the mechanism and the role of water in the unexpected unconventional "on water" nucleophilic addition of methyllithium (MeLi) on 4-chloro-1-phenylbutan-1-one (γ-chloroketone) to yield 2,2-disubstituted tetrahydrofuran, the study is proceeded in stages. First, the nature of aggregation and solvation of the organolithium is studied in the ethereal solvents, diethyl ether (Et_2O) and tetrahydrofuran (THF). Next, the nucleophilic addition reaction is studied in the conventional ethereal solvents (Et_2O and THF) establishing the reaction path and calculation of activation energy for subsequent comparison as well as identifying the descriptor parameters in the metadynamics enhanced sampling method for subsequent use in the "on water" reaction study which constitute the last chapter of the thesis.

A side project conducted at the course of the study on the mechanism and stereoselectivity study of the preparation of amines beared by chiral tertiary carbon by the organometallic 1,2-addition reaction on sulfinyl ketimines is reported in Chapter three of this work. The study entails the elucidation of the high stereoselectivity observed in the 1,2-addition despite the existence in equilibrium of both *E* and *Z* isomers of the sulfinyl ketimines in solution under room temperature. The lower free energy barrier, $\Delta G^{\ddagger}$ for the addition reaction in comparison to the isomerization free energy barrier is suggested to be responsible for the leaning of the reaction towards the product from the more stable isomer. The formation of the product is thermodynamically favoured making the process irreversible. Also, the effect of steric repulsion contributes to the directing of the reaction towards stereoselectivity. The effect of highly coordinating solvent (THF) on the reaction as well as the competition of protonolysis with the 1,2-addition is not negligible. Therefore, in perspective it will be enlightening to carry out the study with explicit solvation.

In the first step of our nucleophilic MeLi addition study, it was determined by DFT calculation (BLYP/def2-TZVPP with D3BJ dispersion correction) that the tetrahedral tetramer MeLi aggregate structure is the more stable configuration among the numerous optimized aggregates studied. The nature of solvation of the MeLi aggregate differ with the solvents and the geometry of the aggregate. For instance, the solvent coordination number on Li^+ ions in cyclic MeLi geometries is higher than the Li^+ ion coordination number in polyhedral MeLi structures. Also, the solvent coordination number with THF is often seen to be higher than with a corresponding Et_2O solvated aggregate. This was found to be due to the higher steric repulsion in the chain-

like Et_2O molecules with flexible wiggling ethyl arms in comparison to the cyclic THF molecule. This effect of steric was seen to limit solvent coordination in especially $(MeLi)_4$—chloroketone complex where mostly only one Li^+ ion is solvated at a time from a QM/MM molecular dynamic simulation study. The occurrence of solvent exchange was observed in the studied systems. For instance, in the $(MeLi)_2$—chloroketone systems in THF and $(MeLi)_4$—chloroketone in Et_2O.

Finding the MeLi dimer and tetrahedral tetramer aggregates to be most commonly isolated aggregates especially in the highly coordinating Et_2O and THF solvents with a further backing from the high stability of the tetrahedral tetramer structure, the reaction mechanism of the nucleophilic addition of the MeLi dimer and tetramer on ketone (acetone and γ-chloroketone) was studied in the conventional Et_2O and THF solvents implicitly by solvation model based on quantum mechanical charge density (SMD) with explicit solvent molecules bonded to the alkyllithium (implicit-explicit model) and explicitly by the well-tempered metadynamics enhanced sampling method. The reaction proceeded by first, the docking of the ketone on the MeLi aggregate via the carbonyl oxygen lone pair. Then, the C—C bond formation is facilitated by the bending of the angle between the carbonyl carbon, carbonyl oxygen and the ketone-bonded lithium (C—O—Li) and by the rotation about the C=O bond which reorients the carbonyl group to be in the plane of the bonding MeLi unit. The methyl group approach the ketone in a direction perpendicular to the carbonyl group plane. The methyl attack on the ketone follows through the Bürgi-Dunitz trajectory for nucleophilic addition on carbonyl compounds in most cases with regards to the CH_3—C=O angle (from the implicit calculation). The effect of solvation in the reaction is by no means negligible. For instance, in THF, the MeLi dimer addition on acetone, seen from metadynamics study, proceeds via the monomeric TS species following splitting of the dimer which later recombined upon the product formation. The corresponding dimer addition in Et_2O on the other hand follows via dimeric TS specie. The nucleophilic addition reaction with the less bulky acetone occur with lower free energy barrier than with the bulky γ-chloroketone. In general, the nucleophilic addition reaction in Et_2O is favoured over the reaction in THF and the reaction proceed with lower activation free energy with the MeLi dimer aggregates in comparison to the MeLi tetramers. However, the calculated free activation energy in both aggregates are within feasible attainable limits.

In the “on water” reaction, it was established that water plays a role on the microscopic scale and not just as a charge reaction surface. The reaction system was modelled as a water—oil (organic) droplet. The reactants are in the Et_2O (organic) phase surrounded by water surface with few water molecules able to diffuse into the organic phase. The diffusing water partially

hydrolyse the MeLi dimer or tetramer as the case may be. The diffusing water are able to form a hydrogen bonding network with the partially hydrolysed dimer, strong enough to prevent complete hydrolysis. It is this partially hydrolysed system that proceed to yield the addition product. In the tetramer, the partial hydrolysis occurs from the easy coordination of water on the three unsolvated Li^+ ions in the $(MeLi)_4$—chloroketone system. The Et_2O coordination at one of the Li^+ makes it less accessible to the diffusing water and therefore the tetramer is partially hydrolysed. Interestingly, the partially hydrolysed system, $[(MeLi)(LiOH)_3]$—chloroketone could undergo the nucleophilic addition at an even lower free activation energy (8 kcal mol^{-1} lower than the corresponding conventional tetramer addition). Therefore, we suggest here, that the "on water" reaction occurs via a combination from the partially hydrolysed dimer and partially hydrolysed tetramer system and hydrogen bond network playing an important role in preventing complete hydrolysis of the organolithium reagent. However, much remain to be done.

As the biasing in the metadynamics simulation to promote the transitioning from the reactant to product is highly a function of the collective variable set, the choice of the collective variable (CV) is an important one for accurate sampling of the metastable states. Neural network has been used in the construction of CV. Parinello and co-workers have shown an improved use of NN in the construction of CV set with multiple descriptors (atomic coordinates such as bond distances, angles and coordination number) by directly expressing the CV as the NN output layer. The CV distribution is designed to match a preassigned target in which the metastable states are well-discriminated. This new-found method can reduce the number of CVs leading to construction of a simple and better comprehensible energy profile.[123] It will be worth trying to use this neural network based method to generate CV sets for our studied system for validation of our selected CV and generation of simplified potential surface which may yield a more improved (precise) determination of activation energy. It is recommended also, to apply the infrequent metadynamics method to study the nucleophilic MeLi addition on the γ-chloroketone so as to estimate and compare the kinetic rates of the reaction in the conventional solvent and in the unconventional "on water" media.

Since our calculation involves using QM/MM where the bulk of the solvent molecules are treated at the classical level, it is undisputable that some approximations are embedded in the treatment of our system. It will be considered better to treat the whole system at the same quantum level (*ab-initio* molecular dynamics, AIMD) allowing the whole solvents to be involve in the reaction especially in our system where fluctuation of hydrogen bond network is feasible and the Grotthuss mechanism is not far-fetched. Unfortunately, it will be costly to carry out an

AIMD calculation on our system given the large number of atoms if we want to carry out a thorough sufficient large scale sampling of our system. Parinello and co-workers have demonstrated the use of neural network to build a reactive potential (and by no means the only example of the use of machine learning in this context) in the quality of *ab initio* level, for the study of the decomposition of urea in water.[124] Having done a metadynamics study and established the collective variables and a propose reaction path, machine learning can be handful in constructing a reactive potential for treating our system. Therefore, as a proposed future work, our system can be learned by the use of neural network and then develop a reactive potential for treating these class of "on water" reaction.

REFERENCE

(1) Thayer, J. S. Cadet's Fuming Liquid: An Historical Survey. *J. Chem. Educ.* **1966**, *43* (11), 594. https://doi.org/10.1021/ed043p594.

(2) Seyferth, D. Cadet's Fuming Arsenical Liquid and the Cacodyl Compounds of Bunsen. *Organometallics* **2001**, *20* (8), 1488–1498. https://doi.org/10.1021/om0101947.

(3) Thayer, J. S. Historical Origins of Organometallic Chemistry. Part I, Zeise's Salt. *J. Chem. Educ.* **1969**, *46* (7), 442. https://doi.org/10.1021/ed046p442.

(4) Zeise, W. C.; Hunt, L. B.; Johnson, T.; Group, M. And His Platinum Complexes.

(5) Thayer, J. S. Historical Origins of Organometallic Chemistry. Part II, Edward Frankland and Diethylzinc. *J. Chem. Educ.* **1969**, *46* (11), 764. https://doi.org/10.1021/ed046p764.

(6) Rheinholdt, H. Fifty Years of the Grignard Reaction. *J. Chem. Educ.* **1950**, *27* (9), 476–488.

(7) Wietelmann, U.; Klett, J. 200 Years of Lithium and 100 Years of Organolithium Chemistry. *Zeitschrift für anorganische und allgemeine Chemie* **2018**, *644* (4), 194–204. https://doi.org/10.1002/zaac.201700394.

(8) Schlenk, W.; Holtz, J. Über die einfachsten metallorganischen Alkaliverbindungen. *Sitzung Vom* **1917**, *50* (1), 262–274. https://doi.org/10.1002/cber.19170500142.

(9) Elschenbroich, C. *Organometallics*; John Wiley & Sons, 2016.

(10) Gupta, B. D.; Elias, A. J. *Basic Organometallic Chemistry: Concepts, Synthesis and Applications*, second.; Universities Press (India) Private Limited, 2013.

(11) Parkins, A. W.; Poller, R. C. *An Introduction to Organometallic Chemistry*; Macmillan International Higher Education, 1986.

(12) Young, W. G.; Roberts, J. D. Highly-Branched Compounds. The Preparation of Triisopropylcarbinol and Diisopropyl-s-Butylcarbinol. *J. Am. Chem. Soc.* **1944**, *66* (9), 1444–1445. https://doi.org/10.1021/ja01237a007.

(13) Bartolo, N. D.; Read, J. A.; Valentín, E. M.; Woerpel, K. A. Reactions of Allylmagnesium Reagents with Carbonyl Compounds and Compounds with C═N Double Bonds: Their Diastereoselectivities Generally Cannot Be Analyzed Using the Felkin–Anh and Chelation-Control Models. *Chem. Rev.* **2020**, *120* (3), 1513–1619. https://doi.org/10.1021/acs.chemrev.9b00414.

(14) Perna, F. M.; Vitale, P.; Capriati, V. Synthetic Applications of Polar Organometallic and Alkali-Metal Reagents under Air and Moisture. *Current Opinion in Green and Sustainable Chemistry* **2021**, *30*, 100487. https://doi.org/10.1016/j.cogsc.2021.100487.

(15) García-Álvarez, J.; Hevia, E.; Capriati, V. The Future of Polar Organometallic Chemistry Written in Bio-Based Solvents and Water. *Chemistry – A European Journal* **2018**, *24* (56), 14854–14863. https://doi.org/10.1002/chem.201802873.

(16) García-Álvarez, J.; Hevia, E.; Capriati, V. Reactivity of Polar Organometallic Compounds in Unconventional Reaction Media: Challenges and Opportunities: Reactivity of Organometallic Compounds in Unconventional Reaction Media. *Eur. J. Org. Chem.* **2015**, *2015* (31), 6779–6799. https://doi.org/10.1002/ejoc.201500757.

(17) Cicco, L.; Sblendorio, S.; Mansueto, R.; Perna, F. M.; Salomone, A.; Florio, S.; Capriati, V. Water Opens the Door to Organolithiums and Grignard Reagents: Exploring and Comparing the Reactivity of Highly Polar Organometallic Compounds in Unconventional Reaction Media towards the Synthesis of Tetrahydrofurans. *Chem. Sci.* **2016**, *7* (2), 1192–1199. https://doi.org/10.1039/C5SC03436A.

(18) Morse, P. M. Diatomic Molecules According to the Wave Mechanics. II. Vibrational Levels. *Phys. Rev.* **1929**, *34* (1), 57–64. https://doi.org/10.1103/PhysRev.34.57.

(19) Jensen, F. *Introduction to Computational Chemistry*, 2nd ed.; John Wiley & Sons, Ltd: The Atrium, Southern Gate, Chichester, West Sussex, England, 2007.

(20) Jones, J. E. On the Determination of Molecular Fields. -II From the Equation of State of a Gas. *Proc. R. Soc. London* **1924**, *106* (738), 463.

(21) Raghavachari, K.; Trucks, G. W.; Pople, J. A.; Head-Gordon, M. A Fifth-Order Perturbation Comparison of Electron Correlation Theories. *Chemical Physics Letters* **1989**, *157* (6), 479–483. https://doi.org/10.1016/S0009-2614(89)87395-6.

(22) Riplinger, C.; Neese, F. An Efficient and near Linear Scaling Pair Natural Orbital Based Local Coupled Cluster Method. *The Journal of Chemical Physics* **2013**, *138* (3), 034106. https://doi.org/10.1063/1.4773581.

(23) Pinski, P.; Riplinger, C.; Valeev, E. F.; Neese, F. Sparse Maps—A Systematic Infrastructure for Reduced-Scaling Electronic Structure Methods. I. An Efficient and Simple Linear Scaling Local MP2 Method That Uses an Intermediate Basis of Pair Natural Orbitals. *The Journal of Chemical Physics* **2015**, *143* (3), 034108. https://doi.org/10.1063/1.4926879.

(24) Riplinger, C.; Pinski, P.; Becker, U.; Valeev, E. F.; Neese, F. Sparse Maps—A Systematic Infrastructure for Reduced-Scaling Electronic Structure Methods. II. Linear Scaling Domain Based Pair Natural Orbital Coupled Cluster Theory. *The Journal of Chemical Physics* **2016**, *144* (2), 024109. https://doi.org/10.1063/1.4939030.

(25) Guo, Y.; Riplinger, C.; Becker, U.; Liakos, D. G.; Minenkov, Y.; Cavallo, L.; Neese, F. Communication: An Improved Linear Scaling Perturbative Triples Correction for the Domain Based Local Pair-Natural Orbital Based Singles and Doubles Coupled Cluster Method [DLPNO-CCSD(T)]. *The Journal of Chemical Physics* **2018**, *148* (1), 011101. https://doi.org/10.1063/1.5011798.

(26) Hohenberg, P.; Kohn, W. Inhomogeneous Electron Gas. *Phys. Rev.* **1964**, *136* (3B), B864–B871. https://doi.org/10.1103/PhysRev.136.B864.

(27) Kohn, W.; Sham, L. J. Self-Consistent Equations Including Exchange and Correlation Effects. *Phys. Rev.* **1965**, *140* (4A), A1133–A1138. https://doi.org/10.1103/PhysRev.140.A1133.

(28) Lee, C.; Yang, W.; Parr, R. G. Development of the Colle-Salvetti Correlation-Energy Formula into a Functional of the Electron Density. *Phys. Rev. B* **1988**, *37* (2), 785–789. https://doi.org/10.1103/PhysRevB.37.785.

(29) Becke, A. D. Density-Functional Exchange-Energy Approximation with Correct Asymptotic Behavior. *Phys. Rev. A* **1988**, *38* (6), 3098–3100. https://doi.org/10.1103/PhysRevA.38.3098.

(30) Becke, A. D. Density-functional Thermochemistry. III. The Role of Exact Exchange. *The Journal of Chemical Physics* **1993**, *98* (7), 5648–5652. https://doi.org/10.1063/1.464913.

(31) P.J. Stephens; F.J. Devlin; C.F. Chabalowski; M.J. Frisch. Ab Initio Calculation of Vibrational Absorption and Circular Dichroism Spectra Using Density Functional Force Fields. *J. Phys. Chem.* **1994**, *98* (45), 11623–11627.

(32) Weigend, F.; Ahlrichs, R. Balanced Basis Sets of Split Valence, Triple Zeta Valence and Quadruple Zeta Valence Quality for H to Rn: Design and Assessment of Accuracy. *Physical Chemistry Chemical Physics* **2005**, *7* (18), 3297–3305. https://doi.org/10.1039/B508541A.

(33) Weigend, F.; Furche, F.; Ahlrichs, R. Gaussian Basis Sets of Quadruple Zeta Valence Quality for Atoms H–Kr. *The Journal of Chemical Physics* **2003**, *119* (24), 12753–12762. https://doi.org/10.1063/1.1627293.

(34) Johnson, E. R.; Becke, A. D. A Post-Hartree-Fock Model of Intermolecular Interactions: Inclusion of Higher-Order Corrections. *The Journal of Chemical Physics* **2006**, *124* (17), 174104. https://doi.org/10.1063/1.2190220.

(35) Grimme, S.; Ehrlich, S.; Goerigk, L. Effect of the Damping Function in Dispersion Corrected Density Functional Theory. *Journal of Computational Chemistry* **2011**, *32* (7), 1456–1465. https://doi.org/10.1002/jcc.21759.

(36) Marenich, A. V.; Cramer, C. J.; Truhlar, D. G. Universal Solvation Model Based on Solute Electron Density and on a Continuum Model of the Solvent Defined by the Bulk Dielectric Constant and Atomic Surface Tensions. *J. Phys. Chem. B* **2009**, *113* (18), 6378–6396. https://doi.org/10.1021/jp810292n.

(37) Neese, F. The ORCA Program System. *WIREs Computational Molecular Science* **2012**, *2* (1), 73–78. https://doi.org/10.1002/wcms.81.

(38) Neese, F. Software Update: The ORCA Program System, Version 4.0. *WIREs Computational Molecular Science* **2018**, *8* (1), e1327. https://doi.org/10.1002/wcms.1327.

(39) Neese, F.; Wennmohs, F.; Becker, U.; Riplinger, C. The ORCA Quantum Chemistry Program Package. *J. Chem. Phys.* **2020**, *152* (22), 224108. https://doi.org/10.1063/5.0004608.

(40) Rassolov, V. A.; Pople, J. A.; Ratner, M. A.; Windus, T. L. 6-31G * Basis Set for Atoms K through Zn. *The Journal of Chemical Physics* **1998**, *109* (4), 1223–1229. https://doi.org/10.1063/1.476673.

(41) Barone, V.; Cossi, M. Quantum Calculation of Molecular Energies and Energy Gradients in Solution by a Conductor Solvent Model. *J. Phys. Chem. A* **1998**, *102* (11), 1995–2001. https://doi.org/10.1021/jp9716997.

(42) M.J Frisch; G. W. Trucks; H. B. Schlegel; G. E. Scuseria; M. A. Robb; J. R. Cheeseman; G. Scalmani; V. Barone; G. A. Petersson; H. Nakatsuji; X. Li; M. Caricato; A. V. Marenich; J. Bloino; B. G. Janesko; R. Gomperts; B. Mennucci; H. P. Hratchian; J. V. Ortiz; A. F. Izmaylov; J. L. Sonnenberg; D. Williams-Young; F. Ding; F. Lipparini; F. Egidi; J. Goings; B. Peng; A. Petrone; T. Henderson; D. Ranasinghe; V. G. Zakrzewski; J. Gao; N. Rega; G. Zheng; W. Liang; M. Hada; M. Ehara; K. Toyota; R. Fukuda; J. Hasegawa; M. Ishida; T. Nakajima; Y. Honda; O. Kitao; H. Nakai; T. Vreven; K. Throssell; J. A. Montgomery; Jr., J. E. Peralta; F. Ogliaro; M. J. Bearpark; J. J. Heyd; E. N. Brothers; K. N. Kudin; V. N. Staroverov; T. A. Keith; R. Kobayashi; J. Normand; K. Raghavachari; A. P. Rendell; J. C. Burant; S. S. Iyengar; J. Tomasi; M. Cossi; J. M. Millam; M. Klene; C. Adamo; R. Cammi; J. W. Ochterski; R. L. Martin; K. Morokuma; O. Farkas; J. B. Foresman; D. J. Fox. Gaussian 16, Revision B.01, 2016.

(43) McCammon, J. A.; Gelin, B. R.; Karplus, M. Dynamics of Folded Proteins. *Nature* **1977**, *267* (5612), 585–590. https://doi.org/10.1038/267585a0.

(44) A. Warshel; M. Levitt. Theoretical Studies of Enzymic Reactions: Dielectric, Electrostatic and Steric Stabilization of the Carbonium Ion in the Reaction of Lysozyme. *J. Mol. Biol.* **1976**, *103*, 227–249.

(45) Bayly, C. I.; Cieplak, P.; Cornell, W.; Kollman, P. A. A Well-Behaved Electrostatic Potential Based Method Using Charge Restraints for Deriving Atomic Charges: The RESP Model. *J. Phys. Chem.* **1993**, *97* (40), 10269–10280. https://doi.org/10.1021/j100142a004.

(46) Case D.A; AKtulga H.M; Belfon K.; Ben-Shalom I.Y; Berryman J.T; Brozell S.R.; Cerutti D.S; Cheatham T.E; Cisneros G.A; Cruzeiro V.WD; Darden T.A; Duke R.E; Giambasu G.; Gilson M.K.; Gohlke H.; Goetz A.W; Harris R.; Izadi S.; Izmailov S.A; Kasavajhala K.; Kaymak M.C; King E.; Kovalenko A.; Kurtzman T.; Lee T.S; LeGrand S.; Li P.; Lin C.; Liu J.; Luchko T.; Luo R.; Machado M.; Man V.; Manathunga M.; Merz K.M; Miao Y.; Mikhailovskii O.; Monard G.; Nguyen H.; O'Hearn K.A; Onufriev A.; Pan F.; Pantano S.; Qi R.; Rahnamoun A.; Roe D.R; Roitberg A.; Sagui C.; Schott-Verdugo S.; Shajan A.; Shen J.; Simmerling C.L; Skrynnikov N.R; Smith J.; Swails J.; Walker R.C; Wang J.; Wang J.; Wei H.; Wolf R.M; Wu X.; Xiong Y.; Xue Y.; York D.M; Zhao S.; Kollman P.A. Amber18, 2018.

(47) Darden, T.; York, D.; Pedersen, L. Particle Mesh Ewald: An $N \cdot \log(N)$ Method for Ewald Sums in Large Systems. *The Journal of Chemical Physics* **1993**, *98* (12), 10089–10092. https://doi.org/10.1063/1.464397.

(48) Essmann, U.; Perera, L.; Berkowitz, M. L.; Darden, T.; Lee, H.; Pedersen, L. G. A Smooth Particle Mesh Ewald Method. *The Journal of Chemical Physics* **1995**, *103* (19), 8577–8593. https://doi.org/10.1063/1.470117.

(49) Adelman, S. A. Generalized Langevin Equation Approach for Atom/Solid-Surface Scattering: General Formulation for Classical Scattering off Harmonic Solids. *J. Chem. Phys.* **1976**, *64* (6), 2375. https://doi.org/10.1063/1.432526.

(50) Meng, X.; Zheng, P.; Wu, J.; Liu, Z. Density and Viscosity Measurements of Diethyl Ether from 243 to 373K and up to 20MPa. *Fluid Phase Equilibria* **2008**, *271* (1–2), 1–5. https://doi.org/10.1016/j.fluid.2008.06.014.

(51) Francesconi, R.; Comelli, F. Excess Molar Volumes of Binary Mixtures Containing Dimethyl Carbonate + Linear and Cyclic Ethers. *J. Chem. Eng. Data* **1994**, *39* (1), 106–107. https://doi.org/10.1021/je00013a028.

(52) VandeVondele, J.; Hutter, J. An Efficient Orbital Transformation Method for Electronic Structure Calculations. *The Journal of Chemical Physics* **2003**, *118* (10), 4365–4369. https://doi.org/10.1063/1.1543154.

(53) Grimme, S.; Antony, J.; Ehrlich, S.; Krieg, H. A Consistent and Accurate *Ab Initio* Parametrization of Density Functional Dispersion Correction (DFT-D) for the 94 Elements H-Pu. *The Journal of Chemical Physics* **2010**, *132* (15), 154104. https://doi.org/10.1063/1.3382344.

(54) Goedecker, S.; Teter, M.; Hutter, J. Separable Dual-Space Gaussian Pseudopotentials. *Phys. Rev. B* **1996**, *54* (3), 1703–1710. https://doi.org/10.1103/PhysRevB.54.1703.

(55) Hartwigsen, C.; Goedecker, S.; Hutter, J. Relativistic Separable Dual-Space Gaussian Pseudopotentials from H to Rn. *Phys. Rev. B* **1998**, *58* (7), 3641–3662. https://doi.org/10.1103/PhysRevB.58.3641.

(56) Krack, M. Pseudopotentials for H to Kr Optimized for Gradient-Corrected Exchange-Correlation Functionals. *Theor Chem Acc* **2005**, *114* (1–3), 145–152. https://doi.org/10.1007/s00214-005-0655-y.

(57) Bussi, G.; Donadio, D.; Parrinello, M. Canonical Sampling through Velocity Rescaling. *The Journal of Chemical Physics* **2007**, *126* (1), 014101. https://doi.org/10.1063/1.2408420.

(58) Kühne, T. D.; Iannuzzi, M.; Del Ben, M.; Rybkin, V. V.; Seewald, P.; Stein, F.; Laino, T.; Khaliullin, R. Z.; Schütt, O.; Schiffmann, F.; Golze, D.; Wilhelm, J.; Chulkov, S.; Bani-Hashemian, M. H.; Weber, V.; Borštnik, U.; Taillefumier, M.; Jakobovits, A. S.; Lazzaro, A.; Pabst, H.; Müller, T.; Schade, R.; Guidon, M.; Andermatt, S.; Holmberg, N.; Schenter, G. K.; Hehn, A.; Bussy, A.; Belleflamme, F.; Tabacchi, G.; Glöß, A.; Lass, M.; Bethune, I.; Mundy, C. J.; Plessl, C.; Watkins, M.; VandeVondele, J.; Krack, M.; Hutter, J. CP2K: An Electronic Structure and Molecular Dynamics Software Package - Quickstep: Efficient and Accurate Electronic Structure Calculations. *J. Chem. Phys.* **2020**, *152* (19), 194103. https://doi.org/10.1063/5.0007045.

(59) A. Laio; M. Parrinello. Escaping Free-Energy Minima. *Proc. Natl. Acad. Sci.* **2002**, *99*, 12562–12566. https://doi.org/10.1073/pnas.202427399.

(60) Ensing, B.; De Vivo, M.; Liu, Z.; Moore, P.; Klein, M. L. Metadynamics as a Tool for Exploring Free Energy Landscapes of Chemical Reactions. *Acc. Chem. Res.* **2006**, *39* (2), 73–81. https://doi.org/10.1021/ar040198i.

(61) Laio, A.; Gervasio, F. L. Metadynamics: A Method to Simulate Rare Events and Reconstruct the Free Energy in Biophysics, Chemistry and Material Science. *Rep. Prog. Phys.* **2008**, *71* (12), 126601. https://doi.org/10.1088/0034-4885/71/12/126601.

(62) Barducci, A.; Bussi, G.; Parrinello, M. Well-Tempered Metadynamics: A Smoothly Converging and Tunable Free-Energy Method. *Phys. Rev. Lett.* **2008**, *100* (2), 020603. https://doi.org/10.1103/PhysRevLett.100.020603.

(63) Bonomi, M.; Branduardi, D.; Bussi, G.; Camilloni, C.; Provasi, D.; Raiteri, P.; Donadio, D.; Marinelli, F.; Pietrucci, F.; Broglia, R. A.; Parrinello, M. PLUMED: A Portable Plugin for Free-Energy Calculations with Molecular Dynamics. *Computer Physics Communications* **2009**, *180* (10), 1961–1972. https://doi.org/10.1016/j.cpc.2009.05.011.

(64) Tribello, G. A.; Bonomi, M.; Branduardi, D.; Camilloni, C.; Bussi, G. PLUMED 2: New Feathers for an Old Bird. *Computer Physics Communications* **2014**, *185* (2), 604–613. https://doi.org/10.1016/j.cpc.2013.09.018.

(65) Bonomi, M.; Bussi, G.; Camilloni, C.; Tribello, G. A.; Banáš, P.; Barducci, A.; Bernetti, M.; Bolhuis, P. G.; Bottaro, S.; Branduardi, D.; Capelli, R.; Carloni, P.; Ceriotti, M.; Cesari, A.; Chen, H.; Chen, W.; Colizzi, F.; De, S.; De La Pierre, M.; Donadio, D.; Drobot, V.; Ensing, B.; Ferguson, A. L.; Filizola, M.; Fraser, J. S.; Fu, H.; Gasparotto, P.; Gervasio, F. L.; Giberti, F.; Gil-Ley, A.; Giorgino, T.; Heller, G. T.; Hocky, G. M.; Iannuzzi, M.; Invernizzi, M.; Jelfs, K. E.; Jussupow, A.; Kirilin, E.; Laio, A.; Limongelli, V.; Lindorff-Larsen, K.; Löhr, T.; Marinelli, F.; Martin-Samos, L.; Masetti, M.; Meyer, R.; Michaelides, A.; Molteni, C.; Morishita, T.; Nava, M.; Paissoni, C.; Papaleo, E.; Parrinello, M.; Pfaendtner, J.; Piaggi, P.; Piccini, G.; Pietropaolo, A.; Pietrucci, F.; Pipolo, S.; Provasi, D.; Quigley, D.; Raiteri, P.; Raniolo, S.; Rydzewski, J.; Salvalaglio, M.; Sosso, G. C.; Spiwok, V.; Šponer, J.; Swenson, D. W. H.; Tiwary, P.; Valsson, O.; Vendruscolo, M.; Voth, G. A.; White, A.; The PLUMED consortium. Promoting Transparency and Reproducibility in Enhanced Molecular Simulations. *Nature Methods* **2019**, *16* (8), 670–673. https://doi.org/10.1038/s41592-019-0506-8.

(66) Jeziorski, B.; Moszynski, R.; Szalewicz, K. Perturbation Theory Approach to Intermolecular Potential Energy Surfaces of van Der Waals Complexes. *Chem. Rev.* **1994**, *94* (7), 1887–1930. https://doi.org/10.1021/cr00031a008.

(67) Hohenstein, E. G.; Sherrill, C. D. Density Fitting of Intramonomer Correlation Effects in Symmetry-Adapted Perturbation Theory. *The Journal of Chemical Physics* **2010**, *133* (1), 014101. https://doi.org/10.1063/1.3451077.

(68) Kendall, R. A.; Dunning, T. H.; Harrison, R. J. Electron Affinities of the First-row Atoms Revisited. Systematic Basis Sets and Wave Functions. *The Journal of Chemical Physics* **1992**, *96* (9), 6796–6806. https://doi.org/10.1063/1.462569.

(69) Smith, D. G. A.; Burns, L. A.; Simmonett, A. C.; Parrish, R. M.; Schieber, M. C.; Galvelis, R.; Kraus, P.; Kruse, H.; Di Remigio, R.; Alenaizan, A.; James, A. M.; Lehtola, S.; Misiewicz, J. P.; Scheurer, M.; Shaw, R. A.; Schriber, J. B.; Xie, Y.; Glick, Z. L.; Sirianni, D. A.; O'Brien, J. S.; Waldrop, J. M.; Kumar, A.; Hohenstein, E. G.; Pritchard, B. P.; Brooks, B. R.; Schaefer, H. F.; Sokolov, A. Yu.; Patkowski, K.; DePrince, A. E.; Bozkaya, U.; King, R. A.; Evangelista, F. A.; Turney, J. M.; Crawford, T. D.; Sherrill, C. D. P SI4 1.4: Open-Source Software for High-Throughput Quantum Chemistry. *J. Chem. Phys.* **2020**, *152* (18), 184108. https://doi.org/10.1063/5.0006002.

(70) Rappoport, Z.; Marek, I. *The Chemistry of Organolithium Compounds*; John Wiley & Sons, 2004.

(71) Brown, T. L. The Structures of Organolithium Compounds. *Advances in Organometallic Chemistry* **1966**, *3*, 365–395. https://doi.org/10.1016/S0065-3055(08)60041-6.

(72) Günther, H.; Moskau, D.; Bast, P.; Schmalz, D. Modern NMR Spectroscopy of Organolithium Compounds. *Angewandte Chemie International Edition in English* **1987**, *26* (12), 1212–1220. https://doi.org/10.1002/anie.198712121.

(73) Ogle, C. A.; Huckabee, B. K.; Johnson, H. C.; Sims, P. F.; Winslow, S. D.; Pinkerton, A. A. Isolation, Characterization, and Crystal Structure of [MeLi.THF]4. *Organometallics* **1993**, *12* (5), 1960–1963. https://doi.org/10.1021/om00029a061.

(74) McKeever, L. D.; Waack, R.; Doran, M. A.; Baker, E. B. Nuclear Magnetic Resonance Study of Structure and Bonding in Methylithium. *J. Am. Chem. Soc.* **1969**, *91* (5), 1057–1061. https://doi.org/10.1021/ja01033a003.

(75) Thomas, R. D.; Clarke, M. T.; Jensen, R. M.; Young, T. Corby. Fluxional Exchange of Tert-Butyllithium Tetramers from Temperature-Dependent Carbon-13-Lithium-6 Coupling. *Organometallics* **1986**, *5* (9), 1851–1857. https://doi.org/10.1021/om00140a016.

(76) Kaufmann, Elmar.; Raghavachari, Krishnan.; Reed, A. E.; Schleyer, P. V. R. Methyllithium and Its Oligomers. Structural and Energetic Relationships. *Organometallics* **1988**, *7* (7), 1597–1607. https://doi.org/10.1021/om00097a024.

(77) Verstraete, P.; Deffieux, A.; Fritsch, A.; Rayez, J. C.; Rayez, M. T. Theoretical Study of a Series of Alkyllithium Clusters. *Journal of Molecular Structure: THEOCHEM* **2003**, *631* (1–3), 53–66. https://doi.org/10.1016/S0166-1280(03)00133-7.

(78) Gérard, H.; de la Lande, A.; Maddaluno, J.; Parisel, O.; Tuckerman, M. E. Revisiting the Structure of $(LiCH_3)_n$ Aggregates Using Car−Parrinello Molecular Dynamics. *J. Phys. Chem. A* **2006**, *110* (14), 4787–4794. https://doi.org/10.1021/jp056326h.

(79) Bates, T. F.; Clarke, M. T.; Thomas, R. D. Unusual Stability of an Alkyllithium Dimer. Preparation, Properties, and Decomposition Mechanism of Tert-Butyllithium Dietherate Dimer. *J. Am. Chem. Soc.* **1988**, *110* (15), 5109–5112. https://doi.org/10.1021/ja00223a032.

(80) Pratt, L. M.; Truhlar, D. G.; Cramer, C. J.; Kass, S. R.; Thompson, J. D.; Xidos, J. D. Aggregation of Alkyllithiums in Tetrahydrofuran. *J. Org. Chem.* **2007**, *72* (8), 2962–2966. https://doi.org/10.1021/jo062557o.

(81) Reich, H. J. Role of Organolithium Aggregates and Mixed Aggregates in Organolithium Mechanisms. *Chem. Rev.* **2013**, *113* (9), 7130–7178. https://doi.org/10.1021/cr400187u.

(82) Cramer, C. J. *Essentials of Computational Chemistry: Theories and Models*, 2nd ed.; Wiley: Chichester, West Sussex, England ; Hoboken, NJ, 2004.

(83) Bryantsev, V. S.; Diallo, M. S.; Goddard III, W. A. Calculation of Solvation Free Energies of Charged Solutes Using Mixed Cluster/Continuum Models. *J. Phys. Chem. B* **2008**, *112* (32), 9709–9719. https://doi.org/10.1021/jp802665d.

(84) Subramanian, V.; Knight, J. S.; Parelkar, S.; Anguish, L.; Coonrod, S. A.; Kaplan, M. J.; Thompson, P. R. Design, Synthesis, and Biological Evaluation of Tetrazole Analogs of Cl-Amidine as Protein Arginine Deiminase Inhibitors. *J. Med. Chem.* **2015**, *58* (3), 1337–1344. https://doi.org/10.1021/jm501636x.

(85) Zhang, J.; Wang, S.; Ba, Y.; Xu, Z. Tetrazole Hybrids with Potential Anticancer Activity. *European Journal of Medicinal Chemistry* **2019**, *178*, 341–351. https://doi.org/10.1016/j.ejmech.2019.05.071.

(86) Venet, M.; End, D.; Angibaud, P. Farnesyl Protein Transferase Inhibitor ZARNESTRA™ R115777 - History of a Discovery. *CTMC* **2003**, *3* (10), 1095–1102. https://doi.org/10.2174/1568026033452050.

(87) He, S.; Senter, T. J.; Pollock, J.; Han, C.; Upadhyay, S. K.; Purohit, T.; Gogliotti, R. D.; Lindsley, C. W.; Cierpicki, T.; Stauffer, S. R.; Grembecka, J. High-Affinity Small-Molecule Inhibitors of the Menin-Mixed Lineage Leukemia (MLL) Interaction Closely Mimic a Natural Protein–Protein Interaction. *J. Med. Chem.* **2014**, *57* (4), 1543–1556. https://doi.org/10.1021/jm401868d.

(88) Sullivan, B. W.; Faulkner, D. J.; Okamoto, K. T.; Chen, M. H. M.; Clardy, J. (6R,7S)-7-Amino-7,8-Dihydro-.Alpha.-Bisabolene, an Antimicrobial Metabolite from the Marine Sponge Halichondria Sp. *J. Org. Chem.* **1986**, *51* (26), 5134–5136. https://doi.org/10.1021/jo00376a014.

(89) Cogan, D. A.; Liu, G.; Ellman, J. Asymmetric Synthesis of Chiral Amines by Highly Diastereoselective 1,2-Additions of Organometallic Reagents to N-Tert-Butanesulfinyl Imines. *Tetrahedron* **1999**, *55* (29), 8883–8904. https://doi.org/10.1016/S0040-4020(99)00451-2.

(90) Davis, F. A.; Kluger, E. W. Chemistry of the Sulfur-Nitrogen Bond. X. Barriers to Planar Inversion in N-(4,4'-Dimethylbenzophenylidene)Arenesulfenamides and -Selenenamides. *J. Am. Chem. Soc.* **1976**, *98* (1), 302–303. https://doi.org/10.1021/ja00417a084.

(91) Hennum, M.; Fliegl, H.; Gundersen, L.-L.; Eisenstein, O. Mechanistic Insights on the Stereoselective Nucleophilic 1,2- Addition to Sulfinyl Imines. *J. Org. Chem.* **2014**, 8.

(92) Smith, S. G.; Charbonneau, L. F.; Novak, D. P.; Brown, T. L. Kinetics of the Reaction of Methyllithium with 2,4-Dimethyl-4'-Methylthiobenzophenone. *J. Am. Chem. Soc.* **1972**, *94* (20), 7059–7063. https://doi.org/10.1021/ja00775a032.

(93) Ashby, E. C.; Laemmle, J. T. Stereochemistry of Organometallic Compound Addition to Ketones. *Chem. Rev.* **1975**, *75* (4), 521–546. https://doi.org/10.1021/cr60296a005.

(94) Al-Aseer, M. A.; Smith, S. G. Kinetics and Mechanism of the Reaction of Ketones with Lithium Reagents in Cyclohexane. *J. Org. Chem.* **1984**, *49* (14), 2608–2613. https://doi.org/10.1021/jo00188a018.

(95) McGarrity, J. F.; Ogle, C. A.; Brich, Z.; Loosli, H. R. A Rapid-Injection (RI) NMR Study of the Reactivity of Butyllithium Aggregates in Tetrahydrofuran. *J. Am. Chem. Soc.* **1985**, *107* (7), 1810–1815. https://doi.org/10.1021/ja00293a002.

(96) McGarrity, J. F.; Ogle, C. A. High-Field Proton NMR Study of the Aggregation and Complexation of n-Butyllithium in Tetrahydrofuran. *J. Am. Chem. Soc.* **1985**, *107* (7), 1805–1810. https://doi.org/10.1021/ja00293a001.

(97) Nichols, M. A.; Williard, P. G. Solid-State Structures of n-Butyllithium-TMEDA, -THF, and -DME Complexes. *J. Am. Chem. Soc.* **1993**, *115* (4), 1568–1572. https://doi.org/10.1021/ja00057a050.

(98) Bailey, W. F.; Bartelson, A. L.; Wiberg, K. B. Contrasting Reactions of Ketones and Thioketones with Alkyllithiums: A Coordinated Experimental and Computational Investigation. *J. Am. Chem. Soc.* **2012**, *134* (6), 3199–3207. https://doi.org/10.1021/ja210847n.

(99) Fressigné, C.; Maddaluno, J.; Marquez, A.; Giessner-Prettre, C. A DFT Theoretical Analysis of Aldehyde Condensation Pathways onto Methyllithium, Lithium

Dimethylamide, and Their Aggregates. *J. Org. Chem.* **2000**, *65* (26), 8899–8907. https://doi.org/10.1021/jo000648u.

(100) Fressigné, C.; Lautrette, A.; Maddaluno, J. A DFT Theoretical Study of the Condensation of Aggregates of Sp^2 Organolithium Compounds on Formaldehyde. *J. Org. Chem.* **2005**, *70* (20), 7816–7828. https://doi.org/10.1021/jo050524n.

(101) Nakamura, M.; Nakamura, E.; Koga, N.; Morokuma, K. Theoretical Studies on the Reaction of Solvated Methyllithium Open Dimer with Aldehydes. *J. Am. Chem. Soc.* **1993**, *115* (23), 11016–11017. https://doi.org/10.1021/ja00076a080.

(102) Hæffner, F.; Sun, C.; Williard, P. G. Mechanistic Variations Due to the Solvation State in the Reaction of MeLi in Dimer and Trimer Aggregates with Formaldehyde. *J. Am. Chem. Soc.* **2000**, *122* (50), 12542–12546. https://doi.org/10.1021/ja002380u.

(103) Bürgi, H. B.; Dunitz, J. D.; Shefter, Eli. Geometrical Reaction Coordinates. II. Nucleophilic Addition to a Carbonyl Group. *J. Am. Chem. Soc.* **1973**, *95* (15), 5065–5067. https://doi.org/10.1021/ja00796a058.

(104) Bürgi, H. B.; Dunitz, J. D.; Lehn, J. M.; Wipff, G. Stereochemistry of Reaction Paths at Carbonyl Centres. *Tetrahedron* **1974**, *30* (12), 1563–1572. https://doi.org/10.1016/S0040-4020(01)90678-7.

(105) Bürgi, H. B.; Dunitz, J. D. From Crystal Statics to Chemical Dynamics. *Acc. Chem. Res.* **1983**, *16* (5), 153–161. https://doi.org/10.1021/ar00089a002.

(106) Taylor, R. Novel Preparation of Tritium- and Trimethylsilyl-Labelled Aromatics. *Tetrahedron Lett., no. 7, pp. 435-436* **1975**. https://doi.org/10.1016/S0040-4039(00)71886-7.

(107) Levine, R.; Karten, M. J.; Kadunce, W. M. Reactions of Organolithium Compounds and Grignard Reagents with Lithium Carboxylates. *J. Org. Chem.* **1975**, *40* (12), 1770–1773. https://doi.org/10.1021/jo00900a020.

(108) Narayan, S.; Muldoon, J.; Finn, M. G.; Fokin, V. V.; Kolb, H. C.; Sharpless, K. B. "On Water": Unique Reactivity of Organic Compounds in Aqueous Suspension. *Angewandte Chemie International Edition* **2005**, *44* (21), 3275–3279. https://doi.org/10.1002/anie.200462883.

(109) Rideout, D. C.; Breslow, R. Hydrophobic Acceleration of Diels-Alder Reactions. *J. Am. Chem. Soc.* **1980**, *102* (26), 7816–7817. https://doi.org/10.1021/ja00546a048.

(110) Jung, Y.; Marcus, R. A. On the Theory of Organic Catalysis "on Water." *J. Am. Chem. Soc.* **2007**, *129* (17), 5492–5502. https://doi.org/10.1021/ja068120f.

(111) Otto, S.; Engberts, J. B. F. N. Hydrophobic Interactions and Chemical Reactivity. *Org. Biomol. Chem.* **2003**, *1*, 2809–2820.

(112) Meijer, A.; Otto, S.; Engberts, J. B. F. N. Effects of the Hydrophobicity of the Reactants on Diels−Alder Reactions in Water. *J. Org. Chem.* **1998**, *63* (24), 8989–8994. https://doi.org/10.1021/jo981359x.

(113) Mallardo, V.; Rizzi, R.; Sassone, F. C.; Mansueto, R.; Perna, F. M.; Salomone, A.; Capriati, V. Regioselective Desymmetrization of Diaryltetrahydrofurans via Directed Ortho-Lithiation: An Unexpected Help from Green Chemistry. *Chem. Commun.* **2014**, *50* (63), 8655–8658. https://doi.org/10.1039/C4CC03149K.

(114) Osztrovszky, G.; Holm, T.; Madsen, R. Ultrafast Grignard Addition Reactions in the Presence of Water. *Org. Biomol. Chem.* **2010**, *8* (15), 3402. https://doi.org/10.1039/c0ob00170h.

(115) Vidal, C.; García-Álvarez, J.; Hernán-Gómez, A.; Kennedy, A. R.; Hevia, E. Introducing Deep Eutectic Solvents to Polar Organometallic Chemistry: Chemoselective Addition of Organolithium and Grignard Reagents to Ketones in Air. *Angewandte Chemie International Edition* **2014**, *53* (23), 5969–5973. https://doi.org/10.1002/anie.201400889.

(116) Rodríguez-Álvarez, M. J.; García-Álvarez, J.; Uzelac, M.; Fairley, M.; O'Hara, C. T.; Hevia, E. Introducing Glycerol as a Sustainable Solvent to Organolithium Chemistry: Ultrafast Chemoselective Addition of Aryllithium Reagents to Nitriles under Air and at Ambient Temperature. *Chemistry – A European Journal* **2018**, *24* (7), 1720–1725. https://doi.org/10.1002/chem.201705577.

(117) Abbott, A. P.; Capper, G.; Davies, D. L.; Rasheed, R. K.; Tambyrajah, V. Novel Solvent Properties of Choline Chloride/Urea MixturesElectronic Supplementary Information (ESI) Available: Spectroscopic Data. See Http://Www.Rsc.Org/Suppdata/Cc/B2/B210714g/. *Chem. Commun.* **2003**, No. 1, 70–71. https://doi.org/10.1039/b210714g.

(118) Smith, E. L.; Abbott, A. P.; Ryder, K. S. Deep Eutectic Solvents (DESs) and Their Applications. *Chem. Rev.* **2014**, *114* (21), 11060–11082. https://doi.org/10.1021/cr300162p.

(119) Cortes-Clerget, M.; Yu, J.; Kincaid, J. R. A.; Walde, P.; Gallou, F.; Lipshutz, B. H. Water as the Reaction Medium in Organic Chemistry: From Our Worst Enemy to Our Best Friend. *Chem. Sci.* **2021**, *12* (12), 4237–4266. https://doi.org/10.1039/D0SC06000C.

(120) Barr, D.; Raithby, P. R.; Schleyer, P. V. R.; Snaith, R.; Wright, D. S. The First Lithiated Organic Compound Containing Water as a Ligand: Synthesis and A Crystal Structure of 2-Merca Tobenzoxazolyl(Tetramethylethylenediamine)Lithium Monohydrate,

6H40C(,A).L.i(t.Meda)H20,a Model Acid-Base Intermediate. *J. Chem. Soc., Chem. Commun* **1990**, 643–645.

(121) Gimbert, Y.; Lesage, D.; Fressigné, C.; Maddaluno, J. Lithium Amide Protected against Hydrolysis by Aggregated Lithium Halides: An MS + DFT Investigation. *J. Org. Chem.* **2017**, *82* (15), 8141–8147. https://doi.org/10.1021/acs.joc.7b01419.

(122) Pocker, Y.; Exner, J. H. Deuterium Isotope Effects in the Decomposition of Organometals by Proton Donors. *J. Am. Chem. Soc.* **1968**, *90* (24), 6764–6773. https://doi.org/10.1021/ja01026a036.

(123) Trizio, E.; Parrinello, M. From Enhanced Sampling to Reaction Profiles. *J. Phys. Chem. Lett.* **2021**, *12* (35), 8621–8626. https://doi.org/10.1021/acs.jpclett.1c02317.

(124) Yang, M.; Bonati, L.; Polino, D.; Parrinello, M. Using Metadynamics to Build Neural Network Potentials for Reactive Events: The Case of Urea Decomposition in Water. *Catalysis Today* **2022**, *387*, 143–149. https://doi.org/10.1016/j.cattod.2021.03.018.

Résumé

L'utilité des organolithiens et organomagnésiens pour les chimistes de synthèse n'est plus à démontrer. Ces composés et, plus généralement, les composés organométalliques fortement polaires du bloc s (R-Li, R-Mg, ..) demandent néanmoins à être manipulés dans des conditions strictes : solvant aprotique, atmosphère inerte, et souvent basse température. Mais récemment, ces dérivés ont pu être utilisés dans des milieux totalement inattendus comme l'eau et cela à température ambiante et avec d'excellents rendements voire sélectivité !

Cette thèse vise à comprendre le mécanisme de cette réaction et le rôle de l'eau, en mettant l'accent sur la synthèse du tétrahydrofurane 2,2-disubstitué par réaction de la 4-chloro-1-phényl butan-1-one (chlorocétone) avec le méthyllithium "sur l'eau" par des méthodes de modélisation de type DFT et par des dynamique QM/MM biaisée comme la métadynamique. Nous avons d'abord étudié les différents états d'agrégation et la nature de la solvatation du MeLi dans les solvants éthérés (éther diéthylique et THF). Les états d'agrégation dominants sont le dimère et le tétramère, le tétramère étant l'état le plus stable. Le nombre de coordination du solvant observé avec le THF est plus élevé que la solvatation correspondante dans l'éther diéthylique. Ceci est principalement dû à la répulsion stérique exercée par les chaînes alkyle de l'éther diéthylique. Une tendance similaire a été observée pour les clusters avec une cétone coordonné (acétone, chlorocétone) au lithium du méthyllithium (clusters MeLi-Ketone). L'étude de l'énergie d'interaction intermoléculaire entre les solvants ou les cétones et les clusters de MeLi a été réalisé en utilisant SAPT (Symmetry Adapted Perturbation Theory) et a montré une relation directe entre l'énergie d'interaction et le nombre de solvants coordonnés en raison de la réduction de la densité électronique sur le cluster de MeLi par l'attraction des solvants coordonnés.

Le mécanisme de réaction de l'addition des agrégats de MeLi aux cétones a été étudié dans les milieux conventionnels (éther diéthylique et THF) et non conventionnels ("sur l'eau"). Les solvants se sont avérés avoir un effet significatif sur les réactions. Pour la réaction sur l'eau, un réseau de liaison hydrogène formé par l'eau et le système cétone-cluster partiellement hydrolysé permet cette réaction sans consommation complète du réactif organométallique par l'eau.

Nous avons également étudié l'addition nucléophile organométallique de sulfinylcétimines et avons trouvé que la différence de stabilité et la rapidité de l'addition par rapport à l'isomérie des diastéréoisomères et l'effet du stérique sont les raisons de la haute sélectivité de l'addition 1,2 obtenue pour la réaction.